

DISSERTATION

Model Order Reduction of Redundant Multibody System Dynamics

ausgeführt zum Zwecke der Erlangung des akademischen Grades
eines Doktors der technischen Wissenschaften (Dr. techn.)
eingereicht an der TU Wien, Fakultät für Maschinenwesen und Betriebswissenschaften von

Dipl.Ing. Daniel Stadlmayr

Mat.Nr.: 0530880

unter der Leitung von

Priv. Doz. Dipl.-Ing. Dr. Wolfgang Steiner

Institut für Mechanik und Mechatronik

Abteilung für Mechanik fester Körper

begutachtet von

Ao.Univ.Prof. Dipl.-Ing. Dr. Alois Steindl

Technische Universität Wien

Institut für Mechanik und Mechatronik

Getreidemarkt 9, 1060 Wien

Univ.-Prof. Dr.-Ing. habil. Alexander Lion

Universität der Bundeswehr München

Institut für Mechanik

Werner-Heisenberg-Weg 39, 85577 Neubiberg

Diese Arbeit wurde von der Österreichischen Forschungsförderungsgesellschaft mbH (FFG) im Rahmen des Projekts ProtoFrame (Projektnr. 839074) unterstützt.

Ich nehme zur Kenntnis, dass ich zur Drucklegung meiner Arbeit unter der Bezeichnung Dissertation nur mit Bewilligung der Prüfungskommission berechtigt bin.

Eidesstaatliche Erklärung

Ich erkläre an Eides statt, dass die vorliegende Arbeit nach den anerkannten Grundsätzen für wissenschaftliche Abhandlungen von mir selbstständig erstellt wurde. Alle verwendeten Hilfsmittel, insbesondere die zugrunde gelegte Literatur, sind in dieser Arbeit genannt und aufgelistet. Die aus den Quellen wörtlich entnommenen Stellen, sind als solche kenntlich gemacht.

Das Thema dieser Arbeit wurde von mir bisher weder im In- noch Ausland einer Beurteilerin/einem Beurteiler zur Begutachtung in irgendeiner Form als Prüfungsarbeit vorgelegt. Diese Arbeit stimmt mit der von den Begutachterinnen/Begutachtern beurteilten Arbeit überein.

Wien, 17. Mai 2018

Daniel Stadlmayr

... to my wife Tanja:
Forse per il mondo sei solo una persona, ma per qualche persona sei tutto il mondo. (Gabriel García Márquez)

Danksagung

Diese Arbeit wäre ohne die Unterstützung meiner Betreuer, Mentoren, Kollegen, und nicht zuletzt meiner Familie nicht denkbar gewesen.

Mein Dank gilt Herrn Priv.Doz. Dipl.-Ing. Dr.techn Wolfgang Steiner, welcher es mir ermöglicht hat diese Arbeit am Institut für Mechanik und Mechatronik an der Technischen Universität Wien anzufertigen. Seine konstruktive Unterstützung und wissenschaftliche Leitung haben wesentlich zum Gelingen dieser Arbeit beigetragen.

Besonders Bedanken möchte ich mich ebenso bei Herrn Dipl.-Ing. Dr.techn. Wolfgang Witteveen, der mir über die vergangenen Jahre die wissenschaftlich/akademische Welt eröffnet, und maßgeblich zum Abschluss dieser Arbeit beigetragen hat.

Großer Dank gebührt ebenso meiner Familie, welche mich stets unterstützt und ermutigt haben.

Kurzfassung

Ein Grund für die zunehmende Bedeutung der Mehrkörpersimulation (MKS) im virtuellen Entwicklungsprozess ist die Verfügbarkeit automatisierter Modellerzeugungsverfahren. Die so erstellten mathematischen Modelle verwenden redundante Freiheitsgrade und Zwangsbedingungen zur Beschreibung des MKS Modells. Im Vergleich zu einer Minimalkoordinatenbeschreibung ist die Simulationsdauer, bedingt durch die größere Anzahl zu lösender Gleichungen, in der Regel deutlich höher. Ziel der vorliegenden Arbeit ist die Ableitung eines Modellreduktionsverfahrens für die MKS zum Zwecke der Effizienzsteigerung.

Aufgrund der geforderten Anwendbarkeit an beliebige Mehrkörpermodelle wurde ein datengestütztes Reduktionsverfahren, basierend auf der „Proper Orthogonal Decomposition“ (POD), ausgewählt. Das Verfahren wurde in folgenden Punkten an die Besonderheiten der MKS adaptiert: (1) Verwendung von Geschwindigkeitsdaten anstatt der üblichen Positionsdaten. (2) Trennung der Koordinaten hinsichtlich ihrer physikalischen Bedeutung (anstatt der üblichen, gemischten Berücksichtigung). (3) Erweiterung der Projektion um ein Residuum, welches die korrekte Abbildung der Anfangsbedingungen sicherstellt.

Der durch die adaptierte POD erzeugte Unterraum enthält bereits Informationen über die Zwangsbedingungen des MKS Systems. Aus diesem Grund wird in dieser Dissertation ein Verfahren vorgestellt, welches redundante Zwangsbedingungen im reduzierten Modell erkennt und eliminiert. Im Gegensatz zu den bisherigen Vorschlägen in der Literatur ist das auf diese Weise reduzierte Gleichungssystem immer lösbar und gut konditioniert.

Die Effizienz der Methode wird anhand praxisrelevanter Beispiele demonstriert. Unter Einhaltung einer hohen Ergebnisqualität kann die Anzahl der zu lösenden Gleichungen um bis zu 90% Prozent reduziert werden. Abschließend wird die Methode auch im Rahmen der Parameteridentifikation angewandt. Hierbei wird der aufgespannte Unterraum auch zur Reduktion von adjungierten Gleichungen verwendet.

Abstract

Multibody system (MBS) simulations see an increasing relevance in the field of automated modeling strategies due to several reasons. A redundant set of coordinates in combination with constraint coordination equations are required for such modeling strategies. Consequently, the numerical challenge of solving such models is much higher than it might be if a minimal set of coordinates representation is used. The current dissertation will explain the development of a model order reduction (MOR) technique, which allows to decrease the number of equations, and increase the numerical efficiency of such redundant multibody systems.

A databased MOR approach has been chosen since the focus is on a general applicability to arbitrary multibody systems. It is based on the Proper Orthogonal Decomposition (POD), which is adapted to the special needs of multibody systems by: (1) Using velocity data of the MBS (instead of the commonly used position data). (2) Separate handling of each coordinate type due to its physical meaning (instead of the commonly used mixed coordinate approach). (3) Adding a residual term to the applied projection which ensures the initial conditions to be met.

Due to the use of a data-driven reduction approach, the resulting reduction subspace includes constraint information of the original MBS model. Therefore, the present dissertation introduces a constraint reduction method, which determines and eliminates redundant constraint equations of the reduced order model. In contrast to known literature regarding MBS reduction, the herein derived coordinate and constraint reduced order model is therefore always solvable and well-conditioned.

The efficiency of the MOR approach is outlined by several practical numerical examples, evolving from automotive tasks. The results underline the efficiency of the novel approach, which ensures high result consistency, while at the same time, the dimension of the mathematical model is reduced up to 90+%. Finally, the approach is also applied to parameter identification tasks in the context of multibody systems. In addition to the previous mentioned reduction, the adjoint equations are reduced as well, by projecting them onto the same subspace as the original MBS model.

Contents

Kurzfassung	v
Abstract	vi
Contents	vii
1 Introduction	1
1.1 Dissertation Objectives and Outline	3
2 Multibody System Dynamics	5
2.1 Euler Parameter	5
2.2 Equations of Motion of an Unconstrained Rigid Body	8
2.3 Equations of Motion of an Unconstrained Flexible Body	10
2.4 Unconstrained Multibody Systems	12
2.5 Constrained Multibody Systems	13
2.5.1 HHT solver algorithm	15
3 Model Order Reduction	17
3.1 The Idea of Model Order Reduction	17
3.2 Projection Based Model Order Reduction	18
3.2.1 Flat Projection	19
3.3 A Priori Model Order Reduction	20
3.3.1 Component Mode Synthesis	21
3.3.2 Moment Matching	23
3.3.3 Balanced Truncation	24
3.3.4 Coordinate Partitioning	26
3.3.5 Nonlinear Galerkin Projection	29
3.3.5.1 Center Manifold Theory	29
3.3.6 Applicability of A Priori Methods	32
3.4 A Posteriori Model Order Reduction	37
3.4.1 Singular Value Decomposition	37

3.4.1.1	The Generalized Singular Value Decomposition . . .	39
3.4.2	(Auto)-Covariance Matrices	41
3.4.3	POD - Proper Orthogonal Decomposition	45
3.4.4	SOD - Smooth Orthogonal Decomposition	55
3.4.5	Applicability of A Posteriori Methods	58
4	Physical and Constraint Coordinate Reduction of Redundantly Formulated Flexible Multibody Systems Based on Adapted POD	65
4.1	Different Coordinate Scales	66
4.1.1	Coordinate-Type Sensitive POD	67
4.2	Deviation of Initial Conditions	70
4.3	Reducing Constraint Equations	71
4.3.1	A Simple Projection Approach	72
4.3.2	A Generalized Projection Approach	76
4.4	Model Order Reduction Scheme	77
4.5	Comments with Respect to the Constraint Forces in the Reduced Model	79
4.6	Effect of the Reduction Approach on the HHT-Solver	81
5	Application to Large Scale Multibody Systems	83
5.1	A Rigid V8 Crank Drive	83
5.1.1	Results	84
5.2	A Rigid V8 Crank Drive in Mounting Condition	90
5.2.1	Results	91
5.3	A Partially Flexible Front Suspension	98
5.3.1	Results	100
5.4	A Rigid Junior Dirtbike	107
5.4.1	Results	108
5.4.2	Discussion	114
6	Application to Parameter Identification Tasks in Multibody Systems	115
6.1	Parameter Identification utilizing the Adjoint Method	116
6.1.1	The Adjoint Method in the Context of Reduced Order Multibody Systems	117
6.1.2	Numerical Example	120
6.1.3	Discussion	122
7	Conclusion	130
	List of Figures	132

List of Tables	134
List of Symbols	135
Bibliography	138
Appendix	148

Introduction

In the last two decades, multibody system simulation have been established as a scarcely replaceable tool in the product development process in various fields like the automotive industry, aerospace, training simulators, and several more. Commercial multibody system (MBS) software emphasize on the automated modeling of a broad variety of multibody systems based on user input of joints and body orientations. Per today, to achieve results of these simulations redundant coordinate formulations are commonly used, which are typically of much higher degree of freedom (DOF) dimension than with a minimal set of coordinates description. Rigid and flexible MBS simulation have become state of the art these days. Deformable bodies are typically derived from Finite Element (FE) models, and imported into the MBS model by well known modal reduction processes like Component Mode Synthesis, cf. [22, 23]. Thus, the set of rigid DOFs is extended by flexible coordinates, originating from the modal reduction. As the FE body import is highly dependent on the user's knowledge of the system, too large a number of flex-body modes are often chosen resulting in a large set of flex DOFs.

In contrast to the minimal set of coordinates representation, the equations of motion for a redundant formulation of the underlying dynamical system do not include joint information. Therefore, the redundant MBS model includes a set of constraint equations, to represent such coordinate interactions. The MBS under consideration is therefore represented by a set of second order differential algebraic equations (DAEs) with differential index three. Such MBS formulation is due to its definition in most cases computationally less efficient than a minimal set of coordinate model.

For this reason, this dissertation aims to derive a model order reduction (MOR) method, which allows to reduce the number of rigid and flexible coordinates, as well as the number of constraint equations. Ideally, this MOR approach allows to

reduce the MBS model into a system with a minimal set of coordinates. In fact, the present MBS formulation is nonlinear as well as time and state dependent which makes a priori MOR method not applicable. Therefore, the character of MOR methods is most likely limited to an a posteriori approach, which allows to reduce the MBS model based on collected model data. This data must be collected along a time history of the original results from MBS models simulation. The class of reducible MBS models is naturally limited to repetitive simulation tasks which need to be carried out at least twice.

The following examples for typical repetitive MBS simulations can be considered within the automotive industry:

- Load data acquisition for follow-up investigations like finite element computations and component design
- parameter identification of production-related uncertainties like inertia parameters, body mass or the exact location of the center of mass (CoM),
- optimal control tasks
- control unit design
- part design studies.

From these circumstances, an application to the parameter identification of production related uncertainties will be given in this dissertation. Several MBS reduction methods have been proposed to handle available computational resources in the last decades and can be roughly divided into two groups of reduction methods. The first group includes methods that eliminate the Lagrange's multipliers and thereby reduce the DAEs into ordinary differential equations (ODEs), cf. [82]. This group of reduction methods is in the need of severely changing the system of DAEs. It is hence not considered in this work since the focus is on automated modeling strategies and the possible application to commercial MBS software. The second group reduces the index of the governing equations of motion into index-one differential equations, but keeps the algebraic equations and therefore preserves the DAE manner, cf. [60]. A potential method of this group is the Proper Orthogonal Decomposition (POD), also known as Karhunen-Loeve Decomposition, cf. [56, 18, 54, 109]. It has been proposed as a reduction method to index-one DAEs evolving from MBS by Ebert [30]. Further, Ersal et al. [31] applied DOF-type sensitive POD reduction to bond-graph models of MBS, and Masoudi et al. [69] recently applied POD model reduction to automotive suspension systems in ODE representation. Furthermore, Smooth Orthogonal Decomposition (SOD) has been presented as a model reduction method for linear mechanical systems subject to

local nonlinearities, cf. [20, 21, 19, 51, 52], recently. While POD and SOD model reduction are usually applied by linear (flat) Galerkin projection, Heirman et al. [48, 49] presented a nonlinear model reduction method based on the Global Modal Parametrization (GMP), cf. [14]. GMP may be related to the first group of reduction methods. In contrast to POD and SOD the therein presented method projects the MBS onto a curvilinear instead of a fixed vector space to reduce the number of generalized coordinates and eliminate the constraints. As a matter of fact, none of the known MOR approaches are applied to the present mathematical representation of the MBS. The set of DAEs is, at least, transformed into a first order system or, by reducing the differential index, into a system of ODEs.

The processing of constraint equations has been and is still an open field of research by various authors. Originating from overdeterminacy, constraint miss-modeling and several other intentions, constraint reduction in terms of the singular value decomposition was discussed intensely, cf. [45, 26, 115, 116]. Nevertheless, when dealing with the special case of the MOR of redundantly formulated MBS, the reduction of constraint equations has, to the best knowledge of the author, not been addressed yet. It is only Ebert [30] who deals with this topic. He therein states that due to the loss of physical phenomena MBS reduction must be restricted to the differential part only (the system DOFs). The algebraic part (the constraint equations) must not be touched.

1.1 Dissertation Objectives and Outline

This dissertation aims to derive a novel model order reduction approach which allows to improve redundantly formulated multibody systems, as generated by MBS software like MSC.Adams [75] or FreeDyn [41]. Focusing repetitive simulation tasks, the novel approach allows to significantly reduce the number of physical coordinates (DOFs) and the number of constraint equations. This results in a considerable reduction of simulation time, without the need of reducing the system's order or the differential index.

It is assumed, that the multibody system modeling part has already been performed by an automated pre-processor. As a consequence, this dissertation does not focus on the modal reduction of flexible bodies. For deep insight into the topic of flexible body import into the multibody system the interested reader is referred to Besselink et al. [11], Lehner [62], Koutsovasilis et al. [57] and Witteveen [114]. The dissertation is outlined as follows:

- **Chapter 2: Introduction to the multibody system under consideration**

The set of DAEs describing a redundantly formulated MBS model is briefly

summarized. The mathematical model presented in this chapter forms the MBS basis and is referred to as the *original* or *full* model throughout this dissertation.

- **Chapter 3: Characterization of applicable model order reduction methods**

This chapter presents an overview of commonly used model order reduction approaches without entitlement to completeness. Suitable approaches are identified and investigated on their applicability to the present mathematical model. The outcome of this applicability study forms the basis of the derived novel model order reduction approach.

- **Chapter 4: Derivation of the novel model order approach**

In this chapter a novel model order reduction approach is derived, based on the findings of Chapter 3. The approach takes into account the special nature of the mathematical model under consideration. It further allows to reduce both, the number of DOFs and the number of constraint equations, based on ideas of POD and principal component analysis. The approach is outlined in detail based on academical examples, allowing insight into the approaches nature.

- **Chapter 5: Application of the novel approach to large scale multi-body systems**

The novel model order reduction approach is tested based on large-size numerical examples, pointing out the approaches potential and capabilities.

- **Chapter 6: Application of the novel approach to parameter identification tasks in multibody system dynamics**

The novel model order reduction approach is applied to parameter identification tasks in multibody system dynamics, utilizing a reduced order adjoint system.

- **Chapter 7: Summary and conclusion**

Multibody System Dynamics

This chapter briefly reviews the set of DAEs, which characterizes the MBS formulation used in the software package FreeDyn. Such software bear much of the burden of modeling multibody systems. Still, they are not able to identify a minimum set of coordinates representation but introduce a redundant set of generalized coordinates. Body interactions (boundary conditions, joints, etc.) are represented by constraint equations. In combination with the equations of motion they set up the previously introduced redundant and nonlinear system of second order differential algebraic equations with differential index three. The chapter is outlined as follows:

First, the description of rotational degrees of freedom by a set of four Euler parameters is summarized. The equations of motion of a single rigid body are introduced next. As the MBS under consideration may consist of rigid and flexible bodies, the equations of motion of a single flexible body are reviewed thereafter. Following up, the unconstrained MBS in terms of several acting bodies is derived. The chapter concludes by introducing constraint equations which enable us to define the constrained multibody system.

2.1 Euler Parameter

For the kinematics of a rigid body, several formulations of a body's motion in space exist. While the description of the three translational degrees of freedom is rather facile, describing body rotations is more complex.

In order to avoid a singular Jacobian matrix, the MBS formulation considered in FreeDyn utilizes four rotational coordinates to this end. These four coordinates are called Euler parameters or Quaternions, cf. [27, 81]. They basically describe

a rotation in 3D space by a unit vector $\mathbf{u} \in \mathbb{R}^3$, representing the axis of rotation, and by the angle of rotation Φ around this vector. As depicted in Fig. 2.1, the

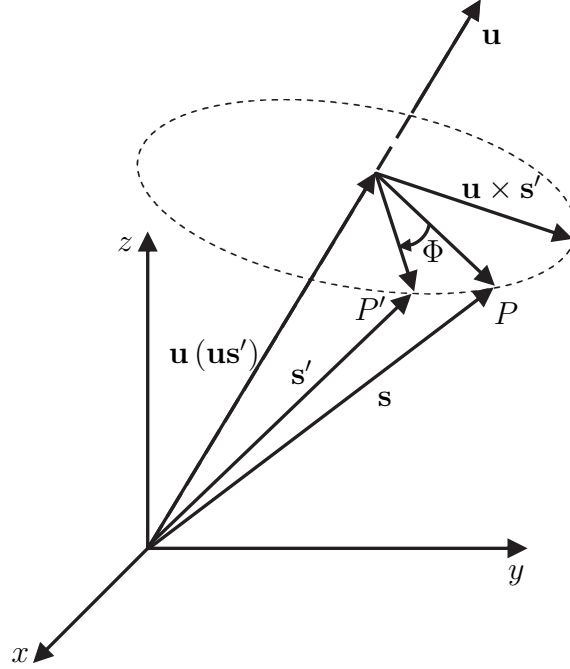


Figure 2.1: Vector diagram for derivation of rotation formula [81, p. 158]

rotation formula from an arbitrary point P to it's actual position P' is described by Nikravesh [81, pp. 158-159] as

$$\mathbf{s} = \mathbf{s}' \cos \Phi + \mathbf{u} (\mathbf{u} \cdot \mathbf{s}') (1 - \cos \Phi) + \mathbf{u} \times \mathbf{s}' \sin \Phi. \quad (2.1)$$

By using the trigonometric relations

$$1 - \cos \Phi = 2 \sin^2 \frac{\Phi}{2} \text{ and} \quad (2.2)$$

$$\sin \Phi = 2 \sin \frac{\Phi}{2} \cos \frac{\Phi}{2}, \quad (2.3)$$

the rotation formula in Eq. (2.1) can be re-expressed. In terms of the four Euler parameters e_0, e_1, e_2, e_3 it reads

$$\mathbf{s} = (2e_0^2 - 1) \mathbf{s}' + 2e_1 (\mathbf{e} \cdot \mathbf{s}') + 2e_0 \mathbf{e} \times \mathbf{s}', \quad (2.4)$$

with

$$\mathbf{e} = [e_1, e_2, e_3]^\top = \mathbf{u} \sin \frac{\Phi}{2}, \quad (2.5)$$

and

$$e_0 = \cos \frac{\Phi}{2}. \quad (2.6)$$

In matrix notation the rotation formula (2.4) reduces to

$$\mathbf{s} = \mathbf{B}\mathbf{s}', \quad (2.7)$$

with the rotation matrix

$$\mathbf{B} = \begin{bmatrix} e_0^2 + e_1^2 - e_2^2 - e_3^2 & 2e_1e_2 - 2e_0e_3 & 2e_1e_3 + 2e_0e_2 \\ 2e_1e_2 + 2e_0e_3 & e_0^2 + e_2^2 - e_3^2 - e_1^2 & 2e_2e_3 - 2e_0e_1 \\ 2e_1e_3 - 2e_0e_2 & 2e_2e_3 + 2e_0e_1 & e_0^2 + e_3^2 - e_1^2 - e_2^2 \end{bmatrix}. \quad (2.8)$$

Where the constraint

$$e_0^2 + e_1^2 + e_2^2 + e_3^2 = 1 \quad (2.9)$$

must be satisfied. The Euler parameter constraint is needed to overcome the issue of non-independent rotational coordinates. Each single body of the MBS introduces such a constraint, which will be denoted as the "inner" constraint throughout this work.

Finally, the matrix

$$\mathbf{G} = 2 \begin{bmatrix} -e_1 & e_0 & e_3 & -e_2 \\ -e_2 & -e_3 & e_0 & e_1 \\ -e_3 & e_2 & -e_1 & e_0 \end{bmatrix} \in \mathbb{R}^{3 \times 4} \quad (2.10)$$

maps the vector of generalized rotational velocities $\dot{\mathbf{q}}^r$ to the angular velocity vector [81]

$$\boldsymbol{\Omega} = \mathbf{G}\dot{\mathbf{q}}^r. \quad (2.11)$$

Therein, $\dot{\mathbf{q}}^r$ is the time derivative of the vector of rotational coordinates $\mathbf{q}^r = [e_0, e_1, e_2, e_3]^\top$. Concluding, Euler parameters not only allow to overcome issues arising from singular system configurations. They also enable efficient numerical simulations as no trigonometric functions must be evaluated to describe \mathbf{B} .

2.2 Equations of Motion of an Unconstrained Rigid Body

As indicated by its name, a multibody system consists of several bodies, which are somehow interacting with each other and/or the ground. We start off by reviewing the motion of a single unconstrained rigid body in 3D space. This section details its equations of motion (EoM) due to the Euler parameter description, following [92]. Later on in this chapter we will combine several of such rigid bodies into a multibody system. According to Fig. 2.2 the position of each material point of a

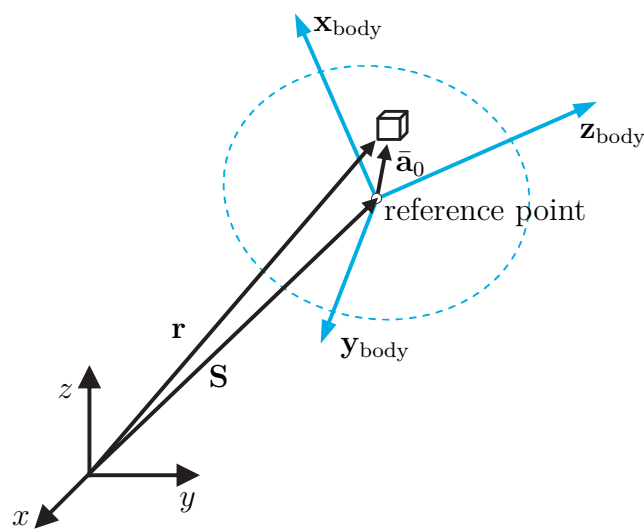


Figure 2.2: Definition of a body fixed coordinate system

rigid body, with respect to the body's reference point, is given by

$$\mathbf{r} = \mathbf{S} + \mathbf{B}\bar{\mathbf{a}}_0. \quad (2.12)$$

Quantities described in the body fixed coordinate system are denoted with an overbar. The vector $\bar{\mathbf{a}}_0$ represents the position vector of a material point with respect to the bodies reference point, which is typically the Center of Gravity (CoG). Further, \mathbf{S} is the position vector from the global time-invariant origin in the global coordinate system to the body origin in the body fixed coordinate system. Time dependencies will be omitted due to better readability. The orientation of the body fixed coordinate system is represented by the unit vectors \mathbf{x}_{body} , \mathbf{y}_{body} , \mathbf{z}_{body} , which are combined in the global rotation matrix \mathbf{B} in terms of Euler parameters.

The vector of seven generalized coordinates of a rigid body reads

$$\mathbf{q} = [\mathbf{q}^t, \mathbf{q}^r]^\top, \quad (2.13)$$

with $\mathbf{q}^t \in \mathbb{R}^3$ as the vector of translational coordinates and $\mathbf{q}^r \in \mathbb{R}^3$ (or $\mathbf{q}^r \in \mathbb{R}^4$ in the case of Euler parameters) representing the vector of rotational coordinates. In the general, unconstrained case, the equations of motion of a single rigid body read $\mathbf{M}\ddot{\mathbf{q}} = \mathbf{Q}$ or

$$\begin{bmatrix} m\mathbf{I} & \mathbf{0} \\ \mathbf{0} & \mathbf{G}^\top \mathbf{J} \mathbf{G} \end{bmatrix} \begin{pmatrix} \ddot{\mathbf{q}}^t \\ \ddot{\mathbf{q}}^r \end{pmatrix} = \sum_{j=1}^{n_{\text{forces}}} \begin{pmatrix} \mathbf{f}_j \\ \hat{\mathbf{a}}_{Fj} \mathbf{B}^\top \mathbf{f}_j \end{pmatrix} + \begin{pmatrix} \mathbf{0} \\ \frac{1}{2} \mathbf{G} \dot{\mathbf{G}}^\top \mathbf{J} \dot{\mathbf{G}} \mathbf{q}^r \end{pmatrix} \quad (2.14)$$

The body mass matrix of the i -th rigid body is defined as

$$\mathbf{M} = \begin{bmatrix} \mathbf{M}_{tt} & \mathbf{0} \\ \mathbf{0} & \mathbf{M}_{rr} \end{bmatrix} = \begin{bmatrix} m\mathbf{I} & \mathbf{0} \\ \mathbf{0} & \mathbf{G}^\top \mathbf{J} \mathbf{G} \end{bmatrix}. \quad (2.15)$$

Here, m holds the body mass and $\mathbf{J} \in \mathbb{R}^{3 \times 3}$ is the body inertia tensor

$$\mathbf{J} = \int_m \hat{\mathbf{a}}_0^\top \hat{\mathbf{a}}_0 \, dm. \quad (2.16)$$

Therein, the skew symmetric matrix

$$\hat{\mathbf{a}}_0 = \begin{bmatrix} 0 & -Z & Y \\ Z & 0 & -X \\ -Y & X & 0 \end{bmatrix} \quad (2.17)$$

represents the cross product $\bar{\mathbf{a}}_0 \times ()$ in terms of a matrix product. The body inertia tensor is mapped to the angular velocity vector by the matrix \mathbf{G} . Note the use of the rotation matrix $\mathbf{B} \in \mathbb{R}^{3 \times 3}$, as introduced in Sec. 2.1.

A rigid body is, in any case, subject to gyroscopic, centrifugal and Coriolis forces, and further perhaps to applied, external forces. These forces are collected in the force vector

$$\begin{aligned} \mathbf{Q} = \begin{bmatrix} \mathbf{Q}^t \\ \mathbf{Q}^r \end{bmatrix} &= \mathbf{Q}_{\text{generalized}} + \mathbf{Q}_V \\ &= \underbrace{\sum_{j=1}^{n_{\text{forces}}} \begin{pmatrix} \mathbf{f}_j \\ \hat{\mathbf{a}}_{Fj} \mathbf{B}^\top \mathbf{f}_j \end{pmatrix}}_{\text{generalized force vector}} + \underbrace{\begin{pmatrix} \mathbf{0} \\ \frac{1}{2} \mathbf{G} \dot{\mathbf{G}}^\top \mathbf{J} \dot{\mathbf{G}} \mathbf{q}^r \end{pmatrix}}_{\text{quadratic velocity vector}}. \end{aligned} \quad (2.18)$$

It is subdivided into the vector of generalized forces, and into the vector of gyroscopic, centrifugal and Coriolis force terms. This vector is referred to as the quadratic velocity vector \mathbf{Q}_V . Therein, \mathbf{f}_j represents an external force in vector notation, and n_{forces} is the total number of external forces acting on the body. Further, $\hat{\mathbf{a}}_{Fj}$ denotes a skew symmetric matrix representing the force application point of the j -th force with respect to the body fixed coordinate system.

2.3 Equations of Motion of an Unconstrained Flexible Body

If the simulation of a body is expected to result in notable deformations, the rigid body formulation introduced before is insufficient. This section summarizes the EoM of a single unconstrained flexible body in 3D space, as presented in detail by Sherif and Nachbagauer [94].

Flexibility can be introduced to the EoM by describing the deformations of the body with respect to a floating reference frame (FRF). Investigating Fig. 2.3 the

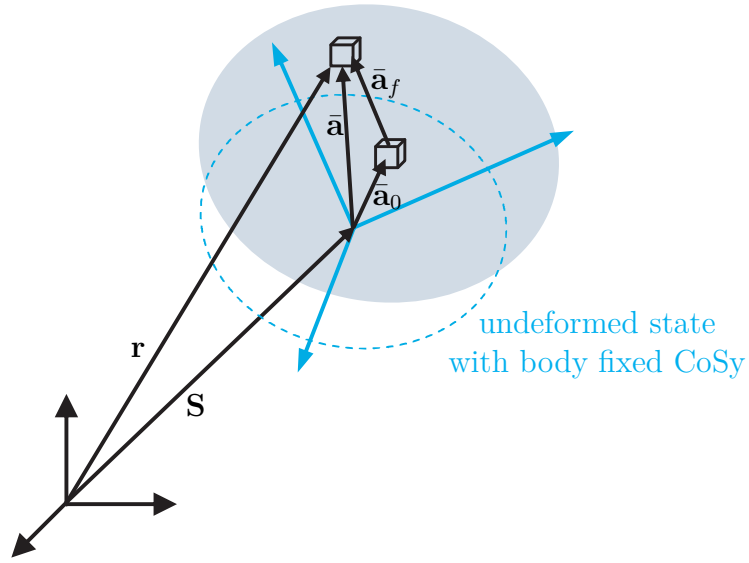


Figure 2.3: Floating reference frame description of a flexible body

absolute position vector of a material point of the flexible body, with respect to the global coordinate system is given by

$$\mathbf{r} = \mathbf{S} + \mathbf{B} \cdot \bar{\mathbf{a}} = \mathbf{S} + \mathbf{B} (\bar{\mathbf{a}}_0 + \bar{\mathbf{a}}_f). \quad (2.19)$$

Quantities described in the body fixed coordinate system are again denoted with an overbar. Vector $\bar{\mathbf{a}}$ represents the position vector of a material point. It is split into the undeformed part $\bar{\mathbf{a}}_0$, and into the deformable part $\bar{\mathbf{a}}_f$. \mathbf{S} is again the position vector from the global, time-invariant model-origin in the global coordinate system, to the body origin in the body fixed coordinate system. \mathbf{B} holds the orthogonal rotation matrix in terms of Euler parameters.

As we are dealing with a flexible body, the deformable part is expanded by the

Ritz approximation

$$\bar{\mathbf{a}}_f = \mathbf{\Theta} \mathbf{q}^f. \quad (2.20)$$

The matrix of shape functions $\mathbf{\Theta} \in \mathbb{R}^{7 \times n_{\text{flex}}}$ discretizes the displacement field of the flexible body. $\mathbf{\Theta}$ is typically derived by modal reduction approaches, and scaled by coefficients $\mathbf{q}^f \in \mathbb{R}^{n_{\text{flex}}}$, denoted as flexible coordinates.

Using this formulation, the vector of state variables reads

$$\mathbf{q} = [\mathbf{q}^t, \mathbf{q}^r, \mathbf{q}^f]^\top \in \mathbb{R}^{(7+n_{\text{flex}})}. \quad (2.21)$$

The rigid body coordinates \mathbf{q}^t and \mathbf{q}^r describe the position of the reference frame, and the flexible coordinates \mathbf{q}^f describe the deformation of the body.

The FRF formulation results in the mass matrix

$$\mathbf{M} = \begin{bmatrix} \mathbf{M}_{\text{tt}} & \mathbf{M}_{\text{tr}} & \mathbf{M}_{\text{tf}} \\ & \mathbf{M}_{\text{rr}} & \mathbf{M}_{\text{rf}} \\ \text{sym.} & & \mathbf{M}_{\text{ff}} \end{bmatrix} \in \mathbb{R}^{(7+n_{\text{flex}}) \times (7+n_{\text{flex}})}, \quad (2.22)$$

introducing the terms

$$\mathbf{M}_{\text{tt}} = m\mathbf{I}, \quad (2.23)$$

$$\mathbf{M}_{\text{rr}} = \mathbf{G}^\top \left[\int_m \hat{\mathbf{a}}^\top \hat{\mathbf{a}} \, dm \right] \mathbf{G}, \quad (2.24)$$

$$\mathbf{M}_{\text{ff}} = \int_m \mathbf{\Theta}^\top \mathbf{\Theta} \, dm, \quad (2.25)$$

$$\mathbf{M}_{\text{tr}} = -\mathbf{B} \left[\int_m \hat{\mathbf{a}} \, dm \right] \mathbf{G}, \quad (2.26)$$

$$\mathbf{M}_{\text{tf}} = \mathbf{B} \int_m \mathbf{\Theta} \, dm, \quad (2.27)$$

$$\mathbf{M}_{\text{rf}} = -\mathbf{G}^\top \int_m \hat{\mathbf{a}}^\top \mathbf{\Theta} \, dm. \quad (2.28)$$

A detailed derivation and explanation of the single submatrices is presented in [94].

As for the mass matrix, also the force vector

$$\mathbf{Q} = \mathbf{Q}_{\text{generalized}} + \mathbf{Q}_V = \begin{bmatrix} \mathbf{Q}^t \\ \mathbf{Q}^r \\ \mathbf{Q}^f \end{bmatrix} \in \mathbb{R}^{(7+n_{\text{flex}})} \quad (2.29)$$

is extended by a subvector of generalized forces $\mathbf{Q}^f \in \mathbb{R}^{n_{\text{flex}}}$. It comprises stiffness and damping forces of the flex body, as well as possibly acting external forces. Further, the quadratic velocity vector

$$\mathbf{Q}_V = [\mathbf{Q}_V^t, \mathbf{Q}_V^r, \mathbf{Q}_V^f]^\top \quad (2.30)$$

is extended by

$$\mathbf{Q}_V^t = -\dot{\mathbf{M}}_{tr}\dot{\mathbf{q}}^r - \dot{\mathbf{M}}_{tf}\dot{\mathbf{q}}^f \quad (2.31)$$

$$\mathbf{Q}_V^r = -(\dot{\mathbf{M}}_{tr})^\top \dot{\mathbf{S}} - \dot{\mathbf{M}}_{rr}\dot{\mathbf{q}}^r - \dot{\mathbf{M}}_{rf}\dot{\mathbf{q}}^f + \left(\frac{\partial T}{\partial \mathbf{q}^r}\right)^\top \quad (2.32)$$

$$\mathbf{Q}_V^f = -(\dot{\mathbf{M}}_{tf})^\top \dot{\mathbf{S}} - (\dot{\mathbf{M}}_{rf})^\top \dot{\mathbf{q}}^r - \dot{\mathbf{M}}_{ff}\dot{\mathbf{q}}^f + \left(\frac{\partial T}{\partial \mathbf{q}^f}\right)^\top. \quad (2.33)$$

Therein, T holds the body's kinetic energy. For a detailed review on the single terms, the interested reader is again referred to [94]. The mass and force vector of a flexible body are rather complex. Thus, special FRF formulations, like the combination of a Buckens frame together with the free-free mode description cf. [93], are commonly used. By using a free-free mode formulation the modes are mass-orthogonal to the translational and to the rotational rigid modes. They are further mass-orthogonal to each other. If the origin of the body coordinate system is congruent with the body's undeformed CoG, the mass matrix of a single flexible body simplifies into

$$\mathbf{M} = \begin{bmatrix} \mathbf{M}_{tt} & \mathbf{0} & \mathbf{0} \\ & \mathbf{M}_{rr} & \mathbf{M}_{rf} \\ sym. & & \mathbf{M}_{ff} \end{bmatrix}. \quad (2.34)$$

The related quadratic velocity vector reduces to

$$\mathbf{Q}_V = [\mathbf{0}, \mathbf{Q}_V^r, \mathbf{Q}_V^f]^\top, \quad (2.35)$$

which can be further simplified to

$$\mathbf{Q}_V^r = -\dot{\mathbf{M}}_{rr}\dot{\mathbf{q}}^r - \dot{\mathbf{M}}_{rf}\dot{\mathbf{q}}^f + \left(\frac{\partial T}{\partial \mathbf{q}^r}\right)^\top \quad (2.36)$$

$$\mathbf{Q}_V^f = -(\dot{\mathbf{M}}_{rf})^\top \dot{\mathbf{q}}^r - \dot{\mathbf{M}}_{ff}\dot{\mathbf{q}}^f + \left(\frac{\partial T}{\partial \mathbf{q}^f}\right)^\top. \quad (2.37)$$

2.4 Unconstrained Multibody Systems

Next, we set up the unconstrained multibody system

$$\mathbf{M}\ddot{\mathbf{q}} = \mathbf{Q}. \quad (2.38)$$

In the present context the term "unconstrained" indicates, that the bodies interact with each other via applied forces. There are no constraint equations introduced

yet.

In Eq. (2.38), $\mathbf{q} \in \mathbb{R}^n$ holds the vector of the n generalized coordinates in the global coordinate system. It is arranged in the body wise manner

$$\mathbf{q} = [\mathbf{q}_1, \mathbf{q}_2, \dots, \mathbf{q}_b]^\top. \quad (2.39)$$

\mathbf{q}_i denotes the coordinate sub vector related to the i -th body, and $b = b_{\text{rigid}} + b_{\text{flex}}$ holds the number of rigid and flexible bodies. As Euler parameters are in need of the already introduced internal Euler constraints, such a formulation is not suitable here. Therefore, we switch to a Euler angle formulation in this section. The number of generalized coordinates is $n = 6 \cdot b$ if $b_{\text{flex}} = 0$, and $n = 6 \cdot b + n_{\text{flex}}$ if $b_{\text{flex}} > 0$.

$\mathbf{Q}(\mathbf{q}, \dot{\mathbf{q}}) \in \mathbb{R}^n$ holds the vector of generalized and gyroscopic forces, which is arranged similarly to \mathbf{q} . Generalized forces may act between a body and ground, or between two bodies. $\mathbf{M}(\mathbf{q}) \in \mathbb{R}^{n \times n}$ represents the block-diagonal global mass matrix

$$\mathbf{M}(\mathbf{q}) = \begin{bmatrix} \mathbf{M}_1(\mathbf{q}) & 0 & & & \\ 0 & \mathbf{M}_2(\mathbf{q}) & & & \\ & & \ddots & & \\ & & & 0 & \\ & & & 0 & \mathbf{M}_b(\mathbf{q}) \end{bmatrix}. \quad (2.40)$$

Therein, \mathbf{M}_i again denotes the sub mass matrix related to the i -th body.

Depending on the rigid or flexible nature of each body, the terms \mathbf{q}_i , \mathbf{M}_i and \mathbf{Q}_i are as introduced in sections 2.2 and 2.3.

In the literature, cf. [74], it is suggested to omit constraint equations by introducing very stiff force elements. Due to the use of such force elements, Eq. (2.38) represents the final set of equations of the MBS. It consists of ordinary differential equations only.

2.5 Constrained Multibody Systems

The final section of this chapter introduces the redundantly formulated constrained MBS, as implemented in the herein utilized simulation software FreeDyn.

The redundant formulation under consideration is characterized by constraint equations, which represent joints, body interactions and inner constraints. Possible constraint equations are classified into holonomic and non-holonomic constraints. Holonomic constraint equations are typically of the form

$$\mathbf{C} = \mathbf{C}(\mathbf{q}, t) = \mathbf{0}. \quad (2.41)$$

Non-holonomic constraints involve the derivative of the generalized coordinates, and typically read

$$\mathbf{C} = \mathbf{C}(\mathbf{q}, \dot{\mathbf{q}}, t) = \mathbf{0}. \quad (2.42)$$

Note that this characterization does not necessarily hold in general. If the time derivative of the constraint equation is eliminable through integration, the resulting constraint equation is again holonomic.

Further, the class of holonomic constraints is subdivided into scleronomic and rheonomic constraints, depending on their explicit time-dependence. For the MBS under consideration, only scleronomic constraints are investigated, which are purely algebraic equations.

Now, the n physical coordinates \mathbf{q} are subject to m scleronomic constraint equations

$$\mathbf{C}(\mathbf{q}) = [C_1(\mathbf{q}), C_2(\mathbf{q}), \dots, C_m(\mathbf{q})]^\top = \mathbf{0}. \quad (2.43)$$

They represent joints (e.g. a hinge, a ball joint, etc.) between two bodies, between a single body and ground. The inner constraint of each body, due to the Euler parameter description, see Eq. (2.9), is another type of constraint. Note that $m < n$ must hold at any time as otherwise the MBS would be overconstrained. The impact of constraints on the EoM is accounted for by extending the equations of motion by generalized constraint forces. As it is shown in [92] the constraint forces are perpendicular to the constraint equations. Therefore, the direction of the j -th constraint C_j is denoted by

$$\mathbf{C}_{j,q} = \left[\frac{\partial C_j}{\partial q_1} \quad \frac{\partial C_j}{\partial q_2} \quad \dots \quad \frac{\partial C_j}{\partial q_n} \right]^\top. \quad (2.44)$$

The generalized constraint force related to C_j is obtained by multiplying the constraint force direction $\mathbf{C}_{j,q}$ with the generalized amplitude λ_j , called the Lagrangian multiplier. Note that λ_j is an additional unknown of the system and hence has to be calculated during simulation.

In order to account for all m constraint equations, the constraint Jacobian

$$\mathbf{C}_q^\top(\mathbf{q}) = \begin{bmatrix} \frac{\partial C_1(\mathbf{q})}{\partial q_1} & \dots & \frac{\partial C_m(\mathbf{q})}{\partial q_1} \\ \vdots & & \vdots \\ \frac{\partial C_1(\mathbf{q})}{\partial q_n} & \dots & \frac{\partial C_m(\mathbf{q})}{\partial q_n} \end{bmatrix} \in \mathbb{R}^{n \times m} \quad (2.45)$$

is introduced. Therein, the j -th column holds the direction of the generalized constraint force related to the j -th constraint equation. Accordingly, all m Lagrangian

multipliers are collected in the vector $\boldsymbol{\lambda} \in \mathbb{R}^m$, introducing m additional unknowns to the system.

By adding the constraint equations $\mathbf{C} = \mathbf{0}$ to the unconstrained MBS in Eq. (2.38) the redundant and nonlinear second order differential algebraic system

$$\begin{aligned} \mathbf{M}(\mathbf{q}) \ddot{\mathbf{q}} &= \mathbf{Q}(\mathbf{q}, \dot{\mathbf{q}}) - \mathbf{C}_q^T(\mathbf{q}) \boldsymbol{\lambda} \\ \mathbf{C}(\mathbf{q}) &= \mathbf{0} \end{aligned} \quad (2.46)$$

with differential index three arises. Note that Eq. (2.46) holds $n + m$ equations necessary to solve for the $n + m$ unknowns \mathbf{q} and $\boldsymbol{\lambda}$.

A FreeDyn specific issue is that constraint equations acting on a flexible body are of different structure than for a rigid body. In order not to define each type of constraint equation in terms of rigid and flexible bodies separately, FreeDyn introduces a rigid zero mass and inertia body (ZIB) to the MBS. ZIBs are used as coupling elements, which are glued to the interaction nodes of a flexible body, by a special flexible body fixed joint. The ZIB itself is a rigid body and the actual joint is then established between the ZIB and the joint's counterpart (a rigid body, another ZIB or the ground) by rigid body constraints.

Due to the use of these ZIBs a flexible body fix joint had to be derived only. Any other type of joint is described in terms of interacting rigid bodies.

Note that as the ZIB is of zero mass and zero inertia, it does not influence the behavior nor the energy of the MBS. Still, it adds a set of seven rigid coordinates to the vector of generalized coordinates \mathbf{q} . Further, each ZIB introduces a set of six external constraint equations due to the fix joint, and an inner constraint equation.

Concluding, each flexible body interaction adds seven rigid body coordinates and seven constraint equations to the MBS.

2.5.1 HHT solver algorithm

The resulting MBS model is solved utilizing a Hilber-Hughes-Taylor (HHT) solver algorithm, cf. [79]. The HHT method may be seen as an extension to the class of Newmark solvers, cf. [80]. It has been extended to the present nonlinear MBS formulation in [79], and is used as the standard solver algorithm in FreeDyn.

This section briefly summarizes the HHT solver algorithm, as implemented in FreeDyn [41]. It is used to compute the numerical MBS examples presented in this dissertation.

In order to solve the MBS system in Eqs. (2.46), Newmark integration formulas are used. They express \mathbf{q} and $\dot{\mathbf{q}}$ as a function of $\ddot{\mathbf{q}}$ at time t_{n+1} from the values at

t_n :

$$\mathbf{q}_{n+1} = \mathbf{q}_n + h\dot{\mathbf{q}}_n + \frac{h^2}{2}[(1 - 2\beta)\ddot{\mathbf{q}}_n + 2\beta\ddot{\mathbf{q}}_{n+1}] \quad (2.47)$$

$$\dot{\mathbf{q}}_{n+1} = \dot{\mathbf{q}}_n + h[(1 - \gamma)\ddot{\mathbf{q}}_n + \gamma\ddot{\mathbf{q}}_{n+1}]. \quad (2.48)$$

Therein, the parameters

$$\beta = \frac{(1 - \alpha)^2}{4} \quad \gamma = \frac{1 - 2\alpha}{2}, \quad (2.49)$$

are determined from the parameter $\alpha \in [-\frac{1}{3}, 0]$. Furthermore, h is the (variable) time step size.

The equations of motion are discretized such that

$$(\mathbf{M}\ddot{\mathbf{q}})_{n+1} + (1 + \alpha)(\mathbf{C}_q^\top \boldsymbol{\lambda} - \mathbf{Q})_{n+1} - \alpha(\mathbf{C}_q^\top \boldsymbol{\lambda} - \mathbf{Q})_n = \mathbf{0}. \quad (2.50)$$

Introducing the scaling factor $\frac{1}{1+\alpha}$, which is due to implementation reasons, the discretized system reads

$$\begin{aligned} \frac{1}{1 + \alpha}(\mathbf{M}\ddot{\mathbf{q}})_{n+1} + (\mathbf{C}_q^\top \boldsymbol{\lambda} - \mathbf{Q})_{n+1} - \frac{\alpha}{1 + \alpha}(\mathbf{C}_q^\top \boldsymbol{\lambda} - \mathbf{Q})_n &= \mathbf{0} =: e_1 \\ \mathbf{C}(\mathbf{q}_{n+1}, t_{n+1}) &= \mathbf{0} =: e_2. \end{aligned} \quad (2.51)$$

By utilizing Newton's method, the correction terms $\Delta\ddot{\mathbf{q}}_{n+1}$ and $\Delta\boldsymbol{\lambda}_{n+1}$ are computed from

$$\underbrace{\begin{bmatrix} \mathbf{M}_{\text{ext}} & \mathbf{C}_q^\top \\ \mathbf{C}_q & \mathbf{0} \end{bmatrix}}_{\text{Jacobian } \mathbf{J}} \begin{bmatrix} \Delta\ddot{\mathbf{q}}_{n+1} \\ \Delta\boldsymbol{\lambda}_{n+1} \end{bmatrix}^{(k)} = \begin{bmatrix} -e_1 \\ -e_2 \end{bmatrix}^{(k)}. \quad (2.52)$$

Where $\mathbf{M}_{\text{ext}} = \frac{1}{1+\alpha}\mathbf{M} + \left(\frac{1}{1+\alpha}(\mathbf{M}\ddot{\mathbf{q}})_q + (\mathbf{C}_q^\top \boldsymbol{\lambda})_q - \mathbf{Q}_q\right)\beta h^2 - \mathbf{Q}_{\dot{\mathbf{q}}}h\gamma$.

Including the corrections of the Jacobian matrix, the system is solved and the numerical solution is improved after each iteration by

$$\begin{aligned} \ddot{\mathbf{q}}_{n+1}^{(k)} &= \ddot{\mathbf{q}}_{n+1}^{(k-1)} + \Delta\ddot{\mathbf{q}}_{n+1}^{(k)}, \\ \boldsymbol{\lambda}_{n+1}^{(k)} &= \boldsymbol{\lambda}_{n+1}^{(k-1)} + \Delta\boldsymbol{\lambda}_{n+1}^{(k)}. \end{aligned} \quad (2.53)$$

Model Order Reduction

This chapter introduces typical projection based model order reduction methods. It further investigates their applicability to the redundantly formulated multibody system, introduced in Chapter 2. The chapter is outlined as follows:

After an introduction to the fundamental idea of model order reduction, projection based model order reduction approaches are reviewed first. Second, commonly used projection based model order reduction subspace generation methods are summarized. They can be roughly divided into a priori and a posteriori methods depending on whether the method is in need of collected simulation data or not. Finally, the presented methods are investigated on their applicability to the second order, nonlinear, index three DAE system, we are dealing with.

3.1 The Idea of Model Order Reduction

Numerical modeling techniques often result in a large number of mathematical equations. The intention of model order reduction is to significantly reduce the number of equations, and the simulation time. The model order reduction method further has to ensure, that the approximation error in the simulation results is small. From a mathematical point of view, the aim of model order reduction is to approximate a set of differential equations

$$\dot{\mathbf{x}} = \mathbf{f}(\mathbf{x}), \quad (3.1)$$

with $\mathbf{x} \in \mathbb{R}^n$ unknowns, by some smaller set

$$\dot{\mathbf{x}}_r = \mathbf{g}(\mathbf{x}_r). \quad (3.2)$$

Here, $\mathbf{x}_r \in \mathbb{R}^r$ denotes the new unknowns. If we set

$$\mathbf{x} = \mathbf{h}(\mathbf{x}_r) + e \approx \mathbf{h}(\mathbf{x}_r), \quad (3.3)$$

with $r \ll n$ and e as approximation error, the task of model order reduction approach is to find an efficient representation of $\mathbf{h}(\mathbf{x}_r)$.

Within this dissertation, the focus is on projection based model order reduction approaches. They define $\mathbf{h}(\mathbf{x}_r)$ as a projection to a flat or curvilinear subspace. Several approaches will be considered in the subsequent sections of this chapter. Nevertheless, the interested reader is referred to the books by Antoulas [6], Qu [84] and Schilders et al. [89] for a vast review on this extensive topic.

3.2 Projection Based Model Order Reduction

In the field of (nonlinear) dynamical systems, a computationally efficient model is typically given by the system's minimal set of coordinate representation. This description is usually not derivable in a straightforward manner for complex systems. Therefore, the actually available redundant description of the underlying dynamical system is enhanced by projection based model order reduction approaches. The fundamentals of these approaches are reviewed by investigating the linear and time-invariant system

$$\begin{aligned} \dot{\mathbf{x}}(t) &= \mathbf{A}\mathbf{x}(t) + \mathbf{B}\mathbf{u}(t) \\ \mathbf{y}(t) &= \mathbf{D}\mathbf{x}(t), \end{aligned} \quad (3.4)$$

subject to initial conditions $\mathbf{x}(0) = \mathbf{x}_0$. Here, $\mathbf{x} \in \mathbb{R}^n$ is the vector of unknown state variables, and $\mathbf{A} \in \mathbb{R}^{n \times n}$ represents the system matrix. $\mathbf{B} \in \mathbb{R}^{n \times u}$ maps the vector of input signals $\mathbf{u} \in \mathbb{R}^u$ to the particular state. Further, $\mathbf{D} \in \mathbb{R}^{y \times n}$ maps the state vector to the vector of system outputs $\mathbf{y} \in \mathbb{R}^y$.

Recalling Eq. (3.3), model order reduction is based on a sufficient representation of the term $\mathbf{h}(\mathbf{x}_r)$. To this end the Galerkin transformation

$$\mathbf{x} = \mathbf{V}\mathbf{x}_r + \mathbf{U}\mathbf{x}_{n-r}, \quad (3.5)$$

is considered. Note that this is simply a transformation of the original state vector. In a mathematical sense we try to construct an orthogonal subspace \mathcal{Y}_1 of the original space \mathcal{H} , which is typically not described by a set of orthogonal basis vectors. \mathcal{Y}_1 is further split into \mathcal{Z}_r and \mathcal{Z}_{n-r} , which are spanned by the orthogonal bases $\mathbf{V} \in \mathbb{R}^{n \times r}$ and $\mathbf{U} \in \mathbb{R}^{n \times (n-r)}$. This approach is also-called *flat* projection, as \mathbf{V} and \mathbf{U} are time-invariant and hence

$$\frac{d}{dt}\mathbf{V} = \mathbf{0} \text{ and } \frac{d}{dt}\mathbf{U} = \mathbf{0}. \quad (3.6)$$

The related variables are $\mathbf{x}_r \in \mathbb{R}^r$ and $\mathbf{x}_{n-r} \in \mathbb{R}^{n-r}$.

3.2.1 Flat Projection

The main task of a projection based model order reduction method is to generate the reduction subspace. Therefore, an introduction to the most frequently used subspace generation methods is presented in the upcoming sections. The flat (Petrov-)Galerkin projection neglects the second term of Eq. (3.5). Hence, the transformation is of the form

$$\mathbf{x} \approx \mathbf{h}(\mathbf{x}_r) = \mathbf{V}\mathbf{x}_r \quad (3.7)$$

with $\mathbf{V} \in \mathbb{R}^{n \times r}$ and $\mathbf{x}_r \in \mathbb{R}^r$, $r \ll n$.

Due to neglecting the subspace spanned by \mathbf{U} , the method loses its exactness. It turns into an approximation on the subspace \mathcal{Z}_r . The system therefore reduces to

$$\begin{aligned} \mathbf{V}\dot{\mathbf{x}}_r &= \mathbf{A}\mathbf{V}\mathbf{x}_r + \mathbf{B}\mathbf{u}(t) + \mathbf{e} \\ \mathbf{y}(t) &= \mathbf{D}\mathbf{V}\mathbf{x}_r, \end{aligned} \quad (3.8)$$

including the residual term \mathbf{e} .

By choosing a suitable *test-subspace* \mathcal{Y}_2 on which we force $\mathbf{e} = \mathbf{0}$, we get an orthogonal basis $\mathbf{W} \in \mathbb{R}^{n \times r}$ of \mathcal{Y}_2 , with $\mathbf{W}^\top \mathbf{e} = \mathbf{0}$. This method with $\mathbf{V} \neq \mathbf{W}$ is called flat Petrov-Galerkin projection and the related reduced order model reads

$$\begin{aligned} \mathbf{W}^\top \mathbf{V}\dot{\mathbf{x}}_r &= \mathbf{W}^\top \mathbf{A}\mathbf{V}\mathbf{x}_r + \mathbf{W}^\top \mathbf{B}\mathbf{u} \\ \mathbf{y} &= \mathbf{D}\mathbf{V}\mathbf{x}_r. \end{aligned} \quad (3.9)$$

In the case of using \mathcal{Y}_1 as the test-subspace ($\mathbf{V} = \mathbf{W}$), the method is called flat Galerkin projection, and the related reduced order model reads

$$\begin{aligned} \mathbf{V}^\top \mathbf{V}\dot{\mathbf{x}}_r &= \mathbf{V}^\top \mathbf{A}\mathbf{V}\mathbf{x}_r + \mathbf{V}^\top \mathbf{B}\mathbf{u} \\ \mathbf{y} &= \mathbf{D}\mathbf{V}\mathbf{x}_r. \end{aligned} \quad (3.10)$$

A geometric interpretation of the flat (Petrov-)Galerkin projection in a 3D space is shown in Fig. 3.1. The flat projection is the most commonly used projective model order reduction method as it is applicable in a very straight-forward manner.

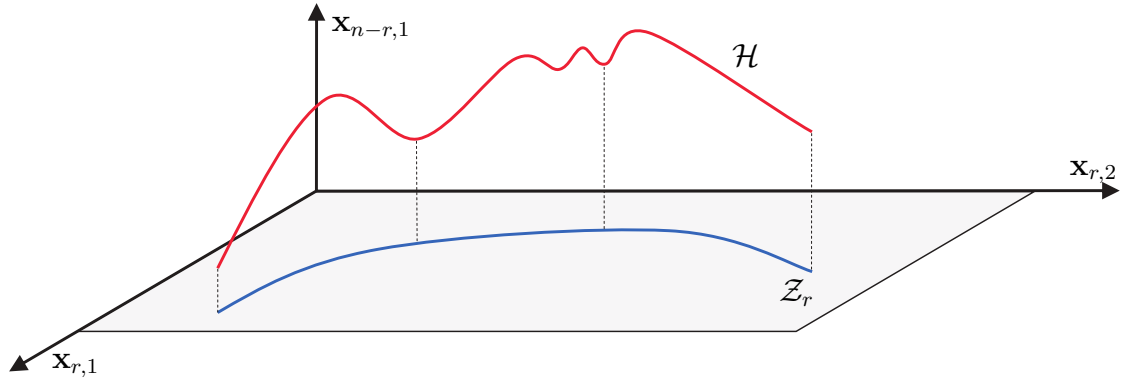


Figure 3.1: Geometric interpretation of the linear Galerkin projection in \mathbb{R}^3 following [71]

3.3 A Priori Model Order Reduction

A priori methods mostly predict the reduced order model utilizing the system's mass, stiffness and damping matrices, as well as the vector of applied forces. This class of approaches is typically applied to (nonlinear) systems of ODEs, like dynamical FEM models. In order to characterize these methods we introduce the linear system

$$\begin{aligned} \mathbf{M}\ddot{\mathbf{x}} + \mathbf{K}\mathbf{x} &= \mathbf{B}\mathbf{u} \\ \mathbf{y} &= \mathbf{D}\mathbf{x}. \end{aligned} \quad (3.11)$$

$\mathbf{x} \in \mathbb{R}^n$ is the vector of DOFs and $\mathbf{M} \in \mathbb{R}^{n \times n}$ is the time-invariant mass matrix. $\mathbf{K} \in \mathbb{R}^{n \times n}$ holds the time-invariant stiffness matrix, and the matrix $\mathbf{B} \in \mathbb{R}^{n \times u}$ maps the load vector $\mathbf{u} \in \mathbb{R}^u$ to the corresponding DOFs. Further, matrix $\mathbf{D} \in \mathbb{R}^{y \times n}$ maps the DOFs to the vector of outputs $\mathbf{y} \in \mathbb{R}^y$. The system is considered symmetric with $\mathbf{M} = \mathbf{M}^\top$ and $\mathbf{K} = \mathbf{K}^\top$.

We now apply the flat (Petrov-)Galerkin projection to generate the corresponding reduced order models. The Petrov-Galerkin projected reduced order model reads

$$\begin{aligned} \mathbf{W}^\top \mathbf{M} \mathbf{V} \ddot{\mathbf{x}}_r + \mathbf{W}^\top \mathbf{K} \mathbf{V} \mathbf{x}_r &= \mathbf{W}^\top \mathbf{B} \mathbf{u} \\ \mathbf{y} &= \mathbf{D} \mathbf{V} \mathbf{x}_r, \end{aligned} \quad (3.12)$$

and the Galerkin projected reduced order model evaluates to

$$\begin{aligned} \mathbf{V}^\top \mathbf{M} \mathbf{V} \ddot{\mathbf{x}}_r + \mathbf{V}^\top \mathbf{K} \mathbf{V} \mathbf{x}_r &= \mathbf{V}^\top \mathbf{B} \mathbf{u} \\ \mathbf{y} &= \mathbf{D} \mathbf{V} \mathbf{x}_r, \end{aligned} \quad (3.13)$$

with $\mathbf{V} \in \mathbb{R}^{n \times r}$, $\mathbf{W} \in \mathbb{R}^{n \times r}$, $\mathbf{x}_r \in \mathbb{R}^r$ and $r \ll n$. The three most commonly used projection approaches *Component Mode Synthesis* (CMS), *Balanced Truncation* (BT) and *Moment Matching* (MM) will be introduced in this section. CMS

represents the class of modal model order reduction approaches. The according reduced order model is built of vibration modes and static displacement fields of the original system. BT and MM originate from control theory and are based on rather mathematical considerations. While BT is based on the Gramian controllability and observability matrices of the original system, MM tries to approximate the system's transfer function by a set of Krylov vectors. For a comprehensive comparison of this class of methods, see [32, 114].

Further, the curvilinear *Global Modal Parametrization* (GMP) approach, which may be seen as a kind of a-priori approach, is reviewed.

3.3.1 Component Mode Synthesis

Component mode synthesis describes a class of modal model order reduction methods which utilize the Eigenvalue decompositions (EVD) and static displacement fields of the original model. This method is typically used to approximate the flexible behavior of finite element bodies for multibody system simulation. It may be assigned to the class of Galerkin projections, as $\mathbf{W} = \mathbf{V}$. A commonly used CMS method, also known as the Craig-Bampton method [24], is presented here.

We assume a linear FEM body, subject to constraints and external forces. The according linear system is depicted in Eq. (3.11). This type of model order reduction is based on a combination of statical condensation, called Guyan reduction, and modal reduction. To this end, the vector of FEM degrees-of-freedom is sorted, such that

$$\mathbf{x} = \begin{bmatrix} \mathbf{x}_m, \mathbf{x}_s \end{bmatrix}^T. \quad (3.14)$$

Therein, $\mathbf{x}_m \in \mathbb{R}^{n_m}$ are n_m master coordinates, and $\mathbf{x}_s \in \mathbb{R}^{n_s}$ are n_s slave coordinates, with $n = n_m + n_s$. We want to describe the deformation of the FEM body by the displacements of the master coordinates. The displacements of the slave coordinates are then expressed by the master coordinates. Due to this classification of coordinates, the linear system in Eq. (3.11) is rearranged into

$$\begin{bmatrix} \mathbf{M}_{m,m} & \mathbf{M}_{m,s} \\ \mathbf{M}_{s,m} & \mathbf{M}_{s,s} \end{bmatrix} \begin{bmatrix} \ddot{\mathbf{x}}_m \\ \ddot{\mathbf{x}}_s \end{bmatrix} + \begin{bmatrix} \mathbf{K}_{m,m} & \mathbf{K}_{m,s} \\ \mathbf{K}_{s,m} & \mathbf{K}_{s,s} \end{bmatrix} \begin{bmatrix} \mathbf{x}_m \\ \mathbf{x}_s \end{bmatrix} = \begin{bmatrix} \mathbf{F}_m \\ \mathbf{F}_s \end{bmatrix}. \quad (3.15)$$

Therein, $\mathbf{F} = [\mathbf{F}_m, \mathbf{F}_s]^T$ is the vector of applied forces. In order to generate the reduced order model, a combination of static modes and vibration modes is used: First, the vector of slave coordinates \mathbf{x}_s is processed by a Guyan reduction. It estimates the displacements of the slave coordinates by considering the static deformation of the master coordinates. Unit loads are applied to each master coordinate separately while, at the same time, all other master coordinates are fixed.

The according static problem reads

$$\begin{bmatrix} \mathbf{K}_{m,m} & \mathbf{K}_{m,s} \\ \mathbf{K}_{s,m} & \mathbf{K}_{s,s} \end{bmatrix} \begin{bmatrix} \mathbf{x}_m \\ \mathbf{x}_s \end{bmatrix} = \begin{bmatrix} \mathbf{F}_m \\ \mathbf{0} \end{bmatrix}. \quad (3.16)$$

The motion of the slave coordinates is then directly computed from

$$\begin{aligned} \mathbf{x}_s &= \mathbf{V}_{\text{stat}} \mathbf{x}_m \\ &= -\mathbf{K}_{s,s}^{-1} \mathbf{K}_{s,m} \mathbf{x}_m, \end{aligned} \quad (3.17)$$

and the full vector of coordinates is given by

$$\mathbf{x} = \begin{bmatrix} \mathbf{I}_{m,m} \\ \mathbf{V}_{\text{stat}} \end{bmatrix} \mathbf{x}_m = \begin{bmatrix} \mathbf{I}_{m,m} \\ -\mathbf{K}_{s,s}^{-1} \mathbf{K}_{s,m} \end{bmatrix} \mathbf{x}_m. \quad (3.18)$$

Second, Eigenvectors ϕ of the dynamical system are computed from the Eigenvalue decomposition

$$\mathbf{K}_{s,s} \phi = \lambda \mathbf{M}_{s,s} \phi, \quad (3.19)$$

where all master coordinates \mathbf{x}_m are locked. Each Eigenvector ϕ_i is related to the Eigenvalue λ_i explicitly. Furthermore, the Eigenvalues of the FEM body under consideration are directly related to the body's Eigenfrequencies by $\omega_i^2 = \lambda_i$. Hence, the number of vibration modes ϕ_i used to describe the dynamical behavior of the FEM body is due to a user-defined Eigenfrequency bound ω_{max} . All Eigenvectors ϕ_i up to ω_{max} are collected as column vectors in the vibration mode matrix \mathbf{V}_{vib} .

Finally, by combining the static modes and the vibration modes the Craig-Bampton model order reduction matrix reads

$$\mathbf{V} = \begin{bmatrix} \mathbf{I}_{m,m} & \mathbf{0} \\ \mathbf{V}_{\text{stat}} & \mathbf{V}_{\text{vib}} \end{bmatrix}. \quad (3.20)$$

The Galerkin projection is given by

$$\begin{bmatrix} \mathbf{x}_m \\ \mathbf{x}_s \end{bmatrix} \approx \begin{bmatrix} \mathbf{I}_{m,m} & \mathbf{0} \\ \mathbf{V}_{\text{stat}} & \mathbf{V}_{\text{vib}} \end{bmatrix} \begin{bmatrix} \mathbf{x}_m \\ \mathbf{q}_{\text{vib}} \end{bmatrix} = \mathbf{V} \mathbf{x}_r, \quad (3.21)$$

where \mathbf{q}_{vib} are modal coordinates, related to the vibration modes \mathbf{V}_{vib} and \mathbf{x}_r is the vector of $r = n_m + n_{\text{vib}}$ reduced coordinates.

During the last decades several improvements and variations of the above method have been proposed. For an extensive review on the method, the interested reader is referred to [24, 22, 23, 25, 114, 84] and references therein.

3.3.2 Moment Matching

Moment matching determines a reduced order model which approximates the system transfer function with sufficient accuracy. Thereby, not only the input/output behavior is approximated but also the complete time-history of the state variables in $\mathbf{x}(t)$. The method is of the group of flat Petrov-Galerkin projection, as in general $\mathbf{V} \neq \mathbf{W}$. It is briefly summarized, following [64, 62]:

Let us assume the first order ODE system

$$\begin{aligned} \mathbf{E}\dot{\mathbf{x}} &= \mathbf{A}\mathbf{x} + \mathbf{B}\mathbf{u} \\ \mathbf{y} &= \mathbf{D}\mathbf{x}. \end{aligned} \quad (3.22)$$

The Laplace transformed transfer function of the first order system reads

$$\mathbf{H}(s) = \frac{\mathbf{Y}(s)}{\mathbf{U}(s)} = \mathbf{D}(s\mathbf{E} - \mathbf{A})^{-1}\mathbf{B}, \quad (3.23)$$

with s holding the Laplace variable. The transfer function is approximated by the power series

$$\mathbf{H}(s) = \sum_{j=0}^{\infty} \mathbf{T}_j^{s_0} (s_0 - s)^j, \quad (3.24)$$

around an expansion point $s_0 \in \mathbb{C}$, which must not be a pole of the the transfer function. Here, $\mathbf{T}_j^{s_0}$ represents the j -th moment

$$\mathbf{T}_j^{s_0} = \mathbf{D} \left((s_0\mathbf{E} - \mathbf{A})^{-1} \mathbf{E} \right)^j (s_0\mathbf{E} - \mathbf{A})^{-1} \mathbf{B} \quad (3.25)$$

of the transfer function around s_0 .

Now, the moment matching method determines a reduced order model by projecting the original system to a Krylov subspace, which is again spanned by the column vectors of matrices \mathbf{W} and \mathbf{V} . One approach is to choose \mathbf{W} and \mathbf{V} as

$$\mathbf{W} = [\mathbf{P}_V^{r-1} \mathbf{Q}_V \ \dots \ \mathbf{P}_V^1 \mathbf{Q}_V \ \mathbf{Q}_V] \quad (3.26)$$

$$\mathbf{V} = [\mathbf{P}_W^{r-1} \mathbf{Q}_W \ \dots \ \mathbf{P}_W^1 \mathbf{Q}_W \ \mathbf{Q}_W], \quad (3.27)$$

with

$$\mathbf{P}_V = (s_0\mathbf{E} - \mathbf{A})^{-1} \mathbf{E}, \quad \mathbf{Q}_V = (s_0\mathbf{E} - \mathbf{A})^{-1} \mathbf{B} \quad (3.28)$$

$$\mathbf{P}_W = (s_0\mathbf{E} - \mathbf{A})^{-\top} \mathbf{E}^\top, \quad \mathbf{Q}_W = (s_0\mathbf{E} - \mathbf{A})^{-\top} \mathbf{D}^\top. \quad (3.29)$$

It can be shown, cf. [64], that thereon the first $2r$ moments of the reduced system hold

$$\mathbf{T}_j^{s_0} = \tilde{\mathbf{T}}_j^{s_0} \quad j = 1, \dots, 2r. \quad (3.30)$$

Note that for equal input/output matrices, and for symmetric mass and stiffness matrices, \mathbf{W} evaluates to \mathbf{V} .

Originating from control theory, the method was adapted for second order systems and (flexible) FEM discretized multibody systems within the last couple of years. Furthermore, advanced algorithms for the construction of \mathbf{V} and \mathbf{W} were introduced, cf. [10, 66, 88, 6, 64, 63, 62, 89].

3.3.3 Balanced Truncation

Balanced Truncation constructs the projection subspaces due to the controllability and observability of the underlying system, cf. [6, 84].

For simplicity, we transform the first order system in Eqs. (3.22) such that $\mathbf{E} = \mathbf{I}$:

$$\begin{aligned}\dot{\mathbf{x}} &= \mathbf{A}\mathbf{x} + \mathbf{B}\mathbf{u} \\ \mathbf{y} &= \mathbf{D}\mathbf{x}\end{aligned}\tag{3.31}$$

The system is investigated on its observability and controllability, utilizing the Ljapunov equations

$$\begin{aligned}\mathbf{A}\mathbf{W}_C + \mathbf{W}_C\mathbf{A}^\top &= -\mathbf{B}\mathbf{B}^\top \\ \mathbf{A}^\top\mathbf{W}_O + \mathbf{W}_O\mathbf{A} &= -\mathbf{D}^\top\mathbf{D}.\end{aligned}\tag{3.32}$$

The system is controllable on the interval $t \in [0, T]$, if the controllability Gramian

$$\mathbf{W}_C(T) = \int_0^T e^{\mathbf{A}t}\mathbf{B}\mathbf{B}^\top e^{\mathbf{A}^\top t} dt\tag{3.33}$$

is nonsingular. The system is further observable on the interval $t \in [0, T]$, if the observability Gramian

$$\mathbf{W}_O(T) = \int_0^T e^{\mathbf{A}^\top t}\mathbf{D}^\top\mathbf{D}e^{\mathbf{A}t} dt\tag{3.34}$$

is nonsingular. A stable system is called *balanced*, if

$$\mathbf{W}_C = \mathbf{W}_O = \text{diag}(\sigma_1, \dots, \sigma_n),\tag{3.35}$$

holds. This means that each state in the system is equally controllable and observable.

In general, the BT method first balances the system via a state-space transformation. This transformation rearranges the state vector in descending order, based on each state's controllability and observability. In a second step, states which are

negligible due to their controllability and observability are truncated. For the first step, the Cholesky factors

$$\mathbf{S}^\top \mathbf{S} = \mathbf{W}_C \quad (3.36)$$

$$\mathbf{R}^\top \mathbf{R} = \mathbf{W}_O \quad (3.37)$$

of the Gramians \mathbf{W}_C and \mathbf{W}_O are computed. Next, the singular value decomposition of

$$\mathbf{S}\mathbf{R}^\top = \mathbf{\Phi}\mathbf{\Sigma}\mathbf{\Psi}^\top = [\mathbf{\Phi}_1 \ \mathbf{\Phi}_2] \begin{bmatrix} \mathbf{\Sigma}_1 & \mathbf{0} \\ \mathbf{0} & \mathbf{\Sigma}_2 \end{bmatrix} \begin{bmatrix} \mathbf{\Psi}_1^\top \\ \mathbf{\Psi}_2^\top \end{bmatrix}, \quad (3.38)$$

with $\mathbf{\Sigma}_1 = \text{diag}(\sigma_1, \dots, \sigma_r)$ and $\mathbf{\Sigma}_2 = \text{diag}(\sigma_{r+1}, \dots, \sigma_n)$ is computed. Therefrom, the left and right projection matrices

$$\mathbf{W}^\top = \mathbf{\Sigma}_1^{-\frac{1}{2}} \mathbf{\Psi}_1^\top \mathbf{R}, \quad (3.39)$$

$$\mathbf{V} = \mathbf{S}^\top \mathbf{\Phi}_1 \mathbf{\Sigma}_1^{-\frac{1}{2}} \quad (3.40)$$

of the Petrov-Galerkin projection are derived. Equation (3.38) is already subdivided such that matrices with the subindex $(\cdot)_1$ hold the dominant part. Matrices with the subindex $(\cdot)_2$ hold the truncated part. Therefore, $\mathbf{\Sigma}_1 = \text{diag}(\sigma_1, \dots, \sigma_r)$, consists of the r dominant singular values. Accordingly, $\mathbf{\Sigma}_2$ holds the set of the $2n - r$ truncated singular values. Thus, the omitted projection matrix \mathbf{U} holds the truncated part $(\cdot)_2$ of the singular value decomposition.

The derived reduced order model consists of those states only, which require little energy to be controlled by the inputs and, at the same time, forward a lot of energy to the outputs. As a special feature of this method, the a priori error bound

$$\|\mathbf{y} - \tilde{\mathbf{y}}\|_2 \leq 2 \sum_{j=r+1}^{2n} \sigma_j \quad (3.41)$$

exists. As r is the number of the considered singular values, the error bound is the sum of the energy which is included in the truncated part of Eq. (3.38).

Balanced Truncation is extensively used in terms of control systems. As for the moment matching method, BT has been expanded to various fields of application. It was further proposed for (flexible) FEM discretized multibody systems and for second-order dynamical systems. For further insight into the method, the interested reader is referred to [70, 113, 10, 84, 6, 62, 117, 89].

3.3.4 Coordinate Partitioning

According to [82], the goal of coordinate partitioning is, to represent a redundantly formulated MBS

$$\begin{aligned} \mathbf{M}(\mathbf{q}) \ddot{\mathbf{q}} &= \mathbf{Q}(\mathbf{q}, \dot{\mathbf{q}}) - \mathbf{C}_q^\top(\mathbf{q}) \boldsymbol{\lambda} \\ \mathbf{C}(\mathbf{q}) &= \mathbf{0}, \end{aligned} \quad (3.42)$$

by an ODE system of the form

$$\hat{\mathbf{M}} \ddot{\mathbf{q}}_{\text{ind}} = \hat{\mathbf{Q}}, \quad (3.43)$$

with $\hat{\mathbf{M}}$ and $\hat{\mathbf{Q}}$ obtained from the partitioning strategy. The vector of Lagrange's multipliers $\boldsymbol{\lambda}$ is eliminated, and the original MBS system is described in terms of so-called independent coordinates \mathbf{q}_{ind} only. Coordinate partitioning approaches have been studied intensely in the 1980s, by, amongst others, Haug and Wehage [46, 112]. The coordinate partitioning strategy is summarized, following mainly [82] and [60]:

First, a novel set of independent coordinates $\mathbf{q}_{\text{ind}} \in \mathbb{R}^f$, with $f < n$ is introduced. In order to establish a connection between these and the original set of generalized coordinates $\mathbf{q} \in \mathbb{R}^n$, additional constraint equations

$$\mathbf{C}_{\text{ind}}(\mathbf{q}, \mathbf{q}_{\text{ind}}) = \mathbf{0} \quad (3.44)$$

are introduced. These, together with the original set of constraints equations, are then combined in the novel vector of constraint equations

$$\bar{\mathbf{C}}(\mathbf{q}, \mathbf{q}_{\text{ind}}) = \begin{pmatrix} \mathbf{C}(\mathbf{q}) \\ \mathbf{C}_{\text{ind}}(\mathbf{q}, \mathbf{q}_{\text{ind}}) \end{pmatrix} = \mathbf{0}, \quad (3.45)$$

with $\bar{\mathbf{C}} \in \mathbb{R}^{(m+f) \times 1}$. In order to achieve the ODE representation of the present system under consideration, constraint orthogonalization is applied. It is based on the idea of constructing the null space $\boldsymbol{\Gamma}$ to the constraints $\bar{\mathbf{C}}$, which dates back to G.A. Maggi, cf.[82, 60]. Due to the definition of the null space of a matrix the orthogonality condition

$$\bar{\mathbf{C}}_q \boldsymbol{\Gamma} = \mathbf{0} \quad (3.46)$$

holds for time-independent constraint equations. Note that as the constraints are in general state dependent, its null space has to be computed repetitively as $\boldsymbol{\Gamma} = \boldsymbol{\Gamma}(\mathbf{q}, \mathbf{q}_{\text{ind}}) \in \mathbb{R}^{(n \times f)}$.

The ODE representation of the original system

$$\boldsymbol{\Gamma}^\top \mathbf{M} \boldsymbol{\Gamma} \ddot{\mathbf{q}}_{\text{ind}} = \boldsymbol{\Gamma}^\top \mathbf{Q} - \underbrace{\boldsymbol{\Gamma}^\top \bar{\mathbf{C}}_q^\top}_{\mathbf{0}} \boldsymbol{\lambda} \quad (3.47)$$

is then derived by projection onto the constructed null space utilizing the linear projection $\ddot{\mathbf{q}} = \mathbf{\Gamma}\ddot{\mathbf{q}}_{\text{ind}}$. It must be noted, that this is the case for constant $\mathbf{\Gamma}$ only. By setting $\hat{\mathbf{M}} = \mathbf{\Gamma}^T \mathbf{M} \mathbf{\Gamma}$ and $\hat{\mathbf{Q}} = \mathbf{\Gamma} \mathbf{Q}$, the system finally reads

$$\hat{\mathbf{M}}\ddot{\mathbf{q}}_{\text{ind}} = \hat{\mathbf{Q}}, \quad (3.48)$$

consisting of f unknowns only.

The difficulty of the coordinate partitioning approach is the computation of the null space matrix $\mathbf{\Gamma}$. Several possible algorithms allowing to compute $\mathbf{\Gamma}$ for various types of problems are summarized in [82, 60]. The Global Modal Parametrization (GMP), an approach explicitly concerning the multibody system formulation of the present thesis, is detailed exemplarily.

It was introduced in the early 2000s in terms of a model order reduction approach for controlled (flexible) multibody dynamics by Brüls et al., cf. [15, 14]. Later, Heirman et al., cf. [48, 49], extended the method to MBS acting close to singular configurations. It is outlined following the work of Heirman et al. [49] and Bruels et al. [14].

Let us consider the MBS with b bodies, as shown at the beginning of this subsection. The vector of state variables \mathbf{q} is expanded into rigid and flexible coordinates

$$\mathbf{q} = \mathbf{q}^{\text{rgd}} + \mathbf{q}^{\text{f}}. \quad (3.49)$$

Therein, \mathbf{q}^{rgd} denotes the vector of rigid coordinates, and \mathbf{q}^{f} holds the vector of flexible coordinates, which are treated as small deviations from the rigid movement. Let us first deal with the rigid coordinates:

The vector \mathbf{q} is sorted such that

$$\mathbf{q}^{\text{rgd}} = \left[\mathbf{q}_r^{\text{rgd}} \quad \mathbf{q}_{\text{dep}}^{\text{rgd}} \right]^T. \quad (3.50)$$

Therein, a set of r independent coordinates $\mathbf{q}_r^{\text{rgd}}$, with $\mathbf{q}_r^{\text{rgd}} \subset \mathbf{q}^{\text{rgd}}$ and $r < n$ exists. Hence, there exists some mapping

$$\mathbf{q}_r^{\text{rgd}} \mapsto \mathbf{q}^{\text{rgd}} = \boldsymbol{\rho} \left(\mathbf{q}_r^{\text{rgd}} \right) \quad (3.51)$$

which allows to compute the full vector of rigid coordinates based on the independent coordinates. The mapping $\boldsymbol{\rho}$ may be chosen such that its Jacobian can be interpreted as the systems rigid body modes

$$\frac{\partial \boldsymbol{\rho} \left(\mathbf{q}_r^{\text{rgd}} \right)}{\partial \mathbf{q}_r^{\text{rgd}}} = \boldsymbol{\Phi} \left(\mathbf{q}_r^{\text{rgd}} \right). \quad (3.52)$$

The dependent set of $n - r$ remaining coordinates $\mathbf{q}_{\text{dep}}^{\text{rgd}}$ is derived by evaluating algebraic equations, which describe the coordinate dependency.

Accordingly, in terms of the flexible part \mathbf{q}^f an equivalent set of independent coordinates $\hat{\mathbf{q}}_s^f$, with $\hat{\mathbf{q}}_s^f \subset \mathbf{q}^f$ and $s < n$ exists. As deformations are treated as small deviations from the rigid movement, the flexible coordinates

$$\mathbf{q}^f = \mathbf{q}^f(\mathbf{q}_r^{\text{rgd}}, \hat{\mathbf{q}}_s^f) \quad (3.53)$$

are also a function of the rigid behavior. In the case of a purely rigid motion the flexible coordinates hold

$$\mathbf{q}^f = \mathbf{q}^f(\mathbf{q}_r^{\text{rgd}}, \mathbf{0}) = \mathbf{0}. \quad (3.54)$$

Flexible coordinates are subject to the series expansion

$$\mathbf{q}^f(\mathbf{q}_r^{\text{rgd}}, \hat{\mathbf{q}}_s^f) \cong \frac{\partial \mathbf{q}^f}{\partial \hat{\mathbf{q}}_s^f}(\mathbf{q}_r^{\text{rgd}}, \mathbf{0}) \hat{\mathbf{q}}_s^f = \hat{\Psi}(\mathbf{q}_r^{\text{rgd}}) \hat{\mathbf{q}}_s^f, \quad (3.55)$$

following the concept of small deviations. Therein, $\hat{\Psi}(\mathbf{q}_r^{\text{rgd}})$ holds the configuration dependent flexible mode shape matrix, and $\hat{\mathbf{q}}_s^f$ holds the according modal coordinates. The construction of this mode shape matrix is supposed to be carried out by methods like the CMS approach, the Hurty approach cf. [14], or the approach presented in [49].

As we want to generate a reduced order model, the vector of modal coordinates and the created mode matrix are further investigated. To this end, the mode matrix $\hat{\Psi}$ is split into its dominant and higher-order modes

$$\hat{\Psi}(\mathbf{q}_r^{\text{rgd}}) = \left[\Psi(\mathbf{q}_r^{\text{rgd}}) \quad \tilde{\Psi}(\mathbf{q}_r^{\text{rgd}}) \right]. \quad (3.56)$$

Therein, Ψ holds the dominant modes (in its columns) and $\tilde{\Psi}$ holds the higher-order modes. Accordingly, the vector of modal coordinates is split into dominant and higher-order coordinates

$$\hat{\mathbf{q}}_s^f = \left[\mathbf{q}_s^f \quad \tilde{\mathbf{q}}_s^f \right]^T. \quad (3.57)$$

In this notation the deformation reads

$$\mathbf{q}^f = \Psi(\mathbf{q}_r^{\text{rgd}}) \mathbf{q}_s^f + \tilde{\Psi}(\mathbf{q}_r^{\text{rgd}}) \tilde{\mathbf{q}}_s^f. \quad (3.58)$$

Finally, by projecting the flexible coordinates to a subspace on which $\tilde{\mathbf{q}}_s^f = \mathbf{0}$ holds, the flexible coordinates are approximated by

$$\mathbf{q}^f \approx \Psi(\mathbf{q}_r^{\text{rgd}}) \mathbf{q}_s^f. \quad (3.59)$$

Including this strategy the mapping of the full vector of coordinates \mathbf{q} reads

$$(\mathbf{q}_r^{\text{rgd}}, \mathbf{q}_s^f) \mapsto \mathbf{q} \cong \boldsymbol{\rho}(\mathbf{q}_r^{\text{rgd}}) + \Psi(\mathbf{q}_r^{\text{rgd}}) \mathbf{q}_s^f. \quad (3.60)$$

The differentiation of the mapping with respect to $\mathbf{q}_r^{\text{rgd}}$ and \mathbf{q}_s^{f} generates the non-linear projection matrix

$$\begin{aligned} \mathbf{V}(\mathbf{q}_r^{\text{rgd}}, \mathbf{q}_s^{\text{f}}) &= \frac{\partial \mathbf{q}}{\partial (\mathbf{q}_r^{\text{rgd}}, \mathbf{q}_s^{\text{f}})} \\ &= \left[\Phi(\mathbf{q}_r^{\text{rgd}}) + \frac{\partial}{\partial \mathbf{q}_r^{\text{rgd}}} (\Psi(\mathbf{q}_r^{\text{rgd}}) \mathbf{q}_s^{\text{f}}) \quad \Psi(\mathbf{q}_r^{\text{rgd}}) \right]. \end{aligned} \quad (3.61)$$

In the case of an undeformed state ($\mathbf{q}_s^{\text{f}} = \mathbf{0}$), the projection matrix reads

$$\mathbf{V}(\mathbf{q}_r^{\text{rgd}}, \mathbf{0}) = \left[\Phi(\mathbf{q}_r^{\text{rgd}}) \quad \Psi(\mathbf{q}_r^{\text{rgd}}) \right]. \quad (3.62)$$

As pointed out by this equations, the reduction subspace $\mathbf{V} = \mathbf{V}(\mathbf{q}_r^{\text{rgd}}, \mathbf{q}_s^{\text{f}})$ (including the null space to the constraints) is configuration dependent. As it will be outlined in the upcoming section of this chapter, this may be an issue concerning the methods efficiency and applicability.

For deep insight into the GMP method, the interested reader is referred to [15, 14, 48, 49] and references therein.

3.3.5 Nonlinear Galerkin Projection

The nonlinear Galerkin projection $\mathbf{x} \approx \mathbf{V} \cdot \mathbf{x}_r + \mathbf{U} \cdot \mathbf{x}_{n-r}$, in contrast to the flat Galerkin projection $\mathbf{x} \approx \mathbf{V} \cdot \mathbf{x}_r$, further accounts for the truncated (high frequency) Eigenvectors \mathbf{U} . The system is no longer projected to a flat subspace, but to a manifold of the original space. Thereby, the behavior of the truncated coordinates \mathbf{x}_{n-r} is approximated and accounted for by projection onto the center manifold

$$\mathbf{x}_{n-r} \approx \mathbf{h}(\mathbf{x}_r). \quad (3.63)$$

Applying this relation, the nonlinear Galerkin projection changes to

$$\mathbf{x} = \mathbf{V} \cdot \mathbf{x}_r + \mathbf{U} \cdot \mathbf{h}(\mathbf{x}_r). \quad (3.64)$$

In Fig. 3.2, the nonlinear Galerkin projection to \mathcal{M} is geometrically interpreted in the 3D space, obeying the non flat behavior.

3.3.5.1 Center Manifold Theory

This section briefly introduces the idea of the center manifold theory. Let us assume the nonlinear differential system

$$\dot{\mathbf{x}} = \mathbf{F}(\mathbf{x}), \text{ with } \mathbf{F} : \mathbb{R}^n \rightarrow \mathbb{R}^n, \mathbf{x} \in \mathbb{R}^n \quad (3.65)$$

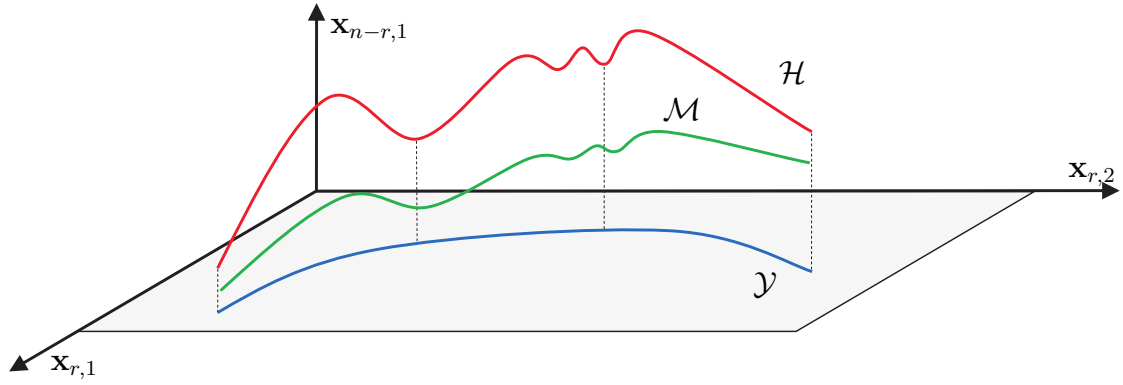


Figure 3.2: Geometric interpretation of the linear and nonlinear (Petrov-)Galerkin projection

and $\mathbf{F}(\mathbf{0}) = \mathbf{0}$. Applying the Taylor series expansion

$$\dot{\mathbf{x}} = \mathbf{A} \cdot \mathbf{x} + \mathbf{f}(\mathbf{x}), \quad (3.66)$$

the system is split into the linear part $\mathbf{A} \cdot \mathbf{x}$, with \mathbf{A} as the resulting coefficient matrix, and into the nonlinear part $\mathbf{f}(\mathbf{x})$.

We first deal with the linear part $\dot{\mathbf{x}} = \mathbf{A} \cdot \mathbf{x}$, and assume the algebraic and geometric multiplicities of the Eigenvalues of \mathbf{A} to be equal. In such a case, the system matrix \mathbf{A} is transformable into a system

$$\dot{\tilde{\mathbf{x}}} = \underbrace{\mathbf{T}^{-1}\mathbf{A}\mathbf{T}}_{\tilde{\mathbf{A}}} \tilde{\mathbf{x}}, \quad (3.67)$$

with the block-diagonal coefficient matrix

$$\tilde{\mathbf{A}} = \begin{bmatrix} \mathbf{A}_c & \mathbf{0} & \mathbf{0} \\ \mathbf{0} & \mathbf{A}_s & \mathbf{0} \\ \mathbf{0} & \mathbf{0} & \mathbf{A}_u \end{bmatrix}, \quad (3.68)$$

using the similarity transformation $\mathbf{x} = \mathbf{T}\tilde{\mathbf{x}}$. This system is then separable into three differential systems

$$\dot{\mathbf{x}}_c = \mathbf{A}_c \cdot \mathbf{x}_c, \quad (3.69)$$

$$\dot{\mathbf{x}}_s = \mathbf{A}_s \cdot \mathbf{x}_s, \quad (3.70)$$

$$\dot{\mathbf{x}}_u = \mathbf{A}_u \cdot \mathbf{x}_u. \quad (3.71)$$

Investigating the Eigenvalues of $\tilde{\mathbf{A}}$, \mathbf{A}_c is characterized by purely imaginary Eigenvalues, \mathbf{A}_s holds Eigenvalues with $Re < 0$ only, and \mathbf{A}_u only holds Eigenvalues with $Re > 0$. The according linear Eigenspaces \mathcal{E}_c , \mathcal{E}_s and \mathcal{E}_u , are called the *center*,

stable and unstable Eigenspaces of $\tilde{\mathbf{A}}$.

Accounting for the nonlinear part $\mathbf{f}(\mathbf{x})$, \mathcal{E}_c , \mathcal{E}_s and \mathcal{E}_u are deformed into nonlinear manifolds. By investigating the behavior of these manifolds it can be shown that, if the unstable manifold \mathcal{E}_u is empty, every trajectory living in \mathcal{E}_s will be attracted by the center manifold \mathcal{E}_c in an exponential way. Therefore, all components living in \mathcal{E}_s will decay exponentially. Now, according to [58], two remarkable properties exist:

1. Trajectories starting on the center manifold stay on it for all positive times (the manifold is said to be invariant under the flow).
2. All trajectories starting off the manifold are attracted to it at an exponential rate, cf. [38]

This implies, that for the long-term behavior of the system only the dynamics restricted to the center manifold need to be investigated. We assume the system to be of that kind, and the set of nonlinear differential equations read

$$\dot{\mathbf{x}}_c = \mathbf{A}_c \cdot \mathbf{x}_c + \mathbf{f}_c(\mathbf{x}_c, \mathbf{x}_s) \quad (3.72)$$

$$\dot{\mathbf{x}}_s = \mathbf{A}_s \cdot \mathbf{x}_s + \mathbf{f}_s(\mathbf{x}_c, \mathbf{x}_s). \quad (3.73)$$

Close to the equilibrium point, and for sufficiently small δ , the center manifold $\mathbf{h}(\mathbf{x}_c)$ can be assumed as

$$\mathcal{M} = \{(\mathbf{x}_c, \mathbf{x}_s) \in \mathbb{R}^c \times \mathbb{R}^s \mid \mathbf{x}_s = \mathbf{h}(\mathbf{x}_c), |\mathbf{x}_c| < \delta, \mathbf{h}(\mathbf{0}) = \mathbf{0}, \mathbf{D}\mathbf{h}(\mathbf{0}) = \mathbf{0}\}, \quad (3.74)$$

with

$$\mathbf{D}\mathbf{h}(\mathbf{0}) = \left. \frac{\partial \mathbf{h}(\mathbf{x}_c)}{\partial \mathbf{x}_c} \right|_{\mathbf{x}_c=\mathbf{0}}. \quad (3.75)$$

Introducing these relations into the original system in Eq. (3.72), the resulting differential equations

$$\dot{\mathbf{x}}_c = \mathbf{A}_c \cdot \mathbf{x}_c + \mathbf{f}_c(\mathbf{x}_c, \mathbf{h}(\mathbf{x}_c)) \quad (3.76)$$

describe the dynamics of the original system close to the equilibrium point of the system. Therefrom, the center manifold is derived by combining the above relations into

$$\begin{aligned} \dot{\mathbf{x}}_s &= \mathbf{A}_s \cdot \mathbf{h}(\mathbf{x}_c) + \mathbf{f}_s(\mathbf{x}_c, \mathbf{h}(\mathbf{x}_c)) \\ &\hat{=} \\ \frac{\partial \mathbf{h}(\mathbf{x}_c)}{\partial \mathbf{x}_c} \cdot \dot{\mathbf{x}}_c &= \mathbf{A}_s \cdot \mathbf{h}(\mathbf{x}_c) + \mathbf{f}_s(\mathbf{x}_c, \mathbf{h}(\mathbf{x}_c)) \\ &\hat{=} \\ \frac{\partial \mathbf{h}(\mathbf{x}_c)}{\partial \mathbf{x}_c} \cdot [\mathbf{A}_c \cdot \mathbf{x}_c + \mathbf{f}_c(\mathbf{x}_c, \mathbf{h}(\mathbf{x}_c))] &= \mathbf{A}_s \cdot \mathbf{h}(\mathbf{x}_c) + \mathbf{f}_s(\mathbf{x}_c, \mathbf{h}(\mathbf{x}_c)), \quad (3.77) \end{aligned}$$

and solving the differential equation (3.77) for $\mathbf{h}(\mathbf{x}_c)$. This center manifold can then be used to solve the reduced system in Eq. (3.76). As a matter of fact, the derivation of the center manifold is a non-trivial task, which is not necessarily successful for any type of differential equations. This is mainly due to the term $\frac{\partial \mathbf{h}(\mathbf{x}_c)}{\partial \mathbf{x}_c} \cdot \mathbf{A}_c \cdot \mathbf{x}_c$ in Eq. (3.77), which may become critical in terms of large systems. One possible approach is to set

$$\frac{\partial \mathbf{h}(\mathbf{x}_c)}{\partial \mathbf{x}_c} \cdot \mathbf{A}_c \cdot \mathbf{x}_c = \mathbf{0}, \quad (3.78)$$

as the insignificant modi \mathbf{x}_s are typically assumed as quasi-static. Due to this simplification, the derivation of the approximated center manifold becomes a purely algebraic operation.

Another approach, presented in Garcia-Archilla et al. [43], proposes the *Post-processed Galerkin method*, which utilizes the linear Galerkin projection for time integration and switches to a nonlinear Galerkin projection only at time-instances worth evaluating. Several more methods for approximating the center manifold were proposed by e.g. Foias or Titi, cf. [38, 39, 106]. Finally, for a detailed discourse on the center manifold theory, the interested reader is referred to, amongst others, the work of Carr, Foias, Robinson, Temam, Reit, Fuchs [104, 87, 40, 17, 86, 42] and references therein.

3.3.6 Applicability of A Priori Methods

The original intention of CMS, BT, and MM was to reduce first and second order ODE systems like FEM models. The strength of these approaches relies on the fact of constant system matrices, which allow to directly reduce a model a priori without any need of generating system information. The nonlinear Galerkin approach, utilizing center manifold theory, is well suited to deal with ordinary and partially differential equations. Detached from these stands the GMP approach. It has been introduced to explicitly handle the present state-dependent MBS system under consideration.

This section first discusses the applicability of the GMP approach. Secondly, it characterizes the CMS, MM and BT model order reduction methods due to the present MBS representation. The section closes with remarks to the nonlinear Galerkin projection.

Global Modal Parametrization

According to Heirman et al. [49, p.7], the major benefit of the GMP is: *'(...)as the elastic deformation is approximated by a limited set of configuration dependent modes, the number of degrees of freedom $[\mathbf{q}_r^{rgd} \ \mathbf{q}_s^f]^\top$ is much smaller than the number of initial coordinates \mathbf{q} and Lagrange multipliers $\boldsymbol{\lambda}$.*'

and further on in the same paragraph:

*'The reduced dimension of the problem, as well as the switch from DAE to ODE, make the projected system equations much cheaper to solve. **However, assembling the reduced system equations requires a considerable effort and can generally only be done numerically.** The cost of this assembly can outweigh the advantage of the small resulting set of equations.'*

The bold depicted statement has to be discussed, as it may be seen as a bottleneck of the GMP approach.

Both, the MBS system and the projection matrix are state dependent. Therefore, a costly offline preparation phase has to be taken into account. In this phase, one has to compute a sufficient set of valid system configurations \mathbf{q}^s and $(\mathbf{q}_r^{\text{rgd}})^s$, respectively. From these, an according set of projection matrices \mathbf{V}^s , and a collection of the according reduced MBS system elements \mathbf{M}^s and \mathbf{Q}^s have to be constructed. During the online phase of the reduced simulation these previously constructed reduced MBS system elements have to be interpolated due to the actual configuration $[\mathbf{q}_r^{\text{rgd}} \ \mathbf{q}_s^f]^\top$. In a second step the ODE involving the interpolated MBS elements is solved for a new set $\mathbf{q}_r^{\text{rgd}}$. These two steps are carried out repetitively throughout the simulation time.

Summing up, the GMP is mainly an interpolation task of locally linearized and reduced MBS systems which are then solved by a sufficient ODE solver algorithm. This might bring up difficulties, mainly concerning the interpolation routine. Although it is stated in [49, p.7], that *'(..)all elements of the projected model equations are defined by smooth functions using inputs that vary smoothly with $\mathbf{q}_r^{\text{rgd}}$ (...)*' and therefore *'(..)the elements of the projected model equations are continuous themselves.'*, the following issues may arise:

1. The set of independent coordinates $\mathbf{q}_r^{\text{rgd}}$ may not be unique within the space of valid system configurations:

According to [14, 49], dead points of the MBS lead the reduced system into a singular configuration.

Therefore, Heirman et al. [49] suggest to apply the GMP approach if the MBS is ensured to act in regular areas of the configuration space only.

2. Evolving from real time implementations and control design, Bruls et al. [14] suggest to choose all controller-relevant actuated coordinates as part of the set $\mathbf{q}_r^{\text{rgd}}$. By doing so, a back transformation of the reduced system solution into the original coordinates \mathbf{q} is obsolete. The needed control parameters are $\mathbf{q}_r^{\text{rgd}}$.

Beside this suggestion to control problems, the choice of $\mathbf{q}_r^{\text{rgd}}$ is left to the user. In principle, the number of independent coordinates is given by the

number of constraint equations

$$n_{\text{ind}} = n - n_{\text{dep}}, \quad (3.79)$$

with $m = n_{\text{dep}}$. Hence, each constraint equation correlates with one dependent coordinate. Still, the actual identification of independent and dependent coordinates may become a non-trivial task. This is especially the case, when dealing with more complex constraint equations, see [92].

3. The offline preparation phase may involve in-depth user knowledge: The configuration space may become high dimensional in the case of several unconstrained coordinates. Therefore, the user probably has to estimate the MBS motion a priori. Otherwise, the configuration space may not be screened sufficiently, resulting in an incomplete set of projection matrices \mathbf{V}^s . In such a case, the online phase may not be able to find corresponding projection matrices. This most likely causes the reduced simulation to fail.
4. The switch from one reduced order model to another may not necessarily be smooth, but depends on the interpolation algorithm: Bruls et al. [14] point out, that the used interpolation algorithm actually determines the accuracy, efficiency and smoothness/continuity of the interpolation. Hence, reduced simulation instabilities and discontinuities may not be negligible in general. Furthermore, these algorithms may be again in need of in-depth knowledge of the upcoming MBS motion, cf. [14].

Concluding the discussion of the GMP approach, the method seems to be highly efficient in terms of control design of well known MBS structures. In the light of a general and simple applicability to industry-used MBS packages, the approach is considered as too advanced. This is, on the one hand, due to the excessive offline phase, which is highly dependent of

- the identifiability of singular configurations of the MBS under consideration,
- the therewith related user-ability to choose the correct set of valid MBS configurations,
- the dimensionality of the MBS, which is the number of independent coordinates, and
- the therewith related user-ability to pick a sufficient set of independent coordinates $\mathbf{q}_r^{\text{rgd}}$.

On the other hand, the online phase of the reduced simulation rests on a new set of ODEs which are in need of

- the user's ability to choose a proper interpolation strategy, which ensures smooth interpolation, and
- a special ODE solver algorithm, which, most likely, has to interact with the interpolation algorithm, and ensures smooth time integration.

Consequently, it can not be taken for granted that the GMP approach is applicable and usable in combination with an industry-used MBS package and non-expert users.

Component Mode Synthesis, Moment Matching and Balanced Truncation

As stated in the beginning of this section, CMS, MM and BT are defined in terms of first and second order ODE systems. Due to this fact, these methods are not able to handle the present MBS description. However, it seems possible to apply the CMS, BT and MM approaches to locally linearized model configurations, following the GMP approach. This idea is briefly outlined and afterwards reasons are given, why this approach is dismissed within this dissertation.

First, the redundant MBS model would have to be transformed into the d-index one ODE system

$$\underbrace{\begin{bmatrix} \mathbf{M} & \mathbf{C}_q^\top \\ \mathbf{C}_q & \mathbf{0} \end{bmatrix}}_{\mathbf{M}_{\text{ext}}} \begin{bmatrix} \ddot{\mathbf{q}} \\ \boldsymbol{\lambda} \end{bmatrix} = \begin{bmatrix} \mathbf{Q} \\ \boldsymbol{\gamma} \end{bmatrix}. \quad (3.80)$$

The already introduced term

$$\boldsymbol{\gamma} = -\dot{\mathbf{C}}_q \dot{\mathbf{q}} = -(\mathbf{C}_q \dot{\mathbf{q}})_q \dot{\mathbf{q}} \quad (3.81)$$

evolves from differentiation of the constraint equations. Pre-multiplication with the inverse of the extended mass matrix \mathbf{M}_{ext} yields

$$\begin{bmatrix} \ddot{\mathbf{q}} \\ \boldsymbol{\lambda} \end{bmatrix} = \begin{bmatrix} \mathbf{M} & \mathbf{C}_q^\top \\ \mathbf{C}_q & \mathbf{0} \end{bmatrix}^{-1} \begin{pmatrix} \mathbf{Q} \\ \boldsymbol{\gamma}(\mathbf{q}, \dot{\mathbf{q}}) \end{pmatrix}. \quad (3.82)$$

This system can be solved for the generalized coordinates \mathbf{q} without evaluating the Lagrange's multipliers. Note that this is only possible in the case of \mathbf{M}_{ext} being invertible. The ODE system in Eq. (3.82) may therefore be seen as the new "original" MBS model, subject to model order reduction based on the CMS,

MM and BT approach. By applying the flat Galerkin projection $\mathbf{q} = \mathbf{V}\mathbf{q}_r$, the corresponding reduced order model would be of the form

$$\begin{bmatrix} \ddot{\mathbf{q}}_r \\ \boldsymbol{\lambda} \end{bmatrix} = \begin{bmatrix} \mathbf{V}^\top \\ \mathbf{I}_{m \times 1} \end{bmatrix} \begin{bmatrix} \mathbf{M} & \mathbf{C}_q^\top \\ \mathbf{C}_q & \mathbf{0} \end{bmatrix}^{-1} \begin{pmatrix} \mathbf{Q} \\ \boldsymbol{\gamma} \end{pmatrix}. \quad (3.83)$$

This means a huge change in the mathematical model, and a considerable increase in the numerical effort. Arising derivatives and Jacobian matrices (e.g. $\dot{\mathbf{C}}_q$) may not be provided by the MBS software and therefore, have to be computed numerically. But, even by accepting these additional numerical costs, the system is still highly state dependent ($\mathbf{M} = \mathbf{M}(\mathbf{q})$, etc.)

Although a priori model order reduction methods have been extended to systems with local nonlinearities, cf. [97], they are based on assumptions handling constant system matrices. Actually, with the GMP approach in mind, one could carry on by locally linearizing the ODE system in Eq. (3.82) and applying the CMS, MM or BT approach to this system.

To this end, a large number of system states $\mathbf{q}^s, \dot{\mathbf{q}}^s$, which comply with the constraint equations, is constructed. Next, the MBS elements $\mathbf{M}^s, \mathbf{C}_q^s, \mathbf{Q}^s$ are evaluated, and afterwards the corresponding reduction subspaces \mathbf{V}^s are generated.

The online phase of the reduced simulation could then be carried out analogously to the GMP approach. Unfortunately, this would bring up the same issues as already summarized for the GMP approach. These issues include system regularity and complexity, solver stability and user knowledge. Therefore, in-depth investigations of this scenario will not be carried out.

Nonlinear Galerkin Projection

The nonlinear Galerkin projection, as presented in this chapter, is based on nonlinear differential equations represented as first order systems. The present set of differential algebraic equations, which describe the redundant set of coordinates for the multibody system, differs vastly from this definition. Similar to the previously described approaches, an index- and order reduction of the multibody system are necessary, in order to transform the mathematical model into a suitable description. To this end, constraint enforcement methods, like the Baumgarte stabilization, would have to be introduced, reducing the performance and determinacy of the multibody model. As the center manifold description is valid within a certain region around an equilibrium point, issues similar to the global modal parametrization occur, when dealing with smooth transition from one center manifold to another. This, in combination with the complex procedure to derive an (approximated) center manifold to the underlying multibody modeling approach excludes the nonlinear Galerkin projection from further considerations.

As a result, the whole group of a priori methods is dismissed for all upcoming considerations.

3.4 A Posteriori Model Order Reduction

The a posteriori model order reduction methods presented in this section do not investigate the original system itself but data originating from it. They are therefore also-called *data-driven* methods. This data is generated by solving the original system, and collecting the time history of e.g. the system states. The application of these methods makes sense if simulation tasks are run repetitively, like in parameter identification or control engineering.

This section reviews the flat projection approaches *Proper Orthogonal Decomposition* (POD) and its generalization the *Smooth Orthogonal Decomposition* (SOD). These approaches utilize the *Singular Value Decomposition* (SVD) and the *Generalized Singular Value Decomposition* (GSVD) in order to investigate the input data. Alternatively, the POD and SOD can also be computed in terms of the (generalized) Eigenvalue decomposition of covariance matrices. The methods are applicable to ODEs, partially differential equations, and systems of DAEs.

This section starts with a brief summary on the main features of the singular value decomposition, generalized singular value decomposition, and covariance before focusing on the POD and SOD in detail.

3.4.1 Singular Value Decomposition

Numerical linear algebra utilizes the so-called *big six matrix decompositions* [102]

- the Cholesky decomposition,
- the LU decomposition,
- the QR algorithm,
- the Spectral decomposition,
- the Schur decomposition,
- **the singular value decomposition decomposition,**

to efficiently handle matrix computations. The goal is to factorize a given matrix into simpler matrices, which can be treated more efficiently. The present subsection reviews the singular value decomposition, following [6, 109, 68, 102]:

Given an arbitrary matrix $\mathbf{A} \in \mathbb{R}^{n \times m}$ with $n \leq m$, the singular value decomposition of this *input-matrix*, is the factorization of \mathbf{A} into the product

$$\mathbf{A} = \underbrace{\Phi}_{n \times n} \underbrace{\Sigma}_{n \times m} \underbrace{\Psi^T}_{m \times m}. \quad (3.84)$$

The column vectors ϕ_i of $\Phi \in \mathbb{R}^{n \times n}$, called *left singular vectors*, span the column space of the input matrix \mathbf{A} . Accordingly, the column vectors ψ_i of $\Psi \in \mathbb{R}^{m \times m}$, called *right singular vectors*, span the row space of the input matrix.

The left and right singular vectors are orthonormal ($\Phi^T \Phi = \mathbf{I}$, $\Psi^T \Psi = \mathbf{I}$). They are further connected by the $n \times m$ matrix Σ . If $n = m$, Σ is of diagonal form $\Sigma = \text{diag}(\sigma_1, \dots, \sigma_n)$, with the n singular values σ_i . In the case of $n < m$, Σ is of the form

$$\Sigma = \left[\begin{array}{c|c} \underbrace{\begin{bmatrix} \sigma_1 & & & \mathbf{0} \\ & \sigma_2 & & \\ & & \ddots & \\ \mathbf{0} & & & \sigma_n \end{bmatrix}}_{n \times n} & \underbrace{\begin{bmatrix} \mathbf{0} \\ \vdots \\ \mathbf{0} \end{bmatrix}}_{n \times m - n} \end{array} \right] \quad (3.85)$$

The singular value decomposition is related to the Eigenvalue decomposition (EVD) of \mathbf{A} . The left singular vectors ϕ_i are the Eigenvectors of

$$(\mathbf{A}\mathbf{A}^T - \lambda_i \mathbf{I}) \phi_i = 0. \quad (3.86)$$

The right singular vectors ψ_i are the Eigenvectors of

$$(\mathbf{A}^T \mathbf{A} - \lambda_i \mathbf{I}) \psi_i = 0, \quad (3.87)$$

respectively.

The singular value decomposition of a matrix can be used for various matrix investigations:

1. The 2-norm of matrix \mathbf{A} equals the largest corresponding singular value

$$\sigma_1 = \|\mathbf{A}\|_2. \quad (3.88)$$

2. In the case of a rank deficient input matrix \mathbf{A} , the singular value decomposition can be expanded into

$$\mathbf{A} = \Phi \Sigma \Psi^T = [\Phi_{\text{ind}} \quad \Phi_{\text{dep}}] \begin{bmatrix} \Sigma_{\text{ind}} & \mathbf{0} \\ \mathbf{0} & \mathbf{0} \end{bmatrix} \begin{bmatrix} (\Psi_{\text{ind}})^T \\ (\Psi_{\text{dep}})^T \end{bmatrix}. \quad (3.89)$$

Therein, $\Sigma_{\text{ind}} \in \mathbb{R}^{l \times l} = \text{diag}(\sigma_1, \dots, \sigma_l)$ holds the independent, singular values of \mathbf{A} . Accordingly, $\Phi_{\text{ind}} \in \mathbb{R}^{n \times l}$ holds the non-zero left singular vectors, and $\Psi_{\text{ind}} \in \mathbb{R}^{l \times m}$ holds the independent right singular vectors.

The rank of the input matrix is given by

$$\text{rank}(\mathbf{A}) = \dim(\Sigma_{\text{ind}}) = l. \quad (3.90)$$

Without losing exactness, Eq. (3.89) can be rewritten in terms of the independent components as

$$\mathbf{A} = \mathbf{\Phi}_{\text{ind}} \mathbf{\Sigma}_{\text{ind}} (\mathbf{\Psi}_{\text{ind}})^\top. \quad (3.91)$$

3. The singular value decomposition can be utilized to find a low rank approximation $\tilde{\mathbf{A}} \in \mathbb{R}^{n \times m}$ of an arbitrary input-matrix $\mathbf{A} \in \mathbb{R}^{n \times m}$ such that it is optimal in the 2-norm.

Suppose $\text{rank } \mathbf{A} = r < n < m$ and $\text{rank } \tilde{\mathbf{A}} = k < r$. Then, we ask the 2-norm of the error matrix $\mathbf{F} = \mathbf{A} - \tilde{\mathbf{A}}$, to be minimized. According to the *Schmidt-Eckart-Young-Mirsky Theorem*[6], this is

$$\min_{\tilde{\mathbf{A}}, \text{rank } \tilde{\mathbf{A}}=k} \|\mathbf{A} - \tilde{\mathbf{A}}\|_2 = \sigma_{k+1}(\mathbf{A}). \quad (3.92)$$

The rank- k approximation is then given by

$$\tilde{\mathbf{A}} = \sigma_1 \phi_1 \psi_1^\top + \cdots + \sigma_k \phi_k \psi_k^\top. \quad (3.93)$$

If we suppose $\mathbf{A} \in \mathbb{R}^{n \times m}$ as n points in an m -dimensional space, optimality in the 2-norm can be interpreted as follows:

The above theorem finds the k -dimensional subspace to which the orthogonal distances of the n points are minimal.

The singular value decomposition has become a very important model reduction tool in terms of the POD method [18, 109, 78]. This method uses the matrix of left singular vectors $\mathbf{\Phi}$ for model order reduction purposes.

3.4.1.1 The Generalized Singular Value Decomposition

The Generalized Singular Value Decomposition (GSVD) has also been utilized as a potential model order reduction method recently. Hence, it is reviewed briefly following [107, 1, 3, 7, 65]:

It allows to decompose arbitrary input matrices $\mathbf{A} \in \mathbb{R}^{m \times n}$ and $\mathbf{B} \in \mathbb{R}^{m \times n}$ both with $m > n$, by

$$\begin{aligned} \mathbf{A} &= \mathbf{\Phi}_I \mathbf{\Sigma}_I \mathbf{\Psi}^\top \\ \mathbf{B} &= \mathbf{\Phi}_{II} \mathbf{\Sigma}_{II} \mathbf{\Psi}^\top. \end{aligned} \quad (3.94)$$

Both lines in Eq. (3.94) may be seen as singular value decompositions. But the input matrices are decomposed such that the row space $\mathbf{\Psi}$ is equal for both input matrices. As a result, the matrices $\mathbf{\Phi}_I, \mathbf{\Sigma}_I, \mathbf{\Phi}_{II}, \mathbf{\Sigma}_{II}, \mathbf{\Psi}$ are of the same structure

as in the case of a singular value decomposition:

The right singular vectors are column vectors $\boldsymbol{\psi}_i$ of the matrix $\boldsymbol{\Psi} \in \mathbb{R}^{m \times m}$. They again span the row space of the input matrices. The m generalized singular values σ_i are computed by the term-by-term division of $\text{diag}(\boldsymbol{\Sigma}_I^\top \boldsymbol{\Sigma}_I)$ and $\text{diag}(\boldsymbol{\Sigma}_{II}^\top \boldsymbol{\Sigma}_{II})$. The generalized left singular vectors are unique for \mathbf{A} and \mathbf{B} . Their column vectors $\boldsymbol{\phi}_i$ span the respective column space. They are collected in matrices $\boldsymbol{\Phi}_I \in \mathbb{R}^{n \times n}$ and $\boldsymbol{\Phi}_{II} \in \mathbb{R}^{n \times n}$ respectively.

The generalized singular value decomposition can also be formulated in terms of the Generalized Eigenvalue Decomposition (GEVD)

$$\left(\frac{1}{m} \mathbf{A}^\top \mathbf{A} - \lambda_i \frac{1}{m} \mathbf{B}^\top \mathbf{B} \right) \boldsymbol{\psi}_i = \mathbf{0}. \quad (3.95)$$

Note that this Eigenvalue decomposition is scaled by the factor $\frac{1}{m}$, with m as the number of lines in \mathbf{A} and \mathbf{B} . This scaling will become important when dealing with auto-correlation matrices. The matrix of generalized right singular vectors is related to the Eigenvector matrix. Furthermore, the Eigenvalues directly correspond to the generalized singular values ($\lambda_i = \sigma_i$).

An interpretation of this decomposition and the characterization of the impact of \mathbf{B} depends on the actual field of application. Following Abdi [1], the generalized singular value decomposition gives a least square estimate of \mathbf{A} by the low-rank approximation $\tilde{\mathbf{A}}$. This estimation is quite similar to the classical singular value decomposition approach. But in contrast to that, the estimate $\tilde{\mathbf{A}}$ is a weighted estimation, with the rows of the "constraint"-matrix \mathbf{B} acting as weights.

The generalized singular value decomposition method has also been used in terms of the Smooth Orthogonal Decomposition by Chelidze et al. [20, 21], which is an extension to the POD method. The relevant model order reduction subspace is spanned by the generalized right singular vectors $\boldsymbol{\Psi}$. An interpretation in terms of the Smooth Orthogonal Decomposition (from an engineers point of view) will be presented in the upcoming section.

The following relations are of special interest in the upcoming part of this chapter:

- For the choice $\mathbf{B} = \mathbf{I}$, the generalized singular value decomposition reduces to the classical singular value decomposition approach

$$\left(\mathbf{A}^\top \mathbf{A} - \lambda_i \mathbf{I} \right) \boldsymbol{\psi}_i = \mathbf{0}. \quad (3.96)$$

- In the case of a quadratic, regular and invertible matrix $\mathbf{B} \in \mathbb{R}^{n \times n}$, the generalized singular value decomposition is replaceable by the singular value decomposition

$$\mathbf{B}^{-1} \mathbf{A} = \boldsymbol{\Phi} \boldsymbol{\Sigma} \boldsymbol{\Psi}^\top. \quad (3.97)$$

It is further describable by the Eigenvalue problem

$$\mathbf{B}^{-1}\mathbf{A}\boldsymbol{\psi}_i = \lambda_i\boldsymbol{\psi}_i. \quad (3.98)$$

- As pointed out in literature, cf. [101, 37, 20], the generalized singular value decomposition approach is ill-conditioned if the "constraint"-matrix \mathbf{B} is singular. As it will turn out later in this work that is a critical issue in terms of the present MBS formulation.

3.4.2 (Auto)-Covariance Matrices

As reviewed in the preceding section the singular value decomposition of an input matrix $\mathbf{A} \in \mathbb{R}^{m \times n}$ can be formulated in terms of the Eigenvalue decomposition

$$\boldsymbol{\Sigma}_\mathbf{A}\boldsymbol{\psi}_i = \lambda_i\boldsymbol{\psi}_i. \quad (3.99)$$

Therein, $\boldsymbol{\Sigma}_\mathbf{A} = \frac{1}{m}\mathbf{A}^\top\mathbf{A}$. Moreover, the generalized singular value decomposition of input matrices $\mathbf{A} \in \mathbb{R}^{m \times n}$ and $\mathbf{B} \in \mathbb{R}^{m \times n}$ is equivalent to the generalized singular value decomposition

$$\boldsymbol{\Sigma}_\mathbf{A}\boldsymbol{\psi}_i = \lambda_i\boldsymbol{\Sigma}_\mathbf{B}\boldsymbol{\psi}_i, \quad (3.100)$$

with $\boldsymbol{\Sigma}_\mathbf{A} = \frac{1}{m}\mathbf{A}^\top\mathbf{A}$, and $\boldsymbol{\Sigma}_\mathbf{B} = \frac{1}{m}\mathbf{B}^\top\mathbf{B}$.

Matrices of the form $\boldsymbol{\Sigma}_\mathbf{A} = \frac{1}{m}\mathbf{A}^\top\mathbf{A}$ are called auto-covariance matrices. Their properties are briefly summarized and interpreted from the dynamicist's point of view.

The auto-covariance $\boldsymbol{\Sigma}_\mathbf{A}$ gives the covariance of a stochastic process (e.g. \mathbf{A}) with itself at given instances of time. An entry of the covariance matrix holds information about direct or indirect proportionality of two variables.

Let us consider a matrix $\mathbf{X} \in \mathbb{R}^{m \times n}$ which holds the time history of a dynamical system. n holds the number of coordinates, and m is the number of collected time samples. Then, the auto-covariance matrix $\boldsymbol{\Sigma}_\mathbf{X} = \frac{1}{m}\mathbf{X}^\top\mathbf{X} \in \mathbb{R}^{n \times n}$ gives the impact of the change of one coordinate to all others. In other words, the auto-covariance matrix is a kind of sensitivity matrix. It highlights linear inter-coordinate relations, due to the time decay of the mechanical system. This interpretation as a sensitivity matrix is justified (at least for linear systems) next.

From the perspective of a dynamicist, one has to distinguish between

- positive valued entries of $\boldsymbol{\Sigma}_\mathbf{X}$. These are due to a positive change in q_i resulting in a positive change in q_j , and

- negative valued entries of $\Sigma_{\mathbf{x}}$, which are due to a positive change in q_i resulting in a negative change in q_j .

Hence, the signs of the single matrix elements show the tendency of the inter-coordinate relation. The magnitude of an (auto)-covariance matrix is not as easy to interpret. But, at least for the normalized case of (auto)-covariance, the magnitude represents the strength of the linear inter-coordinate relation.

An illustrative example is presented by van Wynsberghe and Cui in [108]. Therein, covariance is detailed in terms of the bilinear two mass oscillator shown in Fig. 3.3. The example consists of two bodies with equal mass $m_1 = m_2 = 1$. They are

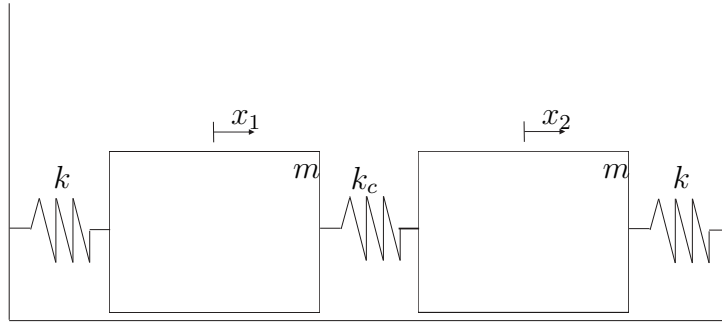


Figure 3.3: Bilinear two mass oscillator, following [108, p.1648]

interconnected by a linear spring with spring stiffness k_c . Both masses are coupled to ground by linear springs with spring stiffness k . The potential energy of this bilinear two mass oscillator reads

$$V = \frac{1}{2}kx_1^2 + \frac{1}{2}kx_2^2 + \frac{1}{2}k_c(x_1 - x_2)^2. \quad (3.101)$$

Therein, x_i is the deviation from the corresponding mass equilibrium. The Eigenvalues λ_i and Eigenvectors Φ_i are calculated from the Hessian matrix

$$\mathbf{H} = \begin{bmatrix} k + k_c & -k_c \\ -k_c & k + k_c \end{bmatrix}. \quad (3.102)$$

They read

$$\boldsymbol{\lambda} = \begin{bmatrix} k \\ k + 2k_c \end{bmatrix}, \text{ and} \quad (3.103)$$

$$\boldsymbol{\Phi} = \begin{bmatrix} 1 & -1 \\ 1 & 1 \end{bmatrix}. \quad (3.104)$$

The Eigenvector matrix contains one symmetric mode Φ_1 , which is the first column vector of Φ . Further, Φ_2 represents the antisymmetric mode related to the second Eigenvalue $\lambda_2 = k + 2k_c$.

By individually investigating the Eigenvector Φ_2 , which is related to Eigenvalue λ_2 , and further assuming $k_c \neq 0$, the Eigenvector suggests a perfectly antisymmetric behavior. Accordingly, in the case of investigating Φ_1 , a perfectly symmetric behavior is pointed out. Hence, in order to represent the actual behavior of the two mass oscillator, which is neither perfectly symmetric nor antisymmetric, both Eigenvectors have to be taken into account.

This is in contrast to the investigation of the covariance matrix $\Sigma_{\mathbf{x}}$. Without detailing the derivation in [108], the normalized position covariance matrix reads

$$\Sigma_{\mathbf{x}} = \begin{bmatrix} 1 & \frac{k_c}{k} \\ \frac{k_c}{k} & 1 \end{bmatrix}. \quad (3.105)$$

Therein, the off-diagonal term k_c/k represents the motion correlation of the two masses in Fig. 3.3. The masses are positively correlated. The magnitude of correlation is linearly depending on the linear coupling spring k_c . This is crucial information, which is not directly predictable from the Eigenvectors.

Next, by applying a constant force F at the left mass the new mass equilibria are statically computed from

$$\mathbf{H} \begin{bmatrix} x_{1,F} \\ x_{2,F} \end{bmatrix} - \begin{bmatrix} F \\ 0 \end{bmatrix} = \mathbf{0}. \quad (3.106)$$

The new equilibrium points are

$$x_{1,F} = \frac{kF}{k^2 - k_c^2}, \text{ and} \quad (3.107)$$

$$x_{2,F} = \frac{k_c F}{k^2 - k_c^2}. \quad (3.108)$$

The sensitivity of $x_{2,F}$, due to a change in $x_{1,F}$, is

$$\frac{x_{2,F}}{x_{1,F}} = \frac{k_c}{k}, \quad (3.109)$$

see [108]. In other words, the force F indirectly affects the second mass with the deflection magnitude depending on k_c .

At this point it should be recalled that k_c/k is the off-diagonal entry of $\Sigma_{\mathbf{x}}$. This enforces the consideration, that the position and velocity covariance matrices may be interpreted as kind of sensitivity matrices.

The assumption of the (auto)-covariance matrix being a kind of sensitivity matrix is further strengthened by the modal representation of an undamped, linear mechanical system.

Consider a system of the form

$$\ddot{\mathbf{x}} + \mathbf{K}\mathbf{x} - \mathbf{f}(t) = \mathbf{0}. \quad (3.110)$$

$\mathbf{x} \in \mathbb{R}^n$ is the vector of DOFs, the constant mass matrix reads $\mathbf{M} = \mathbf{I} \in \mathbb{R}^{n \times n}$, and the constant stiffness matrix is of the form $\mathbf{K} \in \mathbb{R}^{n \times n}$. Further, $\mathbf{f}(t) \in \mathbb{R}^n$ holds the vector of external forces. The n Eigenvectors $\mathbf{v}_i \in \mathbb{R}^n$, are computed from

$$(\mathbf{K} - \omega_i^2 \mathbf{I}) \mathbf{v}_i = \mathbf{0}. \quad (3.111)$$

They are the vibration modes of the system, and ω_i^2 are the according Eigenfrequencies. The system in Eq. (3.110) is approximated by a subset of r relevant modes ($r < n$), which are chosen due to the Eigenfrequencies. Hence, the DOFs are approximated by the Galerkin projection

$$\mathbf{x} \approx \mathbf{V}\mathbf{q}. \quad (3.112)$$

Therein, $\mathbf{V} = [\mathbf{v}_1, \mathbf{v}_2, \dots, \mathbf{v}_r] \in \mathbb{R}^{n \times r}$ and $\mathbf{q} \in \mathbb{R}^r$.

We again collect a matrix $\mathbf{X} \in \mathbb{R}^{n \times m}$ which holds the time history of the n DOFs at m time points. The time history of the DOFs is reformulated as

$$\underbrace{\mathbf{X}}_{n \times m} \approx \underbrace{\mathbf{V}}_{n \times r} \underbrace{\mathbf{Q}}_{r \times m}, \quad (3.113)$$

with

$$\mathbf{Q} = \begin{pmatrix} q_1(t_0) & q_1(t_1) & \dots & q_1(t_m) \\ q_2(t_0) & q_2(t_1) & \dots & q_2(t_m) \\ \dots & \dots & \dots & \dots \\ q_n(t_0) & q_n(t_1) & \dots & q_n(t_m) \end{pmatrix}. \quad (3.114)$$

The according auto-covariance matrix, reads

$$\begin{aligned} \Sigma_{\mathbf{X}} &= \mathbf{X}\mathbf{X}^T \\ &= \begin{bmatrix} \Sigma_{\mathbf{X},11} & \Sigma_{\mathbf{X},12} & \dots & \Sigma_{\mathbf{X},1n} \\ \vdots & \vdots & \vdots & \vdots \\ \Sigma_{\mathbf{X},n1} & \Sigma_{\mathbf{X},n2} & \dots & \Sigma_{\mathbf{X},nn} \end{bmatrix} \\ &= [\mathbf{v}_1, \dots, \mathbf{v}_r] \mathbf{Q}\mathbf{Q}^T [\mathbf{v}_1, \dots, \mathbf{v}_r]^T. \end{aligned} \quad (3.115)$$

Therein, $q_j(t)$ is the time history of the j -th modal coordinate. Obviously, each column in Eq. (3.115) consists of the system modes, scaled by some weighting

factors. As indicated in [35], for the present case of a linear system with $\mathbf{M} = \mathbf{I}$, the matrix elements of $\Sigma_{\mathbf{x}}$ follow the summation rule

$$\{\Sigma_{\mathbf{x}}\}_{jk} = \sum_{l=1}^r v_{jl}v_{kl}\eta_l, \quad (3.116)$$

with

$$\eta_i = \sum_{i=1}^m q_k(t_i)q_k(t_i). \quad (3.117)$$

Therefrom, the following characteristics can be deduced:

1. The auto-covariance matrix is symmetric.
2. The matrix element $\{\Sigma_{\mathbf{x}}\}_{jk}$ connects the physical DOFs x_j and x_k .
3. Each column of $\Sigma_{\mathbf{x}}$ represents a weighted sum of the r modes. Therefore, the system modes should be detectable by e.g. a principal component analysis.
4. Let us consider the transfer function matrix $\mathbf{H}(i\omega) = [H_{jk}(i\omega)]$ in the frequency domain, with i as the imaginary unit. The summation rule of the covariance matrix is then similar to the definition of the single transfer function matrix elements

$$H_{jk}(i\omega) = \sum_{l=1}^r v_{jl}v_{kl}h_l(\omega). \quad (3.118)$$

Therein, $h_l(\omega)$ represents the transfer function of the l -th mode in the frequency domain. Further, the element $H_{jk}(i\omega)$ gives the coupling between the j -th and the k -th DOF of the system. The connection is achieved by the term $v_{jl}v_{kl}$ which can be interpreted as the strength of the coupling. This again strengthens the assumption of the covariance matrix being a kind of sensitivity matrix of the system.

3.4.3 POD - Proper Orthogonal Decomposition

The Proper Orthogonal Decomposition was introduced repeatedly by several researches, in various scientific fields. Probably the first author describing the ideas of POD was Kosambi [56] in 1943. Depending on the particular scientific field, the method's basic intention is also known as Principal Component Analysis ([110, 67, 95]), Karhunen–Loève Expansion [111] or Empirical Orthogonal Functions [73]. POD is utilized to generate low-dimensional approximations of

high-fidelity data in fluid dynamics [96, 61, 103, 13], vibration systems [36, 53, 35], control theory [2], micro electro-mechanical systems [105] and multibody dynamics [31, 30, 69, 100, 99]. This section presents the POD method following [18, 54, 109]: In terms of projection based model order reduction, POD is used to identify an orthogonal subspace \mathcal{Y}_1 to the original space \mathcal{H} . This subspace is split into its dominant part spanned by $\mathbf{V} \in \mathbb{R}^{n \times r}$ with $r \ll n$, and into its less important (and truncated) part spanned by $\mathbf{U} \in \mathbb{R}^{n \times (n-r)}$.

Hence, in analogy with Sec. 3.2.1, POD is applied in terms of a flat Galerkin projection

$$\mathbf{q} \approx \mathbf{V}\mathbf{z}_1. \quad (3.119)$$

For the application of the POD method the original space \mathcal{H} is depicted by measure signals. Consider a time-continuous system of which we take n measures/signals at m discrete instances of time. These are collected in a matrix $\mathbf{X} = [\mathbf{x}_1, \dots, \mathbf{x}_m] \in \mathbb{R}^{n \times m}$ with $m > n$, called the *snapshot matrix*. Following Sec. 3.4.1, POD utilizes the singular value decomposition

$$\mathbf{X} = \mathbf{\Phi}\mathbf{\Sigma}\mathbf{\Psi}^\top, \quad (3.120)$$

to decompose the input matrix \mathbf{X} . It thereby generates an orthogonal subspace \mathcal{Y}_1 based on the signal energy. This subspace is spanned by *Proper Orthogonal Modes* (POMs), which are basis vectors $\phi_i \in \mathbb{R}^n$. They are collected in the matrix $\mathbf{\Phi} \in \mathbb{R}^{n \times n}$. The signal energy is represented by *Proper Orthogonal Values* (POVs) σ_i . These are the singular values, which are collected in the diagonal matrix $\mathbf{\Sigma} \in \mathbb{R}^{n \times m} = \text{diag}(\sigma_1, \dots, \sigma_n)$ in decreasing order. The $m \times m$ matrix $\mathbf{\Psi}$ holds the (in terms of the POD model order reduction unused) right singular vectors.

In analogous manner to the underlying singular value decomposition principles, the POD of the snapshot matrix \mathbf{X} can also be calculated by solving the Eigenproblem

$$(\mathbf{X}\mathbf{X}^\top - \lambda\mathbf{I})\phi_i = \mathbf{0}. \quad (3.121)$$

Note that $\mathbf{X}\mathbf{X}^\top$ is an auto-covariance matrix, as introduced in Sec. 3.4.2. In this case, proper orthogonal modes are directly computed as the Eigenvectors of Eq. (3.121). POVs are given by the square-roots of the Eigenvalues ($\sigma_i = \sqrt{\lambda_i}$). Hence, the POD may be seen as the maximization problem, cf. [109],

$$\max_{\mathbf{\Phi}} \left\{ \lambda(\mathbf{\Phi}) = \|\mathbf{X}\mathbf{\Phi}\|^2 \right\} = \max_{\mathbf{\Phi}} \left\{ \lambda(\mathbf{\Phi}) = \mathbf{\Phi}^\top \mathbf{X}\mathbf{X}^\top \mathbf{\Phi} \right\}. \quad (3.122)$$

Its goal is to find basis vectors $\mathbf{\Phi}_i$ which include the maximum of the signal energy of \mathbf{X} .

The model order reduction subspace is spanned by a subset of r proper orthogonal

modes. These are collected in $\mathbf{\Phi}_r \in \mathbb{R}^{n \times r}$, and hence $\mathbf{V} = \mathbf{\Phi}_r$.

Each POM ϕ_i is uniquely related to its corresponding proper orthogonal value σ_i . According to [53], the energy measured in the direction of a specific proper orthogonal mode is equal to the related squared proper orthogonal value. Hence, the decay of POVs is used to define a set of proper orthogonal modes which spans the model order reduction subspace for the flat Galerkin projection. To this end, the error-measure

$$\varepsilon_{\text{signal-energy}} = 1 - \sum_{k=1}^r \sigma_k^2, \quad (3.123)$$

based on the truncated normalized signal energy, can be utilized, cf. [109]. Note that such absolute error bounds are highly system dependent. Therefore, absolute maximum error values cannot be stated in general. Quantifying the proper orthogonal value decay by plotting them in a logarithmic scale may be a more intuitive method.

The POD method is illustrated by the example of a planar two mass oscillator, depicted in Fig. 3.4. The model consists of two bodies with mass m . The first

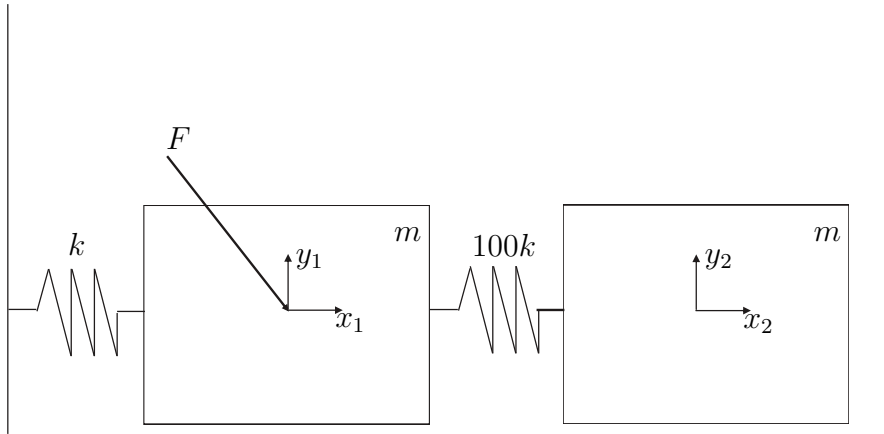


Figure 3.4: Two mass oscillator

body is coupled to ground by a linear spring with spring stiffness $k_1 = k$. Both bodies are connected by another linear spring with spring stiffness $k_2 = 100k$. The mechanism consists of the $n = 4$ DOFs

$$\mathbf{q}(t) = [x_1(t), y_1(t), x_2(t), y_2(t)]^T. \quad (3.124)$$

It is actuated by an external force $F(t)$ acting at the first body's center of gravity. The mass is forced to move in x direction only. Hence, the system is subject to the constraint equations

$$\mathbf{C} = [y_1, y_2]^T = \mathbf{0} \quad (3.125)$$

with the according constraint Jacobian

$$\mathbf{C}_q = \begin{bmatrix} 0 & 1 & 0 & 0 \\ 0 & 0 & 0 & 1 \end{bmatrix}. \quad (3.126)$$

Initial conditions are set to

$$\mathbf{q}_0 = [x_{1,0}, y_{1,0}, x_{2,0}, y_{2,0}]^\top = \mathbf{0}. \quad (3.127)$$

Summing up, the model consists of $n = 4$ differential equations, subject to $m = 2$ algebraic equations.

The system is solved in the time interval $t \in [t_0, t_{\text{end}}]$, and h equally spaced snapshots of the model DOFs are collected as column vectors in the snapshot matrix

$$\mathbf{X} = \begin{bmatrix} q_1(t_0) & \dots & q_1(t_{\text{end}}) \\ q_2(t_0) & \dots & q_2(t_{\text{end}}) \\ q_3(t_0) & \dots & q_3(t_{\text{end}}) \\ q_4(t_0) & \dots & q_4(t_{\text{end}}) \end{bmatrix} = \begin{bmatrix} 0 & \dots & x_{1,h} \\ 0 & \dots & 0 \\ 0 & \dots & x_{2,h} \\ 0 & \dots & 0 \end{bmatrix} \in \mathbb{R}^{n \times h}. \quad (3.128)$$

As long as the excitation does not correlate with the Eigenfrequencies of the second mode (the out of phase mode), the motion of the second mass is dominated by the first mass. This is due to the choice of $k_2 = 100k_1$. The POD method is applied to \mathbf{X} , utilizing the singular value decomposition approach

$$\mathbf{X} = \mathbf{\Phi} \mathbf{\Sigma} \mathbf{\Psi}^\top.$$

For the present example, it reads

$$\underbrace{\begin{bmatrix} x_{1,0} & \dots & x_{1,h} \\ 0 & \dots & 0 \\ x_{2,0} & \dots & x_{2,h} \\ 0 & \dots & 0 \end{bmatrix}}_{\mathbf{X}} = \underbrace{\begin{bmatrix} \phi_{11} & \dots & \phi_{14} \\ \phi_{21} & \dots & \phi_{24} \\ \phi_{31} & \dots & \phi_{34} \\ \phi_{41} & \dots & \phi_{44} \end{bmatrix}}_{\mathbf{\Phi}} \underbrace{\begin{bmatrix} \sigma_1 & 0 & 0 & 0 & \dots & 0 \\ 0 & \sigma_2 & 0 & 0 & \dots & 0 \\ 0 & 0 & \sigma_3 & 0 & \dots & 0 \\ 0 & 0 & 0 & \sigma_4 & \dots & 0 \end{bmatrix}}_{\mathbf{\Sigma}} \mathbf{\Psi}_{h \times h}^\top. \quad (3.129)$$

The normalized and squared singular values compute to

$$\mathbf{\Sigma}^2 = \begin{bmatrix} 0.897 & 0 & 0 & 0 \\ 0 & 4.0E-8 & 0 & 0 \\ 0 & 0 & 0 & 0 \\ 0 & 0 & 0 & 0 \end{bmatrix}, \quad (3.130)$$

and the matrix of right singular vectors reads

$$\mathbf{\Phi} = \begin{bmatrix} -0.707 & -0.707 & 0 & 0 \\ 0 & 0 & 1 & 0 \\ -0.707 & 0.707 & 0 & 0 \\ 0 & 0 & 0 & 1 \end{bmatrix}. \quad (3.131)$$

In accordance with Sec. 3.2, the POD constructs a subspace \mathcal{Y}_1 to the original space \mathcal{H} . It is spanned by the orthogonal column vectors (POMs) $\phi_i \in \mathbb{R}^n$, of $\Phi \in \mathbb{R}^{n \times n}$.

Investigating the normalized and squared singular values (POVs) σ_i^2 in Eq. (3.130),

- one large (dominant) proper orthogonal value $\sigma_1^2 = 0.897$,
- one small POV $\sigma_2^2 = 4.0E - 8$, and
- two zero valued (irrelevant) POVs σ_3^2 and σ_4^2 are examined.

Each proper orthogonal mode is explicitly related to one proper orthogonal value, (e.g. $\phi_1 \sim \sigma_1$). Therefore, it can be deduced from Eq. (3.131) that

- the dominant part of \mathcal{Y}_1 is represented by the first proper orthogonal mode ϕ_1 . It points out an equal motion of both masses, due to the very stiff coupling $k_2 = 100k_1$.
- the less important part of \mathcal{Y}_1 is represented by the second proper orthogonal mode ϕ_2 , which is the reciprocal to the first.
- the irrelevant part of \mathcal{Y}_1 is represented by the third and fourth proper orthogonal modes ϕ_3, ϕ_4 , which are the (constrained) y - motions of both masses.

Hence, \mathcal{Y}_1 is split by choosing only the first proper orthogonal value σ_1^2 as relevant. The matrix of POMs Φ is split accordingly. The submatrix of dominant proper orthogonal modes is of dimension $\Phi_r \in \mathbb{R}^{n \times r}$ with $r = 1$.

The model order reduction matrix finally reads

$$\Phi_r = [-0.707, 0, -0.707, 0]^T. \quad (3.132)$$

POD has been investigated intensely in the last two decades. Amongst other, the following interesting properties were identified:

1. Centering the input data

Consider a snapshot matrix $\mathbf{X} \in \mathbb{R}^{n \times m}$ of n measure signals taken at m equally spaced instances of time. According to Chatterjee, cf. [18], it is common to subtract the row mean from each row of this matrix \mathbf{X} in a preconditioning step. This preconditioning should ensure the data in \mathbf{X} to be centered around the data origin (mean-centered). Furthermore, as a subspace basis vector (POM) has to pass through the origin POMs are sensitive to such preconditioning, as depicted in Fig. 3.5.

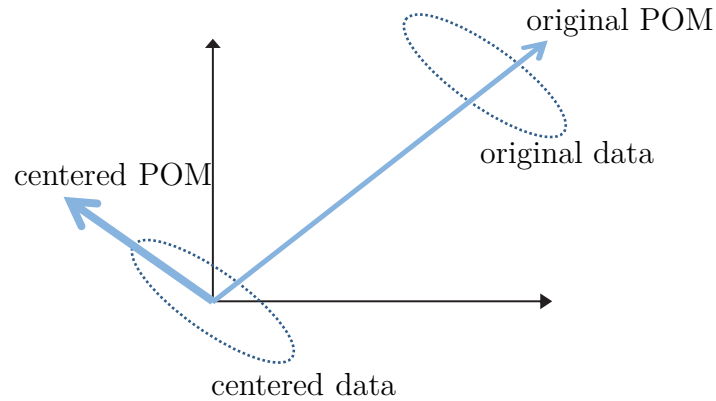


Figure 3.5: Centering the input data, following [18, p.812]

On the other hand, following [72], it can not be clearly stated whether such data-centering is advantageous in general. Therein it is suggested that the user should decide case-sensitively.

From the dynamicist's point of view, this data centering is judged critically. Assume the n rows of \mathbf{X} as the \mathbf{q} coordinates of a body in space measured at m equally spaced instances of time. The proposed row-preconditioning would correspond to calculating the time average of each coordinate q_i and subtracting it from the corresponding coordinate time decay. Hence, any constant offset or steady component of the coordinate time decay would be included in the time average. As a result, such steady components would be lost. The outcome would be an MBS behavior different to the actual.

As an example, consider the two mass oscillator in Fig. 3.6. Both mass positions are measured from the same point $([0; 0])$. Due to this point of

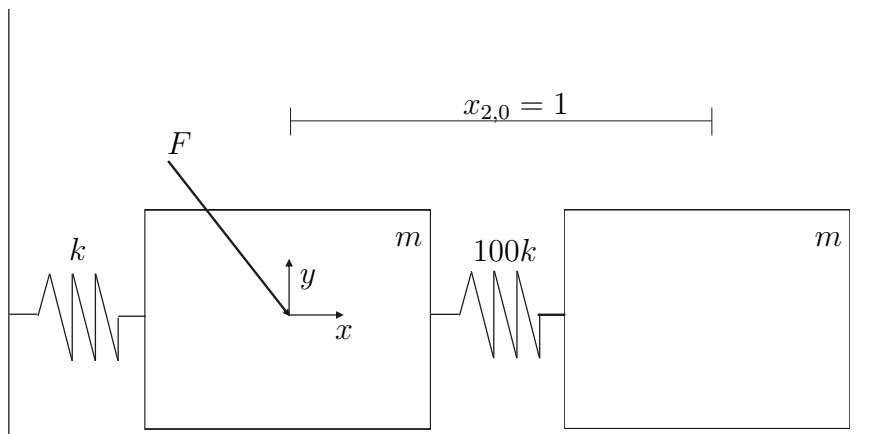


Figure 3.6: Two mass oscillator

measurement, the initial conditions change into

$$\mathbf{q}_0 = [x_{1,0}, y_{1,0}, x_{2,0}, y_{2,0}]^\top = [0, 0, 1, 0]^\top. \quad (3.133)$$

The snapshot matrix reads

$$\mathbf{X} = \begin{bmatrix} q_1(t_0) & \dots & q_1(t_{\text{end}}) \\ q_2(t_0) & \dots & q_2(t_{\text{end}}) \\ q_3(t_0) & \dots & q_3(t_{\text{end}}) \\ q_4(t_0) & \dots & q_4(t_{\text{end}}) \end{bmatrix} = \begin{bmatrix} 0 & \dots & x_{1,h} \\ 0 & \dots & 0 \\ 1 & \dots & x_{2,h} \\ 0 & \dots & 0 \end{bmatrix} \in \mathbb{R}^{n \times h}. \quad (3.134)$$

On the one hand, if this snapshot data is decomposed directly (without mean-centering), the POD of Eq. (3.134) computes to

$$\Sigma^2 = \begin{bmatrix} 0.9969 & 0 & 0 & 0 \\ 0 & 0.0031 & 0 & 0 \\ 0 & 0 & 0 & 0 \\ 0 & 0 & 0 & 0 \end{bmatrix}, \quad (3.135)$$

and

$$\Phi_{nc} = \begin{bmatrix} -0.193 & -0.981 & 0 & 0 \\ 0 & 0 & 1 & 0 \\ -0.981 & 0.193 & 0 & 0 \\ 0 & 0 & 0 & 1 \end{bmatrix}. \quad (3.136)$$

On the other hand, mean-centering of these snapshots is equivalent to subtracting the initial conditions at each time step. The POD results of the mean centered snapshots are equivalent to Eq. (3.131) and read

$$\Phi_c = \begin{bmatrix} -0.707 & -0.707 & 0 & 0 \\ 0 & 0 & 1 & 0 \\ -0.707 & 0.707 & 0 & 0 \\ 0 & 0 & 0 & 1 \end{bmatrix}. \quad (3.137)$$

Nevertheless, both proper orthogonal mode matrices correctly represent the original data. It is only the interpretation of the proper orthogonal modes, which may be easier or not. For the present MBS models under consideration, taken snapshots are naturally not mean-centered. Within this dissertation, mean-centering will not be carried out, as the risk of violating constraint equations appears as too high.

2. Correlation of Proper Orthogonal Modes with Vibration Modes

POMs can be related to normal vibration modes of discrete vibration systems

with constant mass matrices, cf. [36]. This property is briefly outlined for the undamped, linear system

$$\mathbf{M}\ddot{\mathbf{x}} + \mathbf{K}\mathbf{x} = \mathbf{0}. \quad (3.138)$$

We assume symmetric, positive definite mass and stiffness matrices $\mathbf{M} \in \mathbb{R}^{n \times n}$, $\mathbf{K} \in \mathbb{R}^{n \times n}$. $\mathbf{x} \in \mathbb{R}^n$ holds the vector of DOFs. The system can be transformed into

$$\ddot{\hat{\mathbf{x}}} + \mathbf{M}^{-1/2}\mathbf{K}\mathbf{M}^{-1/2}\hat{\mathbf{x}} = \mathbf{0}, \quad (3.139)$$

with \mathbf{I} as the effective mass matrix using the relation $\mathbf{x} = \mathbf{M}^{-1/2}\hat{\mathbf{x}}$. For such a system, the normalized normal modes \mathbf{v}_i satisfy the orthogonality property $\mathbf{v}_i^\top \mathbf{v}_j = \delta_{ij}$. The motion of all DOFs can be expressed by the series of normal modes

$$\mathbf{x}(t) = a_1(t)\mathbf{v}_1 + \cdots + a_n(t)\mathbf{v}_n. \quad (3.140)$$

Therein,

$$\begin{pmatrix} a_1(t_0) & a_1(t_1) & \cdots & a_1(t_m) \\ a_2(t_0) & a_2(t_1) & \cdots & a_2(t_m) \\ \vdots & \vdots & \ddots & \vdots \\ a_n(t_0) & a_n(t_1) & \cdots & a_n(t_m) \end{pmatrix} \quad (3.141)$$

represents the time modulus of the normal modes. The snapshot matrix of this system reads

$$\mathbf{X} = [\mathbf{x}(t_1) \cdots \mathbf{x}(t_m)] = \begin{bmatrix} \underbrace{\mathbf{v}_1}_{n \times 1} \underbrace{\mathbf{a}_1^\top}_{1 \times m} + \cdots + \mathbf{v}_n \mathbf{a}_n^\top \end{bmatrix} \in \mathbb{R}^{n \times m}, \quad (3.142)$$

with m as the number of time samples. According to [36] the proper orthogonal modes of the snapshot matrix can be related to the normal modes. To this end, the POD approach is applied in terms of the Eigendecomposition

$$(\boldsymbol{\Sigma}_{\mathbf{X}} - \lambda \mathbf{I}) \boldsymbol{\phi} = \mathbf{0} \quad (3.143)$$

of the covariance matrix $\boldsymbol{\Sigma}_{\mathbf{X}} = (1/m)\mathbf{X}\mathbf{X}^\top$. In order to show that a proper orthogonal mode $\boldsymbol{\phi}_i$ converges to a modal vector of the underlying mechanical system, the covariance matrix $\boldsymbol{\Sigma}_{\mathbf{X}}$ is multiplied with a modal vector \mathbf{v}_j from the right

$$\boldsymbol{\Sigma}_{\mathbf{X}} \mathbf{v}_j = \frac{1}{m} \left[\mathbf{v}_1 \mathbf{a}_1^\top + \cdots + \mathbf{v}_n \mathbf{a}_n^\top \right] \left[\mathbf{v}_1 \mathbf{a}_1^\top + \cdots + \mathbf{v}_n \mathbf{a}_n^\top \right]^\top \mathbf{v}_j. \quad (3.144)$$

Recalling the orthogonality relation $\mathbf{v}_i^\top \mathbf{v}_j = \delta_{ij}$, Eq. (3.144) reduces to

$$\Sigma_{\mathbf{X}} \mathbf{v}_j = \frac{1}{m} \left[\mathbf{v}_1 \mathbf{a}_1^\top \mathbf{a}_j + \cdots + \mathbf{v}_n \mathbf{a}_n^\top \mathbf{a}_j \right]. \quad (3.145)$$

Let us assume distinct Eigenfrequencies of the mechanical system. Then, due to the orthogonality of the system's normal modes \mathbf{v}_i , the according time moduli vectors \mathbf{a}_i are orthogonal to each other. Therefore, in the case of an infinite set of time samples ($m \rightarrow \infty$)

$$\frac{1}{m} \mathbf{v}_i \mathbf{a}_i^\top \mathbf{a}_j \rightarrow 0, \quad (3.146)$$

if $i \neq j$, cf. [36]. The term $\frac{1}{m} \mathbf{v}_j \mathbf{a}_j^\top \mathbf{a}_j$, which is proportional to \mathbf{v}_j is the only one remaining. Hence, a proper orthogonal mode ϕ_i of $\mathbf{X}\mathbf{X}^\top$ converges to a modal vector \mathbf{v}_j of the vibrating mechanical system.

For further insight into this topic and analogies to nonlinear systems, the interested reader is referred to [36, 35, 53, 55]

3. POD is snapshot-sensitive

POD is very powerful in investigating given input matrices on their essential content. Nevertheless, the quality of the POD approach is related to the quality of the collected snapshots. For instance, in the case of mixing physical coordinates with strain measures of the system, one has to ensure proper scaling of these different input variables. Otherwise, the outcome of the POD method may not be meaningful.

4. POD and cyclic coordinates

As already mentioned, the POD method reproduces an input matrix by a linear combination of proper orthogonal modes, see Eq. (3.93). This brings up limitations, as in the following case:

Consider an arbitrary set of (unnecessary) points on a plane. Further, consider one (meaningful) circle on the same plane, as depicted in Fig. 3.7. The according POD input matrix is of the form $\mathbf{X} \in \mathbb{R}^{n \times m}$, with $n = 2$ rows consisting of the x and y coordinates of all m points. Let us assume, we would like to extract the circle out of the set of arbitrary points and represent it by the one coordinate (the angle) it is characterized by.

The POD of such an input matrix delivers one large valued proper orthogonal value σ_1^2 , and one small valued POV σ_2^2 . Actually, POD is not able to distinguish between the coordinates of the arbitrary points and the circle, cf. [18]. This is pointed out in Fig. 3.7 which shows an insufficient representation

$$\mathbf{X} \approx \tilde{\mathbf{X}} = \sigma_1 \phi_1 \psi_1 \quad (3.147)$$

of the circle due to the use of the first (red colored) proper orthogonal mode only. In order to correctly reproduce the circle all proper orthogonal modes have to be included into

$$\mathbf{X} = \tilde{\mathbf{X}} = \sigma_1 \phi_1 \psi_1 + \sigma_2 \phi_2 \psi_2. \quad (3.148)$$

As it is pointed out, the mentioned data can not be approximated by a low-dimensional representation, as Eq. (3.148) is an exact operation.

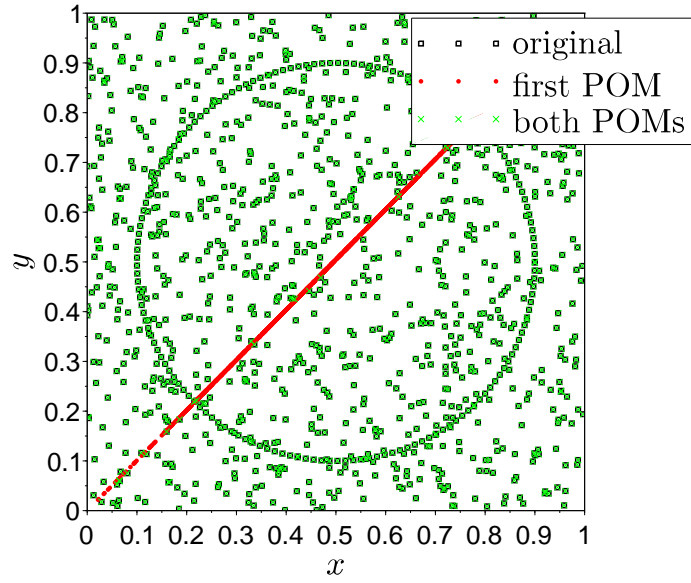


Figure 3.7: POD and cyclic coordinates

To cut a long matter short, POD is (in general) not able to identify trigonometric functions.

5. POD signal energy

The present section reviewed POD as a method which investigates the signal energy of the input matrix. In terms of dynamical systems, it would be wishful to relate the signal energy to the kinetic energy of the underlying system. Although this is not possible in general, see [18], the signal energy can be related to the deformation energy of some systems. This approach is called the *weighted* POD method [109]:

For systems with a constant, symmetric and positive definit stiffness matrix $\mathbf{K} \in \mathbb{R}^{n \times n}$, like Eq. (3.138), the weighted POD method in terms of the

Eigenvalue decomposition reads

$$\mathbf{X}^T \mathbf{K} \mathbf{X} \bar{\boldsymbol{\psi}}_i = \lambda_i \bar{\boldsymbol{\psi}}_i. \quad (3.149)$$

Instead of decomposing the classical correlation matrix $\mathbf{X}^T \mathbf{X}$, the weighted correlation matrix $\mathbf{X}^T \mathbf{K} \mathbf{X}$ is processed. Note that variables denoted with an overbar describe weighted results, like the weighted proper orthogonal value $\bar{\sigma}_i^2 = \bar{\lambda}_i$, or the weighted right singular vector $\bar{\boldsymbol{\psi}}_i$. The unweighted proper orthogonal modes of the original input matrix can be computed therefrom by

$$\begin{aligned} \boldsymbol{\phi}_i &= \mathbf{K}^{-1/2} \bar{\boldsymbol{\phi}}_i \\ &= \frac{1}{\sqrt{\bar{\lambda}_i}} \mathbf{K}^{-1/2} \mathbf{K}^{1/2} \mathbf{X} \bar{\boldsymbol{\psi}}_i \\ &= \frac{1}{\sqrt{\bar{\lambda}_i}} \mathbf{X} \bar{\boldsymbol{\psi}}_i. \end{aligned} \quad (3.150)$$

Hence, the derived proper orthogonal modes $\boldsymbol{\phi}_i$ correspond to the original input data - to the actual mechanical model. But in this case, the proper orthogonal modes are characterized in terms of weighted singular values $\bar{\sigma}_i$, which characterize the deformation energy of the dynamical system. Therefore, the model order reduction subspace is selectable due to an energy measure, which is well-known in the field of mechanics.

3.4.4 SOD - Smooth Orthogonal Decomposition

The Smooth Orthogonal Decomposition (SOD) was introduced by Chelidze & Zhou [20] only a few years ago. The method's original intent was to overcome POD related limitations in the vibration mode identification of (un-)damped free vibration systems. It is shown therein, that the SOD approach allows to identify the normal vibration modes without any knowledge of the underlying mass matrix of the system. In that sense, SOD is a data analysis method, which allows to extract linear normal modes of vibration systems.

The method was extended to systems with local nonlinearities in [19, 9, 34], and it was further applied in terms of biomedical engineering in [91]. Applications as a model reduction tool can be found in [8, 51, 52, 98]. Chelidze and Ilbeigi [19, 51, 52] pointed out that SOD is able to outperform POD in the construction of reduced order models for linear dynamical systems subject to concentrated and state dependent forces.

The upcoming introduction to SOD follows the work of [20, 21, 19], and is related to the reviews of the generalized singular value decomposition and covariance in Sec. 3.4.1.1 and Sec. 3.4.2.

SOD is closely related to the POD method and also applied in terms of a flat Galerkin projection. Similar to POD, snapshots are decomposed and ranked due to their implied signal energy. In contrast to the POD approach, SOD investigates not only position snapshots $\mathbf{X} \in \mathbb{R}^{m \times n}$, but also the velocity snapshot matrix $\dot{\mathbf{X}} \in \mathbb{R}^{m \times n}$. In terms of the present field of application n is the number of coordinates, and m is the number of time points. Hence, a column of \mathbf{X} holds the time decay of a single position coordinate. Accordingly, a column of $\dot{\mathbf{X}}$ represents the time decay of a single velocity coordinate.

The SOD is computed by the generalized singular value decomposition

$$\begin{aligned}\mathbf{X} &= \mathbf{C}\mathbf{D}\mathbf{\Phi}^\top \\ \dot{\mathbf{X}} &= \mathbf{E}\mathbf{F}\mathbf{\Phi}^\top.\end{aligned}\quad (3.151)$$

For the SOD method it is explicitly stated by Chelidze [21], that the column vectors of \mathbf{X} and $\dot{\mathbf{X}}$ have to be mean-centered.

The SOD is characterized in terms of the generalized singular value decomposition approach first. Recalling Sec. 3.4.1.1, both input matrices are decomposed such that their row space $\mathbf{\Phi} \in \mathbb{R}^{n \times n}$ is equal.

The model order reduction subspace \mathbf{V} is spanned by a subset of Smooth Projection Modes (SPM), which are column vectors \mathbf{v}_i of the inverse of the transposed matrix of right basis vectors $\mathbf{\Phi}^{-\top} \in \mathbb{R}^{n \times n}$. The right basis vectors ϕ_i itself are called Smooth Orthogonal Modes (SOM). Smooth proper modes and smooth orthogonal modes are characterized by so-called Smooth Orthogonal Values (SOV).

Note that $\mathbf{D} = \text{diag}(\sigma_{\mathbf{X},1}, \dots, \sigma_{\mathbf{X},n})$ and $\mathbf{F} = \text{diag}(\sigma_{\dot{\mathbf{X}},1}, \dots, \sigma_{\dot{\mathbf{X}},n})$ hold singular values to the corresponding input matrix, but the actual smooth orthogonal values σ_i^2 are derived from the term-by-term division of $\text{diag}(\mathbf{D}^\top \mathbf{D})$ and $\text{diag}(\mathbf{F}^\top \mathbf{F})$. SOD may also be carried out by solving the generalized Eigenvalue decomposition

$$(\mathbf{\Sigma}_{\mathbf{X}} - \lambda_i \mathbf{\Sigma}_{\dot{\mathbf{X}}}) \mathbf{v}_i = \mathbf{0}.\quad (3.152)$$

The used position and velocity auto-correlation matrices read $\mathbf{\Sigma}_{\mathbf{X}} = \frac{1}{m} \mathbf{X}^\top \mathbf{X}$ and $\mathbf{\Sigma}_{\dot{\mathbf{X}}} = \frac{1}{m} \dot{\mathbf{X}}^\top \dot{\mathbf{X}}$. In terms of the generalized Eigenvalue decomposition, smooth orthogonal modes are the Eigenvalues λ_i , and SPMs are the Eigenvectors \mathbf{v}_i .

According to Chelidze [21], the SOD may be interpreted as the maximum variance problem

$$\max_{\mathbf{\Phi}} \left\{ \lambda(\mathbf{V}) = \frac{\|\mathbf{X}\mathbf{V}\|^2}{\|\dot{\mathbf{X}}\mathbf{V}\|^2} \right\} = \max_{\mathbf{\Phi}} \left\{ \lambda(\mathbf{V}) = \frac{\mathbf{V}^\top \mathbf{\Sigma}_{\mathbf{X}} \mathbf{V}}{\mathbf{V}^\top \mathbf{\Sigma}_{\dot{\mathbf{X}}} \mathbf{V}} \right\}.\quad (3.153)$$

This maximization problem may be again interpreted as to find basis vectors \mathbf{v}_i which include the maximum of the signal energy of \mathbf{X} . But, at the same time, the

basis vectors should be as smooth in time as possible. This is indicated by the minimization problem

$$\min_{\Phi} \|\dot{\mathbf{X}}\mathbf{V}\|^2, \quad (3.154)$$

which is the denominator of Eq. (3.153).

When talking about an interpretation of the SOD, the following statements are helpful:

According to Cheldize [21, p.462]:

'The idea [of SOD] is that given noisy multivariate measurements that contain some deterministic (i.e., smooth in time) signals one needs to look for the projections that are smooth in time to identify deterministic trends. At the same time one needs to require the maximum possible variance of the projections to eliminate constant projections.'

Furthermore, Ilbeigi [51, p. 4] defines the magnitude of a smooth orthogonal value as:

'The degree of smoothness of the coordinates is described by the magnitude of the corresponding SOV. Thus, the greater in magnitude the smooth orthogonal value, the smoother in time is the corresponding coordinate.'

Both statements highlight the importance of the minimization problem in Eq. (3.154). The motion of an unforced linear system, subject to free vibration, typically combines two aspects:

1. A smooth motion combines large deflections with slow dynamics.
2. A non-smooth (rough) motion combines small deflections with high dynamics.

SOD emphasis on processes of the first kind. The basis vectors are chosen such that the signal energy of the motions subject to low (smooth) dynamics is maximized. Motions with high dynamics are treated as subordinate. This is the case for linear systems, which are describable by the Eigenvalue problem

$$\mathbf{K}\mathbf{v}_i = \omega_i^2 \mathbf{M}\mathbf{v}_i. \quad (3.155)$$

The covariance matrix $\Sigma_{\mathbf{x}}$ is related to $\mathbf{K}\mathbf{v}_i$, which may be seen as a displacement term that is somehow connected to the potential energy of the linear system. Further, the covariance matrix $\Sigma_{\dot{\mathbf{x}}}$ is related to $\omega_i^2 \mathbf{M}\mathbf{v}_i$, which may be seen as somehow connected to the kinetic energy of the linear system. Hence, SOD performs well if the underlying system is linear and representable by the above Eigenvalue problem.

Its performance is also pointed out by its outstanding ability to identify vibration modes of linear systems, cf. [20]. On the other hand, for the MBS systems under consideration such a connection is not clearly drawable. This is due to MBS being typically configuration dependent, nonlinear, and furthermore, commonly subject to large body motions.

In the upcoming section, the performance of the SOD approach is compared to the POD method, based on a redundantly formulated MBS example.

3.4.5 Applicability of A Posteriori Methods

The presented a posteriori model order reduction methods originate from measurement data analysis. As long as the collected snapshot data is chosen sufficiently, model order reduction subspace generation is possible for ODEs, partial differential equations, and DAEs.

Nevertheless, the universal applicability to arbitrary snapshot data is also a drawback. In order to collect the mandatory snapshots, the original system has to be computed forward in time at least once. This circumstance reduces the applicability of the presented a posteriori methods to repetitive simulation tasks like control engineering, parameter identification, wear monitoring, etc.

MOR of the redundant MBS model in Eqs. (2.46) utilizing the POD approach has been introduced by Ebert [30]. Therein, the POD approach is applied to position level snapshots. It is further stated explicitly, that only the number of physical coordinates is reducible. Ebert points out, that a reduction of the algebraic equations (the constraint equations) is not allowed as this may lead to unphysical phenomena.

Another application to redundant MBS systems can be found in Masoudi et al. [69]. Therein, the system of DAEs is reduced into a Baumgarte stabilized set of ODEs, which is an intense change in the systems character.

The appliance of the SOD approach to a redundant MBS model was first formulated by the author in Stadlmayr & Witteveen [98]. Other applications of the SOD approach to the present MBS are, to the best knowledge of the author, not known. This section compares the POD and SOD approach to the system of DAEs under consideration, following [98].

Starting from the original MBS system

$$\begin{aligned} \mathbf{M}(\mathbf{q}) \ddot{\mathbf{q}} + \mathbf{C}_q^\top(\mathbf{q}) \boldsymbol{\lambda} &= \mathbf{Q}(\mathbf{q}, \dot{\mathbf{q}}) \\ \mathbf{C}(\mathbf{q}) &= \mathbf{0}, \end{aligned} \quad (3.156)$$

the reduced order model

$$\begin{aligned} \mathbf{V}^\top \mathbf{M}(\tilde{\mathbf{q}}) \mathbf{V} \ddot{\tilde{\mathbf{q}}}_r + \mathbf{V}^\top \mathbf{C}_q^\top(\tilde{\mathbf{q}}) \boldsymbol{\lambda} &= \mathbf{V}^\top \mathbf{Q}(\tilde{\mathbf{q}}, \dot{\tilde{\mathbf{q}}}) \\ \mathbf{C}(\tilde{\mathbf{q}}) &= \mathbf{0}, \end{aligned} \quad (3.157)$$

is generated utilizing the flat Galerkin projection

$$\mathbf{q} \approx \tilde{\mathbf{q}} = \mathbf{V}\mathbf{q}_r. \quad (3.158)$$

The reduction subspace $\mathbf{V} \in \mathbb{R}^{n \times r}$ is spanned by proper orthogonal modes or SPMs, respectively. The POD and SOD subspace generation will be compared by the numerical example of a cart-pendulum system, utilizing the above reduced order model.

Example:

The MBS model of the rigid cart-pendulum presented in Fig. 3.8 is generated using the open source tool FreeDyn, cf. [41]. The FreeDyn modeling strategy utilizes a redundant set of three translational coordinates and four rotational Euler parameters. Since the example consists of two bodies, the present MBS model is described by $n = 14$ physical coordinates. The MBS model is forced by a sinusoidal force $F(t) = \sin(4\pi t)[\text{N}]$ at the carts CoG. It is further coupled to ground by a linear spring with spring stiffness $k = 1[\text{N}/\text{mm}]$. The MBS model is subject to gravity, which acts in negative y -direction.

The cart is constrained to a 1D movement along the diagonal of the $x - y$ plane. Furthermore, the pendulum is coupled to the cart by a hinge-joint around the z -axis. In total $m_{\text{ext}} = 8$ external constraints and $m_{\text{inner}} = 2$ Euler constraints are introduced. The MBS model is solved in the open source program Scilab [90]

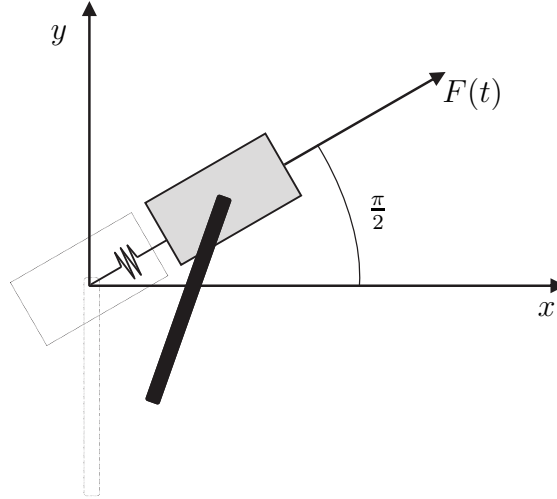


Figure 3.8: Original cart-pendulum model

utilizing an HHT-solver [50] algorithm in the time-interval $t \in [0, 10]$ seconds. The time step size is set to $\Delta t = 0.01$ [s]. Therefore, $h = 1001$ equally spaced position and velocity snapshots of all $n = 14$ physical coordinates are collected in the

snapshot matrices $\mathbf{X} \in n \times h$ and $\dot{\mathbf{X}} \in n \times h$. The time history of the pendulums rotational e_3 parameter is representatively shown in Fig. 3.9. The snapshot matrices

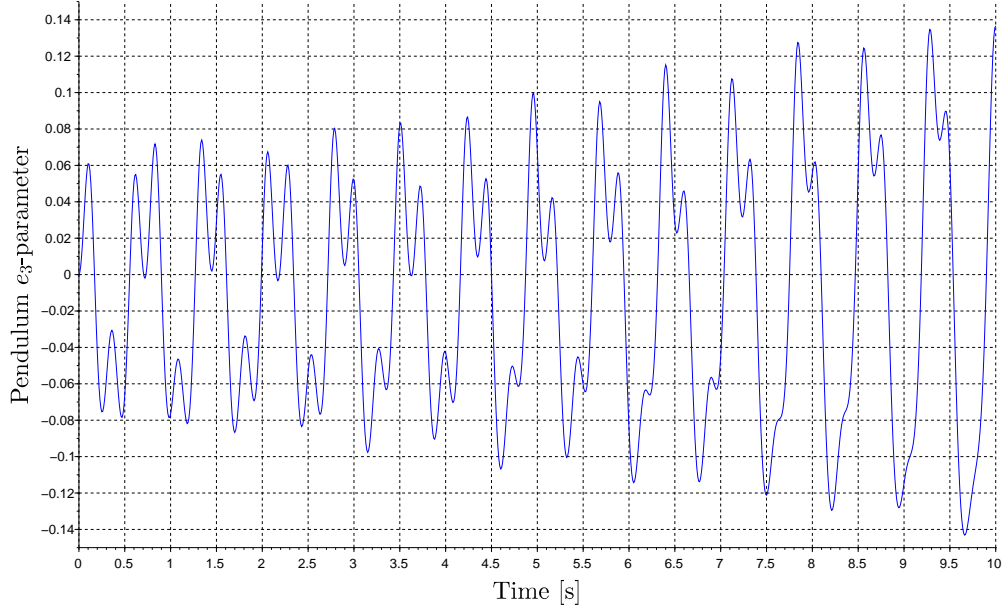


Figure 3.9: Time history of the pendulum's rotational e_3 coordinate

are used to compute proper orthogonal values and smooth orthogonal values, following Sec. 3.4.1. The POD method points out a major decrease in signal energy (about 10^{10} in magnitude) from σ_6 to σ_7 . This is indicated by the vertical blue dashed lines in Fig. 3.10. Hence, the projection matrix $\mathbf{V} \in \mathbb{R}^{n \times r}$ consists of the first six column vectors (POMs) of Φ . Figure 3.11 points out the high consistency of the original MBS model and the POD-reduced MBS model. As SOD is closely related to POD, its model order reduction ability is expected to be of similar quality. Investigating the decay of smooth orthogonal values in Fig. 3.10, a tremendous drop in magnitude from σ_1 to σ_2 is recognized first. Another drop is found from σ_8 to σ_9 , indicated by the vertical red dashed lines. According to these drops, the first potential SOD subspace, is spanned by the first SOM only.

Simulation results point out, that the one dimensional SOD subspace is insufficient to correctly approximate the original system behavior, as the HHT solver is not able to meet its internal error bounds and therefore aborts the simulation.

The simulation of the reduced order model is repeated, utilizing the SOD subspace related to the second drop from σ_8 to σ_9 . This subspace is spanned by the first

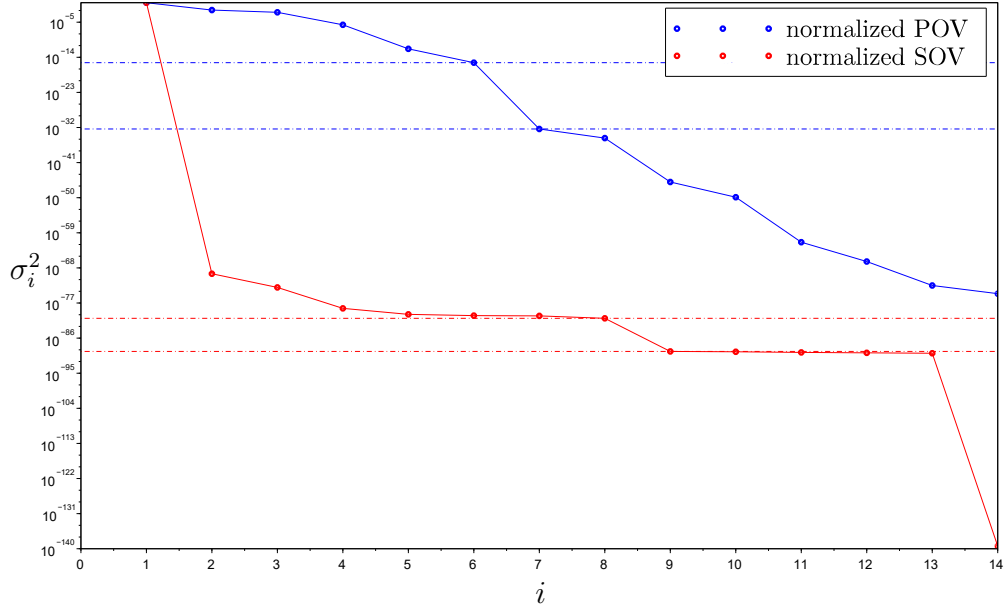


Figure 3.10: Proper orthogonal values - Reduced cart-pendulum model

eight smooth orthogonal modes. Unfortunately, the HHT solver is again not able to successfully solve the resulting reduced order model.

Interestingly, when looking at Fig. 3.10, there is hardly any similarity between the smooth orthogonal value and proper orthogonal value decay. Therefore, the snapshot covariance matrices $\Sigma_{\mathbf{X}} = \mathbf{X}\mathbf{X}^T$ and $\Sigma_{\dot{\mathbf{X}}} = \dot{\mathbf{X}}\dot{\mathbf{X}}^T$ are investigated on their regularity.

Although the MBS model consists of $n = 14$ DOFs, numerical rank computation points out

$$\text{rank}(\Sigma_{\mathbf{X}}) = \text{rank}(\Sigma_{\dot{\mathbf{X}}}) = 5. \quad (3.159)$$

Due to the applied constraint equations the system snapshots consist of five independent and nine dependent measure signals, regardless whether we consider position or velocity DOFs.

As noted in Sec. 3.4.1.1, the generalized singular value decomposition approach struggles in terms of a singular "constraint"-matrix $\dot{\mathbf{X}}$. This is pointed out by the related generalized Eigenvalue value decomposition

$$\Sigma_{\mathbf{X}}\psi_i = \lambda_i\Sigma_{\dot{\mathbf{X}}}\psi_i. \quad (3.160)$$

It is computed in Scilab, utilizing the LAPACK package, cf. [4]. The generalized

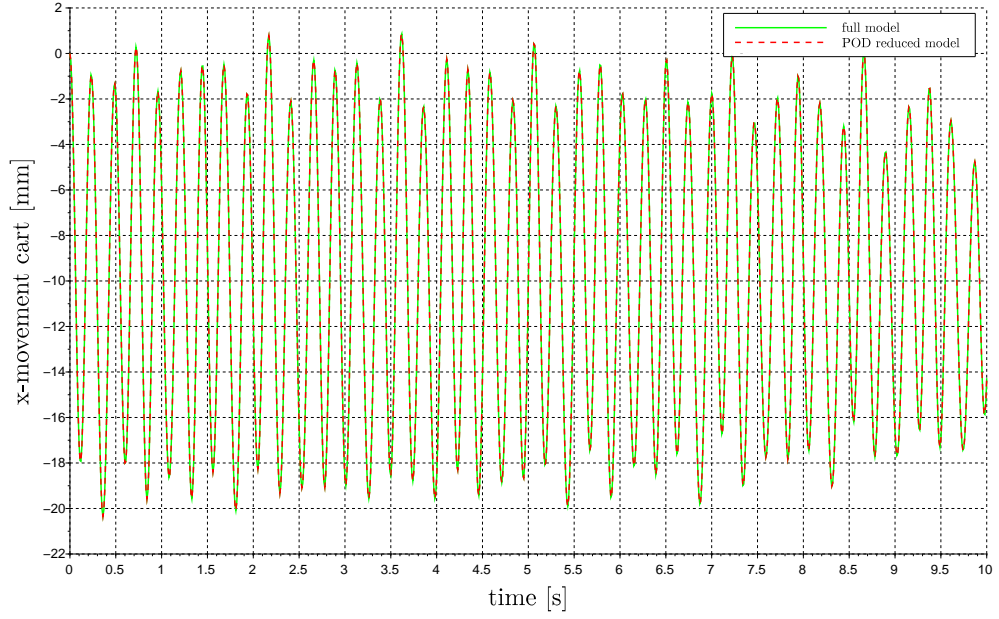


Figure 3.11: Superposition of the cart movement in the original and the POD reduced model

Eigenvalues λ_i , and the generalized singular values σ_i read

$$\lambda = \begin{bmatrix} \infty \\ 4.0 \times 10^{-2} \\ 3.0 \times 10^{-3} \\ 1.0 \times 10^{-3} \\ 4.865 \times 10^{-8} \\ -2.128 \times 10^{-7} \\ -1.459 \times 10^{-5} \\ -3.211 \times 10^{-5} \\ -1.391 \times 10^{-5} \\ -1.511 \times 10^{-4} \\ -2.05 \times 10^{-1} \\ -9.5 \times 10^{-2} \\ \text{NaN} \\ \text{NaN} \end{bmatrix}, \quad \sigma = \begin{bmatrix} 1.924 \times 10^{37} \\ 3.444 \times 10^2 \\ 6.059 \\ 1.2 \times 10^{-2} \\ 2.1 \times 10^{-3} \\ 1.4 \times 10^{-3} \\ 1.35 \times 10^{-3} \\ 6.6 \times 10^{-4} \\ 3.77 \times 10^{-8} \\ 3.39 \times 10^{-8} \\ 2.82 \times 10^{-8} \\ 2.49 \times 10^{-8} \\ 2.20 \times 10^{-8} \\ 4.20 \times 10^{-33} \end{bmatrix}. \quad (3.161)$$

Note that due to the rank-deficient "constraint"-matrix $\dot{\mathbf{X}}$, the numerical generalized Eigenvalue value decomposition approach, included in LAPACK, computes

infinte, negative and even non-defined Eigenvalues. The actual Eigenvalues λ_i are computed as

$$\lambda_i = \frac{\alpha_i}{\beta_i}, \quad (3.162)$$

where α_i and β_i are generalized Eigenvalues, computed by the internal LAPACK routine. In the case of a singular $\dot{\mathbf{X}}$, terms $\beta_i = 0$ result and, due to

$$\lambda_i = \frac{\alpha_i}{0} = \infty, \quad (3.163)$$

they are interpreted as infinite Eigenvalues.

Further, in the case of

$$\lambda_i = \frac{0}{0}, \quad (3.164)$$

the Eigenvalue is not defined and depicted as not-a-number (NaN). Hence, there exist one infinite Eigenvalue, seven negative Eigenvalues, two undefined Eigenvalues and four small positive generalized Eigenvalues.

Based on these theoretical considerations, conclusions on the SOD and its underlying mathematical methods are drawn. In terms of the generalized singular value decomposition and generalized Eigenvalue value decomposition, the following issues refuse the applicability to the present MBS formulation:

- In the case of a singular "constraint"-matrix $\dot{\mathbf{X}}$, the generalized Eigenvalue value decomposition may compute negative, infinite and undefined Eigenvalues.
It should be noted that due to the numerical Eigenvalue decomposition very large Eigenvalues may also represent infinite Eigenvalues due to roundoff errors.
- The generalized singular value decomposition approach does not highlight a singular "constraint" matrix as clear as the generalized Eigenvalue value decomposition does. Though, it still suffers from the singularity, as implausibly high generalized singular values are computed.
- An infinite generalized Eigenvalue corresponds to a very large generalized singular value.
- For a singular "constraint" matrix, the generalized Eigenvalues do not coincide with the generalized singular values, as it is the case for a regular "constraint" matrix.

The following issues make the applicability of SOD to the present MBS formulation questionable:

- In the case of a singular "constraint" matrix, smooth orthogonal modes span a singular subspace which is not applicable for model order reduction.
- MBS snapshots are typically singular and the identification of singular rows and columns might become an inconclusive non-trivial task. Preconditioning the snapshot matrices could easily become a bottle neck in terms of the applicability and efficiency.
- As pointed out in Sec. 3.4.4, the SOD approach emphasis on processes, which are smooth in time. It performs well in terms of linear free vibration systems, for which a clear connection between the system's Eigenmodes and the SOD modes can be drawn. Unfortunately, the present nonlinear MBS systems can not be ensured to follow this behavior. MBS models might be forced to large motions, and these motions might be chosen such that the system is no longer subject to its free vibrations. This might be a drawback in such a sense that the position and velocity snapshots no longer follow the nature as in the linear case but result in uncorrelated behavior.

Summarizing the findings of this section, the SOD method is not able to handle singular system snapshots as they arise with MBS under consideration. In contrast, the POD approach is directly applicable to the present type of MBS. Furthermore, POD highlights the dimension of the reduction subspace by reasonable drops in the computed proper orthogonal values. Thus, the classical POD approach is chosen as basis for the model order reduction method developed in this dissertation. It will be advanced, concerning the special structure and properties of the MBS under consideration.

The formulation of the reduced order model according to Ebert [30] brings up further issues. By restricting the model order reduction to physical coordinates (DOFs) only, the resulting reduced order model consists of $r < n$ reduced DOFs subject to m constraint equations. Depending on the actual MBS model under consideration, the number of reduced coordinates may be $r < m$. Such a reduced order model is over-constrained and most likely ill-conditioned. Hence, the limitation to reduce the DOFs only, has to be relativized such that the resulting reduced order model is well determined. This issue concerning over-constrained reduced order models is also investigated and solved in the upcoming chapter.

Physical and Constraint Coordinate Reduction of Redundantly Formulated Flexible Multibody Systems Based on Adapted POD

The upcoming Chapter introduces a novel flat projection based model order reduction method, which takes into account the pointed out limitations of the preceding Chapter. To this end, the novel model order reduction approach combines both, a physical coordinate reduction and a constraint coordinate reduction.

The physical coordinate reduction is based on the principles of proper orthogonal decomposition. It is specialized such that it takes into account different coordinate scales. As it will be pointed out, it is based on velocity coordinate snapshots. Furthermore, the issue of centered snapshot data is accounted for by introducing an extension to the flat Galerkin projection.

As the resulting reduced order model is probably overconstrained, a constraint coordinate reduction is presented next. Thereby, a null space to the constraints is constructed, which takes into account the reduced physical coordinates. This allows to reduce the set of constraint equations to those, which are not directly met by the extended flat Galerkin projection of the physical coordinates.

4.1 Different Coordinate Scales

One special feature of the redundant MBS formulation in FreeDyn is the use of Euler parameters. These describe the three rotational DOFs of a body in 3D space by a set of four parameters. As Euler parameters are subject to the constraint equation

$$e_0^2 + e_1^2 + e_2^2 + e_3^2 - 1 = 0, \quad (4.1)$$

the magnitude of e_0, e_1, e_2, e_3 is within ± 1 . Hence, when dealing with large body translations together with small body rotations, the classical proper orthogonal decomposition snapshot approach may interpret rotations as insignificant. This issue can be outlined by the following illustrative example:

Example: *Single mass under constant rotation and large translational movement*
The MBS model consists of one body with mass m . The six body DOFs are

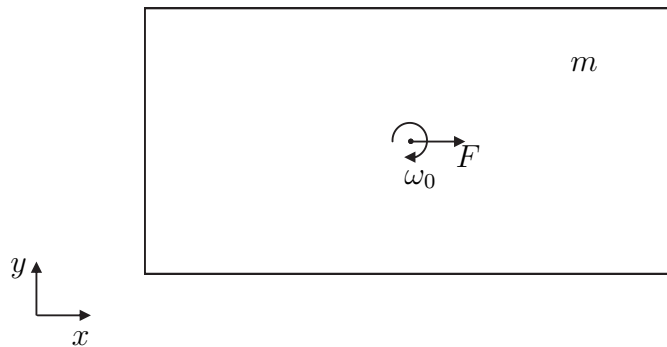


Figure 4.1: Single mass under constant rotation and large translational movement

represented by three translational and four rotational coordinates. As shown in Fig. 4.1, the body is rotating with a constant rotational velocity ω_0 around its z -axis. The body is further actuated by a constant external force F at its center of gravity. The initial conditions are set to

$$\begin{aligned} \mathbf{q}_0 &= [x_0, y_0, z_0, e_{0,0}, e_{1,0}, e_{2,0}, e_{3,0}]^T \\ &= [0, 0, 0, 1, 0, 0, 0]^T. \end{aligned} \quad (4.2)$$

The applied constraint equations force the body to move in x -direction only. While the rotational velocity is constant, the body is constantly accelerating due to the applied force.

Collected position snapshots are of the form

$$\mathbf{X} = \begin{bmatrix} x(t_0) & \dots & x(t_{\text{end}}) \\ y(t_0) & \dots & y(t_{\text{end}}) \\ z(t_0) & \dots & z(t_{\text{end}}) \\ e_0(t_0) & \dots & e_0(t_{\text{end}}) \\ e_1(t_0) & \dots & e_1(t_{\text{end}}) \\ e_2(t_0) & \dots & e_2(t_{\text{end}}) \\ e_3(t_0) & \dots & e_3(t_{\text{end}}) \end{bmatrix} = \begin{bmatrix} 0 & \dots & x(t_{\text{end}}) \\ 0 & \dots & 0 \\ 0 & \dots & 0 \\ 1 & \dots & e_0(t_{\text{end}}) \\ 0 & \dots & 0 \\ 0 & \dots & 0 \\ 0 & \dots & e_3(t_{\text{end}}) \end{bmatrix}. \quad (4.3)$$

By utilizing the classical proper orthogonal decomposition approach, see Chapter 3, a scaling issue due to the large translational movement arises.

The Euler parameters are forced to reside within the numerical range of ± 1 . As a result, the normalized proper orthogonal values

$$\mathbf{\Sigma} = [1, (*) \times 10^{-8}, (*) \times 10^{-10}, (*) \times 10^{-12}, (*) \times 10^{-45}, 0, 0]^\top \quad (4.4)$$

point out a major drop from POV one to POV two. The proper orthogonal mode related to this first proper orthogonal value reads

$$\phi_1 = [1, 0, 0, 0, 0, 0, 0]^\top. \quad (4.5)$$

As it is pointed out, the reduced order model will consist of the original x -coordinate only. Hence, the different scales of translational and rotational coordinates degrade the rotations, although the body is rotating at a high rotational velocity.

4.1.1 Coordinate-Type Sensitive POD

In order to overcome this issue, the coordinate scale sensitive proper orthogonal decomposition approach is introduced. It was first proposed by the author in Stadlmayr et al. [100]. The approach is inspired by the work of Ersal et al. [31], who introduced a body-coordinate-frame orientation approach for bond-graph models. As stated by Ersal et al., POD is used to achieve a structural simplification of the bond-graph model. This is due to re-orienting the given body-coordinate-frames such that their axes point into the direction of motion.

To this end, snapshots

$$\dot{\mathbf{X}} = [\mathbf{v}_x, \mathbf{v}_y, \mathbf{v}_z, \boldsymbol{\omega}_x, \boldsymbol{\omega}_y, \boldsymbol{\omega}_z,] = [\dot{\mathbf{X}}^t \ \dot{\mathbf{X}}^r] \quad (4.6)$$

are collected at velocity level, cf. [31]. They are then split into their translational content $\dot{\mathbf{X}}^t \in \mathbb{R}^{m \times 3}$ and into their rotational content $\dot{\mathbf{X}}^r \in \mathbb{R}^{m \times 3}$, respectively.

These separated observation spaces are processed by the singular value decompositions

$$\dot{\mathbf{X}}^t = \mathbf{\Phi}^t \mathbf{\Sigma}^t \mathbf{\Psi}^{t\top} \text{ and } \dot{\mathbf{X}}^r = \mathbf{\Phi}^r \mathbf{\Sigma}^r \mathbf{\Psi}^{r\top}. \quad (4.7)$$

Possible simplifications in the orientation of a body's body-fixed-coordinate-frame are indicated by zero valued proper orthogonal values.

Due to this separated proper orthogonal decompositions, the following conclusion can be drawn:

Any motion (translational/rotational) along a proper orthogonal mode associated with a zero valued proper orthogonal value is zero. Hence, the body-coordinate-frame orientation is marginal in terms of the acting motion, and the singular values may indicate a more significant frame orientation. For instance, a 3D motion may be reducible into a pure rotation around a directional vector defined by the associated proper orthogonal mode.

The approach by Ersal et al. [31] is described in terms of bond-graph models. The following limitations to the therein proposed approach can be deduced:

- Each body in the model has to be treated separately. This results in a large set of $k = 2b$ possible reduction subspaces, with b as the number of bodies.
- It is not possible to identify equal body motion. This is due to the body wise re-orientation of the according body-coordinate-frames.
- There is no concept to efficiently connect and/or combine the resulting k reduction subspaces. It is rather suggested, to choose either the translational or rotational reduction subspace for each body separately. This choice is left to the user.
- The topic of constraint equations is not covered, as the method is designed for bond-graph models. Hence, issues arising from redundant constraint equations are not addressed at all.
- The approach does not account for flexible bodies.

The physical coordinate reduction approach accounts for the above mentioned limitations. It puts special attention on the characteristics of the redundantly formulated MBS under consideration.

We now want to compare the classical proper orthogonal decomposition approach with the coordinate-type sensitive approach as introduced in this dissertation. Again, consider the simple rotational example from Sec. 4.1. When splitting the

collected snapshots in Eq. 4.3 into

$$\mathbf{X}^t = \begin{bmatrix} 0 & \dots & x(t_{\text{end}}) \\ 0 & \dots & 0 \\ 0 & \dots & 0 \end{bmatrix} \quad \text{and} \quad \mathbf{X}^r = \begin{bmatrix} 1 & \dots & e_0(t_{\text{end}}) \\ 0 & \dots & 0 \\ 0 & \dots & 0 \\ 0 & \dots & e_3(t_{\text{end}}) \end{bmatrix}, \quad (4.8)$$

the coordinate-type sensitive POD results in

$$\mathbf{\Sigma}^t = [1, 0, 0]^T \quad \text{and} \quad \mathbf{\Sigma}^r = [0.72, 0.69, 0, 0]^T. \quad (4.9)$$

These results point out two reduced order models consisting of one translational and two rotational reduced coordinate respectively. The following conclusions can be drawn from the above evaluation of the approach by Ersal et al. [31]: Handling different coordinate types separately is an appropriate method to ensure physical transformations. It is further a suitable approach to account for different snapshot scales.

Besides these features, the following extension is derived within this dissertation: Two or more rigidly coupled bodies should be representable by a common set of reduced coordinates.

MBS position snapshot data is typically not mean-centered by nature. As it furthermore should not be mean-centered at all, see Chapter 4, velocity snapshot data seems to be more sophisticated. This is due to

- static coordinates, which should be of zero velocity (at least within the computational accuracy). Position level snapshots are not ensured to be zero-valued, as static coordinates might be subject to non-zero initial conditions.
- directly connected coordinates, which are subject to constant offsets. Due to not mean-centered snapshot data, such connections should be identifiable more easily investigating velocity data.
- velocity coordinate data being somehow connected to the kinetic energy and therefore the dynamics of the MBS. By investigating velocity data the proper orthogonal decomposition is supposed to be closer connected to the dynamics of the multibody system.

Due to these reasons, velocity data based POD is supposed to identify the reduced order model more easily and precisely. Therefore, the model order reduction approach developed in this dissertation is based on velocity snapshot data. The choice of velocity data will be numerically justified due to a comparison with position based data in Chapter 5.

Snapshots of the MBS model are collected such that the translational velocity coordinates of all bodies are combined in one translational-velocity-coordinate-snapshot matrix

$$\dot{\mathbf{X}}^t = \begin{bmatrix} \dot{\mathbf{x}}_1(t_0) & \dots & \dot{\mathbf{x}}_1(t_{\text{end}}) \\ \dot{\mathbf{y}}_1(t_0) & \dots & \dot{\mathbf{y}}_1(t_{\text{end}}) \\ \dot{\mathbf{z}}_1(t_0) & \dots & \dot{\mathbf{z}}_1(t_{\text{end}}) \\ \vdots & \dots & \vdots \\ \dot{\mathbf{x}}_b(t_0) & \dots & \dot{\mathbf{x}}_b(t_{\text{end}}) \\ \dot{\mathbf{y}}_b(t_0) & \dots & \dot{\mathbf{y}}_b(t_{\text{end}}) \\ \dot{\mathbf{z}}_b(t_0) & \dots & \dot{\mathbf{z}}_b(t_{\text{end}}) \end{bmatrix}. \quad (4.10)$$

Rotational and flexible velocity coordinate snapshots are collected in $\dot{\mathbf{X}}^r \in \mathbb{R}^{n_{\text{rot}} \times h}$ and $\dot{\mathbf{X}}^f \in \mathbb{R}^{n_{\text{flex}} \times h}$ accordingly.

The proper orthogonal decomposition approach

$$\dot{\mathbf{X}}^t = \mathbf{\Phi}^t \mathbf{\Sigma}^t \mathbf{\Psi}^{t\top} \quad (4.11)$$

$$\dot{\mathbf{X}}^r = \mathbf{\Phi}^r \mathbf{\Sigma}^r \mathbf{\Psi}^{r\top} \quad (4.12)$$

$$\dot{\mathbf{X}}^f = \mathbf{\Phi}^f \mathbf{\Sigma}^f \mathbf{\Psi}^{f\top} \quad (4.13)$$

is applied to each snapshot matrix separately. The reduction subspaces $\mathbf{\Phi}_r^t \in \mathbb{R}^{n_{\text{trans}} \times r_{\text{trans}}}$, $\mathbf{\Phi}_r^r \in \mathbb{R}^{n_{\text{rot}} \times r_{\text{rot}}}$ and $\mathbf{\Phi}_r^f \in \mathbb{R}^{n_{\text{flex}} \times r_{\text{flex}}}$ are derived from investigating the proper orthogonal values in $\mathbf{\Sigma}^t$, $\mathbf{\Sigma}^r$ and $\mathbf{\Sigma}^f$.

The final global model order reduction matrix is derived by combining $\mathbf{\Phi}_r^t$, $\mathbf{\Phi}_r^r$ and $\mathbf{\Phi}_r^f$ to

$$\mathbf{V} = \begin{bmatrix} \mathbf{\Phi}_r^t & \mathbf{0} \\ & \mathbf{\Phi}_r^r \\ \mathbf{0} & & \mathbf{\Phi}_r^f \end{bmatrix} \in \mathbb{R}^{n \times r}. \quad (4.14)$$

Therein, $n = n_{\text{trans}} + n_{\text{rot}} + n_{\text{flex}}$ and $r = r_{\text{trans}} + r_{\text{rot}} + r_{\text{flex}}$ and $r < n$.

This global projection matrix allows to project all model coordinates at once. It further accounts for different coordinate scales by utilizing regarding coordinate type reduction subspaces. These are derived from velocity-level snapshots.

4.2 Deviation of Initial Conditions

The proposed model order reduction strategy is based on velocity data of the MBS, which includes initial velocity conditions only. Therefore, it is in lack of information concerning the initial conditions on position level, resulting in a physical offset of the reduced order model. This issue is solved by an extension of the applied Galerkin projection, which has to be taken into account throughout the whole

reduced order simulation:

In order to compensate the lack of information, the initial conditions of the original MBS model are first projected to the reduction subspace

$$\mathbf{q}_{r,0} = \mathbf{V}^T \cdot \mathbf{q}_0. \quad (4.15)$$

They are then projected back into the full space

$$\tilde{\mathbf{q}}_0 = \mathbf{V} \cdot \mathbf{q}_{r,0}. \quad (4.16)$$

Therefrom, the deviation

$$\mathbf{R}_0 = \mathbf{q}_0 - \tilde{\mathbf{q}}_0 \quad (4.17)$$

is computed. By combining these steps

$$\tilde{\mathbf{q}}_0 = \mathbf{V}\mathbf{V}^T \cdot \mathbf{q}_0 \quad (4.18)$$

is a function of the projection matrix and the full model's initial conditions. Note that although the orthogonality criteria ($\mathbf{A}^T\mathbf{A} = \mathbf{A}\mathbf{A}^T = \mathbf{I}$) holds for quadratic matrices, this is not the case for the present rank deficient projection matrix $\mathbf{V} \in \mathbb{R}^{n \times r}$. Hence, the term $\mathbf{V}\mathbf{V}^T \cdot \mathbf{q}_0$ equals to zero for all initial conditions which are not covered by the velocity proper orthogonal modes.

Rewriting Eq. (4.17) and inserting the above relations, the residuum vector \mathbf{R}_0 is defined as

$$\mathbf{R}_0 = \mathbf{q}_0 - \mathbf{V}\mathbf{V}^T \cdot \mathbf{q}_0. \quad (4.19)$$

In order to account for the actual initial conditions, the novel Galerkin projection rule, reads

$$\mathbf{q} \approx \tilde{\mathbf{q}} = \mathbf{V} \cdot \mathbf{q}_r + \mathbf{R}_0. \quad (4.20)$$

As \mathbf{q}_0 and \mathbf{V} are time-invariant, \mathbf{R}_0 is a constant shift from the origin. It is, hence, convenient to identify the residuum vector \mathbf{R}_0 once at $t = t_0$.

This approach accounts for possible residua in the initial conditions, by including a constant offset to the projection rule. Note that this novel Galerkin approach has to be applied throughout the whole reduced order simulation.

4.3 Reducing Constraint Equations

When dealing with multibody systems modeled in 3D MBS software packages, the number of constraint equations is often larger than actually necessary. Take, for instance, a pure planar motion of some mechanism. Due to the general 3D modeling approach, out-of-plane constraints are typically defined. These are theoretically unnecessary for the actual behavior of the mechanism, but relate to the

3D modeling approach. Moreover, depending on the actual excitation, physical body joints (hinges, ball-joints, etc.) may restrict non-actuated coordinates of the MBS.

Besides these modeling-related issues the reduction of physical DOF may cause constraint equations to become irregular and redundant. In order to shed light on this issue, consider the following: By definition, any valid full model simulation fulfills its constraint equations. Therefore, any snapshot matrix \mathbf{X} or $\dot{\mathbf{X}}$ collected from such a simulation contains constraint information. Therein, constraints describing dependencies between two DOFs (e.g. $x - y = 0$) may appear as equal snapshot lines. Further, coordinate restrictions may appear as zero or constant valued lines in the snapshot matrices.

As a natural extension, constraint information included in the snapshot matrix \mathbf{X} or $\dot{\mathbf{X}}$ is also contained in the global reduction matrix \mathbf{V} , which is built from these snapshots. In fact, by reducing the physical coordinates the flat projection ensures constraints which are covered by \mathbf{V} to be met. This is, because the flat Galerkin projection acts as a kind of constraint itself. Hence, covered constraint equations would appear redundantly in the physical coordinate reduced reduced order model

$$\begin{aligned} \mathbf{V}^\top \mathbf{M} \mathbf{V} \ddot{\mathbf{q}}_r + \mathbf{V}^\top \mathbf{C}_q^\top \boldsymbol{\lambda} &= \mathbf{V}^\top \mathbf{Q} \\ \mathbf{C} &= \mathbf{0}. \end{aligned} \quad (4.21)$$

Therefore, reducing the constraint equations is a critical but necessary task. Otherwise, the reduced order model may be overconstrained.

From a more mathematical point of view: If the vector of generalized coordinates $\mathbf{q} \in \mathbb{R}^n$ is reduced to $\mathbf{q}_r \in \mathbb{R}^r$, without reducing the vector of constraint equations $\mathbf{C} \in \mathbb{R}^m$, the resulting system of DAEs might become overdetermined and ill-conditioned, if $m > r$.

4.3.1 A Simple Projection Approach

A first attempt to handle the issue of overdetermined reduced order models is presented by the author in Stadlmayr et al. [100]. It is based on the assumption:

A constraint equation is removable if the corresponding Jacobian line $\mathbf{C}_{q,j}$ evaluates to zero when projected by \mathbf{V} .

A smaller set of constraint equations $\mathbf{C}_l(\mathbf{q}) \in \mathbb{R}^l$, with $l < m$, is found if any line of $\mathbf{C}_q \mathbf{V}$ equals to zero for all instances of time. As \mathbf{C} is in general non-constant the projection must be carried out repeatedly in an offline-phase for each time-step.

To this end, Algorithm 4.1 is defined. It computes the vector *isNeeded* which highlights regular constraint equations by value one. Due to this algorithm constraint equations are removable

Algorithm 4.1: A Simple Constraint Reduction Procedure

```

function ISCONSTRAINTNEEDED(V, Cq, t)    with;
    Cq = [Cq(t0), ..., Cq(ti), ..., Cq(tend)]
    isNeeded = zeros(m, 1);
    for t = t0 : Δt : tend do
        for j = 1 : m do
            if Cq(:, j)V(:, j) ≠ 0 then
                isNeeded(j) = 1;
            end
        end
    end

```

- (a) if they are not acting during simulation, or
- (b) if they are fulfilled by the Galerkin projection.

The constraint DOF reduction method is outlined by the initial value problem in Fig. 4.2.

-

Example: *Rigid Pendulum - Initial Value Problem*

To this end, we switch from Euler parameters to an Euler Angle description (three rotational coordinates) for illustration reasons. The undamped system consists of one body, a pendulum with length $l = 1$, which is modeled in 3D space, see Fig. 4.2. Therefore, the vector of physical coordinates consists of three translational coordinates x, y, z , and the corresponding three rotational coordinates φ, ψ, θ . It defines the pendulum's behavior relative to the global coordinate system, which is located in the hinge joint. The pendulum is subject to the five constraint equations, which force the pendulum to a planar movement within the $x - y$ plane. We further assume $\varphi < 2\pi$, as we do not want to deal with 2π discontinuity issues.

$$\mathbf{C}(\mathbf{q}) = [z, \psi, \theta, \sin(\varphi) - x, \cos(\varphi) - y]^T = \mathbf{0}. \quad (4.22)$$

The corresponding constraint Jacobian reads

$$\mathbf{C}_q(\mathbf{q}) = \begin{bmatrix} 0 & 0 & 1 & 0 & 0 & 0 \\ 0 & 0 & 0 & 0 & 1 & 0 \\ 0 & 0 & 0 & 0 & 0 & 1 \\ -1 & 0 & 0 & \cos(\varphi) & 0 & 0 \\ 0 & -1 & 0 & -\sin(\varphi) & 0 & 0 \end{bmatrix}. \quad (4.23)$$

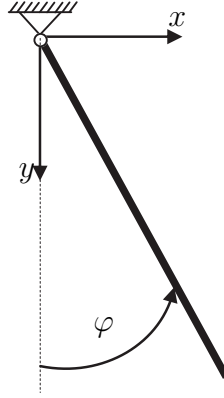


Figure 4.2: Rigid pendulum

Initial conditions are set to satisfy the initial angular deflection $\varphi(t_0)$. The velocity snapshots read

$$\begin{aligned} \dot{\mathbf{X}} &= \begin{bmatrix} \dot{\mathbf{X}}^t \\ \dot{\mathbf{X}}^r \end{bmatrix} \\ &= \begin{bmatrix} \cos(\varphi_0)\dot{\varphi}_0 & \cos(\varphi_1)\dot{\varphi}_1 & \dots & \cos(\varphi_{\text{end}})\dot{\varphi}_{\text{end}} \\ -\sin(\varphi_0)\dot{\varphi}_0 & -\sin(\varphi_1)\dot{\varphi}_1 & \dots & -\sin(\varphi_{\text{end}})\dot{\varphi}_{\text{end}} \\ 0 & 0 & \dots & 0 \\ \dot{\varphi}_0 & \dot{\varphi}_1 & \dots & \dot{\varphi}_{\text{end}} \\ 0 & 0 & \dots & 0 \\ 0 & 0 & \dots & 0 \end{bmatrix}, \end{aligned} \quad (4.24)$$

where $\varphi_0 = \varphi(t_0)$, $\dot{\varphi}_0 = \dot{\varphi}(t_0)$, $\varphi_1 = \varphi(t_1) = \varphi(t_1)$, etc. We apply the proposed proper orthogonal decomposition method to the translational velocity snapshot matrix $\dot{\mathbf{X}}^t$. Two major proper orthogonal values corresponding to the x and y direction and one zero valued proper orthogonal value corresponding to the z direction are found.

Hence, the first two proper orthogonal modes

$$\Phi_r^t = \begin{bmatrix} 1 - \epsilon & 0 + \epsilon \\ 0 + \epsilon & 1 - \epsilon \\ 0 & 0 \end{bmatrix} \quad (4.25)$$

are chosen as the translational part of the reduction matrix \mathbf{V} . The small deviation ϵ between a unit vector and the actual proper orthogonal modes originates from the numerical calculation of the kinematic relationship between x, y and φ , and the therewith related trigonometric functions.

Applying the proper orthogonal decomposition method to $\dot{\mathbf{X}}^r$ one major proper

orthogonal value corresponding to the rotation around φ is found. The other two proper orthogonal values are equal to zero. Hence, the rotational part of \mathbf{V} consists of the proper orthogonal mode

$$\Phi_r^r = [1, 0, 0]^T. \quad (4.26)$$

The global projection matrix reads

$$\mathbf{V} = \begin{bmatrix} \Phi_r^t & \mathbf{0} \\ \mathbf{0} & \Phi_r^f \end{bmatrix} = \begin{bmatrix} 1 - \epsilon & 0 + \epsilon & 0 \\ 0 + \epsilon & 1 - \epsilon & 0 \\ 0 & 0 & 0 \\ 0 & 0 & 1 \\ 0 & 0 & 0 \\ 0 & 0 & 0 \end{bmatrix}. \quad (4.27)$$

Note that for this example, the initial conditions are met directly. Therefore, the residual vector $\mathbf{R}_0 = \mathbf{V}\mathbf{V}^T\mathbf{q}_0$ equals to zero.

In order to identify removable constraints, the proposed constraint reduction algorithm is applied. According to Alg. (4.1), Eq. (4.28) shows entries equal to zero for all instances of time which correspond to the first three constraint equations

$$\mathbf{C}_q \mathbf{V} = [0, 0, 0, *, *]^T. \quad (4.28)$$

The fourth and fifth constraint equations, representing the pendulum's joint, are unequal to zero (denoted by an asterisk in Eq. (4.28)). This is due to the kinematic relation between x, y and ϕ being not detectable. The first three constraint equations do not act during simulation (also indicated by the zero entries in \mathbf{V}). Thus, the constraint reduction vector evaluates to

$$\text{isNeeded} = [0, 0, 0, 1, 1]^T. \quad (4.29)$$

In conclusion, the reduced order model, projected by \mathbf{V} , can be solved sufficiently using $r = 3$ instead of $n = 6$ DOFs. Due to this choice, three out of five constraint equations have to be neglected.

The connection between unnecessary non-moving physical DOFs and the corresponding proper orthogonal values and proper orthogonal modes is pointed out by the outcome of the above constraint reduction process. But it is also observable that the method suffers from the lack of identifying kinematic relations between translational and rotational DOFs. Therefore, the constructed reduced order model may be seen as the minimal derivable representation of the present example. However, this method tends to fail if the constraint equations are defined in any direction other than the global axes directions. Numerical tests have shown, that in terms of a more complex MBS model hardly any constraint equations might be identified as reducible by this approach. This is especially the case for models which consist of boundary conditions in arbitrary directions in space.

4.3.2 A Generalized Projection Approach

This section presents a generalized constraint reduction approach. It is based on the singular value decomposition of the projected constraint Jacobian $\mathbf{C}_{\mathbf{q},r} = \mathbf{C}_{\mathbf{q}}\mathbf{V}$. This approach has been first published by the author in [99], and is closely related to the Principal Component Analysis [67, 95, 110]. It allows to reduce the set of constraint equations even if the constraint's axes directions are chosen arbitrarily.

First, recall that the rank of any matrix $\mathbf{Y} \in \mathbb{R}^{m \times n}$ is calculated by the singular value decomposition

$$\begin{aligned} \mathbf{Y} &= \mathbf{\Phi} \cdot \mathbf{\Sigma} \cdot \mathbf{\Psi}^T \\ &= \begin{bmatrix} \mathbf{\Phi}^i & \mathbf{\Phi}^d \end{bmatrix} \begin{bmatrix} \mathbf{D} & 0 \\ 0 & 0 \end{bmatrix} \begin{bmatrix} \mathbf{\Psi}^{iT} & \mathbf{\Psi}^{dT} \end{bmatrix}. \end{aligned} \quad (4.30)$$

The rank of \mathbf{Y} is given by the number of non-zero entries in $\mathbf{\Sigma} \in \mathbb{R}^{m \times n}$, which is the row/ column size of the quadratic matrix $\mathbf{D} \in \mathbb{R}^{l \times l}$. The matrix of left singular vectors $\mathbf{\Phi} \in \mathbb{R}^{m \times m}$ spans the column-space of \mathbf{Y} . It can be split into independent (superscript ⁱ) and dependent (superscript ^d) left singular vectors. The matrix of right singular vectors $\mathbf{\Psi}^T \in \mathbb{R}^{n \times n}$ spans the row-space and can be split accordingly. With no loss of precision, Eq. (4.30) can be rewritten in terms of the independent components as

$$\mathbf{Y} = \mathbf{\Phi}^i \cdot \mathbf{D} \cdot \mathbf{\Psi}^{iT}. \quad (4.31)$$

Therein, the independent column space $\mathbf{\Phi}^i \in \mathbb{R}^{m \times l}$ spans a subspace solely consisting of the unique column information from \mathbf{Y} .

The matrix of independent left singular vectors is denoted as $\mathbf{\Gamma} = \mathbf{\Phi}^i$ from now. By pre-multiplying \mathbf{Y} with $\mathbf{\Gamma}^T$ the original redundant data is re-expressed as a linear combination of its independent basis vectors:

$$\mathbf{Y}_{\text{unique}} = \mathbf{\Gamma}^T \mathbf{Y}, \quad (4.32)$$

Therein, $\mathbf{Y}_{\text{unique}} \in \mathbb{R}^{l \times m}$ contains, in its columns, only the essential (unique) information of \mathbf{Y} .

The method is applied to the constraint Jacobian $\mathbf{C}_{\mathbf{q},r} \in \mathbb{R}^{m \times r}$ in an offline phase of the simulation procedure. The number of original constraint equations is again denoted by m and r is the number of reduced physical coordinates.

By setting $\mathbf{Y} = \mathbf{C}_{\mathbf{q},r}$ and proceeding as proposed, independent left singular vectors $\mathbf{\Gamma} \in \mathbb{R}^{m \times l}$ and non-zero singular values $\mathbf{D} \in \mathbb{R}^{l \times l}$ are computed. The constraint Jacobian is re-expressed as a linear combination of its independent basis vectors

$$\mathbf{C}_{\mathbf{q},r,l} = \mathbf{\Gamma}^T \mathbf{C}_{\mathbf{q},r}. \quad (4.33)$$

Now, $\mathbf{C}_{\mathbf{q},r,l} \in \mathbb{R}^{l \times r}$, with $l \leq r$, consists of the regular constraint information only. The proposed projection is also applied to the vector of constraint equations

$$\mathbf{C}_l = \mathbf{\Gamma}^\top \mathbf{C}, \quad (4.34)$$

to ensure consistency. Note that if the algebraic constraint equations ($\mathbf{C} = \mathbf{0}$) hold true for the original system any linear combination of these terms, in the sense of Eq. (4.34), meets the zero-condition $\mathbf{C}_l = \mathbf{0}$ as well.

Finally, the physical and constraint DOF reduced model is defined as

$$\begin{aligned} \mathbf{V}^\top \mathbf{M} \mathbf{V} \ddot{\mathbf{q}}_r + \mathbf{V}^\top \mathbf{C}_{\mathbf{q},r,l}^\top \boldsymbol{\lambda}_l &= \mathbf{V}^\top \mathbf{Q} \\ \mathbf{\Gamma}^\top \mathbf{C} &= \mathbf{0}. \end{aligned} \quad (4.35)$$

Note that in Eq. (4.35), one could set

$$\mathbf{C}_{\mathbf{q},r,l}^\top \boldsymbol{\lambda}_l = \mathbf{C}_{\mathbf{q},r}^\top \mathbf{\Gamma} \boldsymbol{\lambda}_l = \mathbf{V}^\top \mathbf{C}_{\mathbf{q}}^\top \mathbf{\Gamma} \boldsymbol{\lambda}_l \quad (4.36)$$

and argue that the last part is similar to a Galerkin projection of the vector of Lagrangian multipliers $\boldsymbol{\lambda} \approx \tilde{\boldsymbol{\lambda}} = \mathbf{\Gamma} \boldsymbol{\lambda}_l$. In fact, this term arises due to the consequent application of the constraint reduction method and is not intended as a Galerkin projection. Nevertheless, the vector of Lagrangian multipliers has to change its dimension according to the remaining number of constraint equations \mathbf{C}_l .

In the case of $l = r$ the reduced MBS model is fully constrained, as the number of remaining constraints equals the number of reduced DOFs. To overcome this issue, the singular values in \mathbf{D} should be investigated similar to the physical DOF reduction in Sec. 3.4.3. Again, a smaller set of reduced constraint equations is indicated by a drop in the singular value decay.

Furthermore, the constraint reduction method introduced in Sec. 4.3.1 is a special case of the present method. Any constraint equation evaluating zero in the sense of the projection $\mathbf{C}_{\mathbf{q}} \mathbf{V}$ is equivalent to a redundant column in $\mathbf{C}_{\mathbf{q}}$. It therefore results in a zero valued singular value in $\boldsymbol{\Sigma}$.

4.4 Model Order Reduction Scheme

Summarizing this Chapter, a model order reduction method is introduced which reduces physical and constraint coordinates. The physical coordinate reduction approach is based on coordinate-scale sensitive proper orthogonal decomposition, applied to velocity data. It further rests on an extended flat projection approach. This extension takes into account possible residuals resulting from non-zero initial conditions.

The constraint coordinate reduction approach is based on the principal component analysis. It extracts redundant constraint information from the reduced order model. The final reduced order model is ensured to be regular and determined within the chosen ROM subspace:

1. Solve the original MBS model

$$\begin{aligned} \mathbf{M}(\mathbf{q}) \ddot{\mathbf{q}} + \mathbf{C}_{\mathbf{q}}(\mathbf{q})^{\top} \boldsymbol{\lambda} &= \mathbf{Q}(\mathbf{q}, \dot{\mathbf{q}}) \\ \mathbf{C}(\mathbf{q}) &= \mathbf{0} \end{aligned} \quad (4.37)$$

forward in time, collecting velocity snapshot data in the snapshot matrix $\dot{\mathbf{X}}$.

2. Subdivide the velocity snapshot data into $\dot{\mathbf{X}}^t$, $\dot{\mathbf{X}}^r$, and $\dot{\mathbf{X}}^f$.
3. Process each coordinate-type-velocity snapshot data separately, using the proper orthogonal decomposition approach

$$\dot{\mathbf{X}}^t = \boldsymbol{\Phi}^t \boldsymbol{\Sigma}^t \boldsymbol{\Psi}^{t\top} \quad (4.38)$$

$$\dot{\mathbf{X}}^r = \boldsymbol{\Phi}^r \boldsymbol{\Sigma}^r \boldsymbol{\Psi}^{r\top} \quad (4.39)$$

$$\dot{\mathbf{X}}^f = \boldsymbol{\Phi}^f \boldsymbol{\Sigma}^f \boldsymbol{\Psi}^{f\top}. \quad (4.40)$$

4. Characterize the regarding reduced subspaces of dimension $r_{\text{trans}} < n_{\text{trans}}$, $r_{\text{rot}} < n_{\text{rot}}$, and $r_{\text{flex}} < n_{\text{flex}}$, by investigating the proper orthogonal value decay in $\boldsymbol{\Sigma}^t$, $\boldsymbol{\Sigma}^r$, and $\boldsymbol{\Sigma}^f$.
5. Combine the chosen subspaces into the global reduction subspace

$$\mathbf{V} = \begin{bmatrix} \boldsymbol{\Phi}_r^t & \mathbf{0} \\ \boldsymbol{\Phi}_r^r & \\ \mathbf{0} & \boldsymbol{\Phi}_r^f \end{bmatrix}. \quad (4.41)$$

6. Identify redundant constraints by investigating the constraint Jacobian due to the proposed principal component analysis

$$\mathbf{C}_{\mathbf{q}} \mathbf{V} = \boldsymbol{\Phi}^i \mathbf{D} \boldsymbol{\Psi}^{i\top}. \quad (4.42)$$

The unique constraint data is derived from the projection onto the subspace spanned by the l left singular vectors $\boldsymbol{\Psi}^i$, collected in $\boldsymbol{\Gamma}$. The set of unique constraints and the corresponding constraint Jacobian are derived from

$$\mathbf{C}_l = \boldsymbol{\Gamma}^{\top} \mathbf{C} \quad (4.43)$$

and

$$\mathbf{C}_{\mathbf{q},r,l} = \boldsymbol{\Gamma}^{\top} \mathbf{C}_{\mathbf{q}} \mathbf{V}. \quad (4.44)$$

7. For upcoming simulations, utilize the reduced order model

$$\begin{aligned} \mathbf{V}^T \mathbf{M} \mathbf{V} \ddot{\mathbf{q}}_r + \mathbf{V}^T \mathbf{C}_{\mathbf{q},r,l}^T \boldsymbol{\lambda}_l &= \mathbf{V}^T \mathbf{Q} \\ \mathbf{C}_l &= \mathbf{0} \end{aligned} \quad (4.45)$$

in an iterative scheme. In order to evaluate the actual configuration dependent system matrices and vectors \mathbf{M} , \mathbf{Q} , \mathbf{C} , $\mathbf{C}_{\mathbf{q}}$ the reduced coordinates \mathbf{q}_r have to be transformed into the approximated full coordinates

$$\tilde{\mathbf{q}} = \mathbf{V} \cdot \mathbf{q}_r + \mathbf{R}_0. \quad (4.46)$$

4.5 Comments with Respect to the Constraint Forces in the Reduced Model

The model order reduction to physical and constraint coordinates allows to construct a reduced order model, which reproduces the original system motion with high consistency. Nevertheless, as the proper orthogonal mode matrix is truncated, the advantage of finding a smaller set of coordinates by a weighted linear combination of the original coordinates, goes hand in hand with a loss of system information.

To ensure correct constraint forces is still an open field of research. Several authors deal with the problem of redundant constraint equations. In [45, 26, 115, 116] and references therein, constraint redundancy resulting from singular configurations, over-constrained modeling (as in the case of a rigid door being modeled using both hinges), etc. is covered.

In the present case, the constraint forces of the reduced order model turn out to differ from the constraint forces of the original system. As a consequence, the reduced order model can not be used to generate load data in joints, as it might be needed for special FEM simulations and fatigue analysis. It can be shown, that the change in the constraint forces is caused by the physical coordinate reduction. If any original coordinate is weighted with factor zero in the reduced order model, which is a zero entry in all related entries of the projection matrix \mathbf{V} , forces acting on this coordinate no longer enter the reduced order model. Therefore, the according constraint force $\mathbf{V} \mathbf{C}_{\mathbf{q}}^T \boldsymbol{\lambda}$ equals to zero.

This issue can be simply demonstrated by the single mass oscillator with mass m , which was already introduced in Chapter 3. It is coupled to ground by a linear spring with spring stiffness k . It is further actuated by an external force F in (x, y) direction. The example is again depicted in Fig. 4.3. Let the original model consist of two degrees of freedom, which are the (x, y) movement of the cart. The model is subject to one constraint equation which reads $C_1 = y = 0$. Hence, the mass is

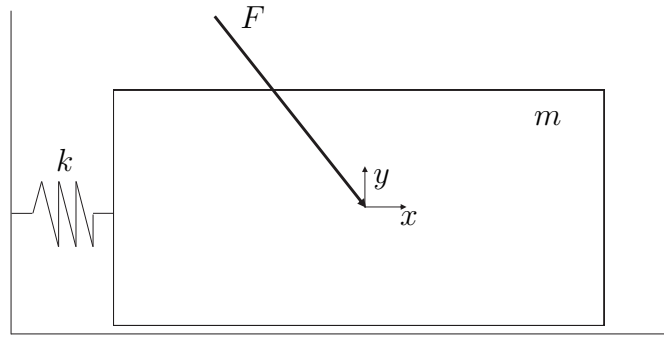


Figure 4.3: Single mass oscillator

forced to move in x direction only. The constraint Jacobian of this example is of the form

$$\mathbf{C}_q = \begin{bmatrix} 0 & 1 \end{bmatrix}. \quad (4.47)$$

The velocity result file $\dot{\mathbf{X}} \in \mathbb{R}^{2 \times h}$ reads

$$\dot{\mathbf{X}} = \begin{bmatrix} \dot{x}(t_0) & \dots & \dot{x}(t_{\text{end}}) \\ \dot{y}(t_0) & \dots & \dot{y}(t_{\text{end}}) \end{bmatrix} = \begin{bmatrix} * & \dots & * \\ 0 & \dots & 0 \end{bmatrix}. \quad (4.48)$$

Hence, the singular value decomposition of this data matrix delivers one non-zero and one zero valued proper orthogonal value. The global projection matrix reads

$$\mathbf{V} = \begin{bmatrix} 1 \\ 0 \end{bmatrix}. \quad (4.49)$$

It reduces the system into a one-DOF reduced order model, as all zero valued proper orthogonal values are omitted. Due to this choice, which is also the minimal set of coordinates representation, the constraint Jacobian is projected to the reduction subspace as

$$\mathbf{C}_q \mathbf{V} = \begin{bmatrix} 0 & 1 \end{bmatrix} \begin{bmatrix} 1 \\ 0 \end{bmatrix} = 0. \quad (4.50)$$

When transforming the reduced system solution back into the full space, the movement of the single mass oscillator is equal to the original system. This is due to the reduced order model consisting of the acting x DOF only. Nevertheless, the constraint force $\mathbf{V}^T \mathbf{C}_q^T \boldsymbol{\lambda}$ equals to zero for all instances of time as $\mathbf{V}^T \mathbf{C}_q^T = \mathbf{0}$. Therefore, this model order reduction method is not usable for simulations concerning the original MBS's constraint forces as important results.

Finally, it must be taken into account, that omitted constraints may become important in the case of critically changing excitation directions or model parameters. It might then be necessary to collect a new set of snapshots to renew the reduction subspace and the set of unique constraints.

4.6 Effect of the Reduction Approach on the HHT-Solver

The example presented in Sec. 4.5 points out the necessity to process the constraint equations to ensure regularity and certainty of the reduced order model. In addition, the constraint reduction and the overall reduction process affect the HHT-solver algorithm in Sec. 2.5.1.

Recall the Jacobian matrix

$$\mathbf{J} = \begin{bmatrix} \mathbf{M}_{\text{ext}} & \mathbf{C}_{\mathbf{q}}^{\top} \\ \mathbf{C}_{\mathbf{q}} & \mathbf{0} \end{bmatrix}, \quad (4.51)$$

which is used to compute correction terms $\Delta \dot{\mathbf{q}}$ and $\Delta \boldsymbol{\lambda}$ during simulation. Therein, the extended mass matrix reads

$$\mathbf{M}_{\text{ext}} = \frac{1}{1+\alpha} \mathbf{M} + \left(\frac{1}{1+\alpha} (\mathbf{M}\ddot{\mathbf{q}})_{\mathbf{q}} + (\mathbf{C}_{\mathbf{q}}^{\top} \boldsymbol{\lambda})_{\mathbf{q}} - \mathbf{Q}_{\mathbf{q}} \right) \beta h^2 - \mathbf{Q}_{\dot{\mathbf{q}}} h \gamma.$$

The Jacobian matrix has to be projected onto the reduction subspace as follows:

$$\mathbf{J}_r = \begin{bmatrix} \mathbf{M}_{\text{ext},r} & \mathbf{V}^{\top} \mathbf{C}_{\mathbf{q}}^{\top} \boldsymbol{\Gamma} \\ \boldsymbol{\Gamma} \mathbf{C}_{\mathbf{q}} \mathbf{V} & \mathbf{0} \end{bmatrix}, \quad (4.52)$$

with

$$\begin{aligned} \mathbf{M}_{\text{ext},r} &= \frac{1}{1+\alpha} \mathbf{V}^{\top} \mathbf{M} \mathbf{V} \\ &+ \left(\frac{1}{1+\alpha} \mathbf{V}^{\top} (\mathbf{M}\ddot{\mathbf{q}})_{\mathbf{q}} \mathbf{V} + \mathbf{V}^{\top} (\mathbf{C}_{\mathbf{q}}^{\top} \boldsymbol{\lambda})_{\mathbf{q}} \mathbf{V} - \mathbf{V}^{\top} \mathbf{Q}_{\mathbf{q}} \mathbf{V} \right) \beta h^2 \\ &- \mathbf{V}^{\top} \mathbf{Q}_{\dot{\mathbf{q}}} \mathbf{V} h \gamma. \end{aligned} \quad (4.53)$$

The individual sub-Jacobians $(\mathbf{M}\ddot{\mathbf{q}})_{\mathbf{q}}$, $(\mathbf{C}_{\mathbf{q}}^{\top} \boldsymbol{\lambda})_{\mathbf{q}}$, etc. are assembled analytically in FreeDyn in a preprocessing step. Therefore, these matrices must be evaluated by the approximated full coordinates $\tilde{\mathbf{q}} = \mathbf{V} \mathbf{q}_r + \mathbf{R}_0$ in each reduced order model iteration.

In terms of a reduced order model which is only reduced in its physical coordinates, single lines up to the whole matrix $\mathbf{C}_{\mathbf{q}}$ would become singular. This would cause the solver to abort immediately in the case of redundant constraints. Consider $\mathbf{C}_{\mathbf{q}}$ as a zero matrix, which is all constraint equations are redundant. Further consider this circumstance as $\mathbf{C}_{\mathbf{q}} = \mathbf{0}$ for illustrative reasons. Then, the according physical coordinate reduced system Jacobian would be of the form

$$\mathbf{J} = \begin{bmatrix} \mathbf{M}_{\text{ext},r} & \mathbf{0} \\ \mathbf{0} & \mathbf{0} \end{bmatrix} \quad (4.54)$$

and, hence, singular.

By applying the introduced generalized constraint reduction approach, the singular value decomposition of the reduced constraint Jacobian identifies such redundant constraints. In the present case all constraint equations would be covered by \mathbf{V} . Therefore, the constraints \mathbf{C} , the constraint Jacobian \mathbf{C}_q and the according Lagrangian multipliers $\boldsymbol{\lambda}$ are completely eliminated from the solver algorithm. The reduced order model is then regular and well-conditioned again, as the system Jacobian reduces to

$$\mathbf{J} = [\mathbf{M}_{\text{ext},r}]. \quad (4.55)$$

Application to Large Scale Multibody Systems

The developed model order reduction method is applied to MBS models consisting of a reasonably large number of bodies, DOFs and constraints. These examples originate from automotive optimization tasks and represent typical complexity faced by industrial users.

The examples are modeled using the FreeDyn software package. They are solved in Scilab [90] utilizing the FreeDyn-Scilab interface. FreeDyn is used for modeling tasks and for computing the system matrices of the MBS according to the actual state vectors. The system matrices are then handed through to Scilab by the FreeDyn-Scilab interface. Scilab is used to solve both, the full and the reduced order MBS. It therefore utilizes the HHT solver algorithm introduced in Chapter 2. It is further used to compute the ROM necessities. These are the global projection matrix, the constraint reduction matrix, and the initial condition residuum.

The numerical examples point out strengths but also limitations of the proposed method.

5.1 A Rigid V8 Crank Drive

The in-plane V8 crank drive shown in Fig. 5.1 is set up in 3D space with a V-angle of 90° . The MBS model consists of 17 rigid bodies. Each connecting rod is connected to the crankshaft by a spherical joint (three constraint equations) and by rotational restrictions (two constraint equations). An equivalent set of five constraint equations is introduced in order to connect the piston rod to the piston. Each piston is further constrained against ground by one translational and one

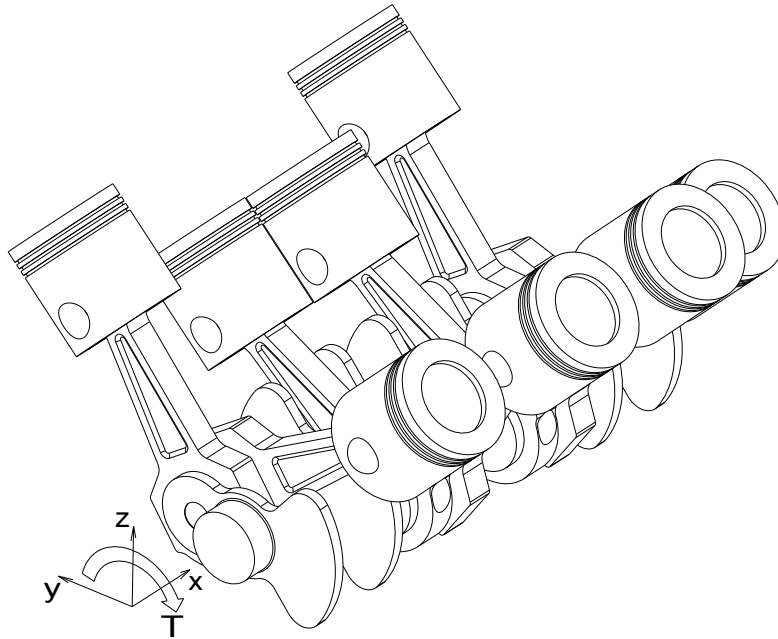


Figure 5.1: V8 crank drive

rotational restriction to its lateral axis at its COG. Thus, each cylinder introduces a set of twelve constraint equations.

Another set of five constraint equations is introduced by the crankshaft at its COG. It is restrained by a spherical joint and two rotational restrictions to its lateral axis. Finally, 17 internal constraints are introduced by the rigid bodies. Summing up, the MBS model consists of $b = 17$ bodies, $n = 119$ physical coordinates and $m = 118$ constraint equations. Detailed model data is summarized in Tab. 1.

The frictionless system is revved up by an idle torque $T = 20$ [Nm] acting on the crankshaft's longitudinal axis. After 1.5 seconds of simulation time, the crankshaft is further revved up to a peak velocity of 4000 [RPM] by a second torque $T_{\text{peak}} = 200$ [Nm]. This peak torque is deactivated after another 1.5 seconds, allowing the crank drive to slow down to idle speed again. The applied torques are opposed by a rotational damping element acting on the crankshaft, in order to achieve constant engine speeds. The acting torques and forces are summarized in Tab. 2. The resulting engine speed curve is shown in Fig. 5.2.

5.1.1 Results

The rigid V8 crank drive is simulated in Scilab, utilizing the FreeDyn-Scilab interface. The derived model order reduction method is applied to the velocity results of the full model simulation. The number of constraint equations is reduced accord-

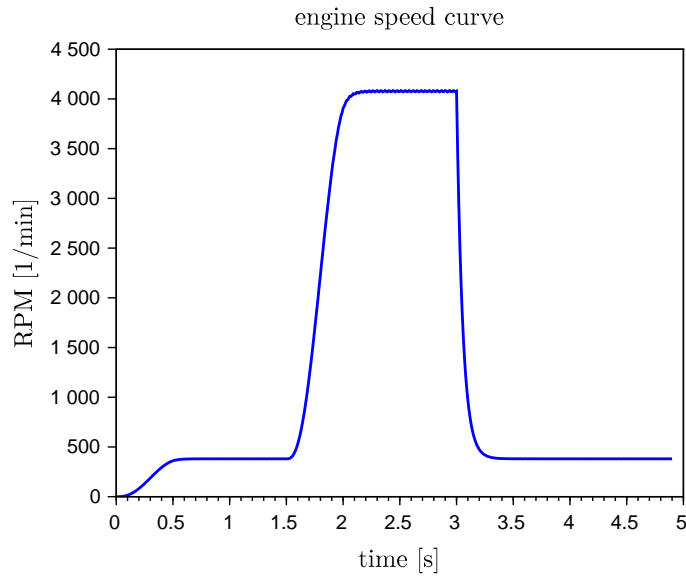


Figure 5.2: V8 RPM plot

ing to the choice of reduced physical coordinates. This new approach is compared to the POD of combined position snapshots. It is also compared to the POD of combined velocity snapshots. Figures 5.3 and 5.4 show the decay of the calculated proper orthogonal values according to the herein derived model order reduction method. The plotted proper orthogonal values are normalized such that

$$\sum_{i=1}^n \sigma_i^2 = 1, \quad (5.1)$$

for each type of coordinates. The decay of translational proper orthogonal values in Fig. 5.3 clearly points out a drop by several orders of magnitude below $1\text{E-}16$ after POV four. Hence, the four proper orthogonal modes corresponding to the first four POVs span the reduced subspace to the translational part of this model. Consequently, the number of reduced translational coordinates is four.

As it will be pointed out by all upcoming examples in this Chapter, an absolute proper orthogonal value value of $1\text{E-}16$ seems to represent a sufficient limit for the POV selection criteria. Note, that this is only valid for the present examples, and only in the case of applying the coordiante-scale sensitive POD. This is not the case for the "classical" POD with combined coordinate snapshots, as under- and overestimations on the impact of single coordinates happen. The herein used limit should therefore not be taken as a general selection criteria.

In analogous manner, the proper orthogonal value decay of the rotational velocity

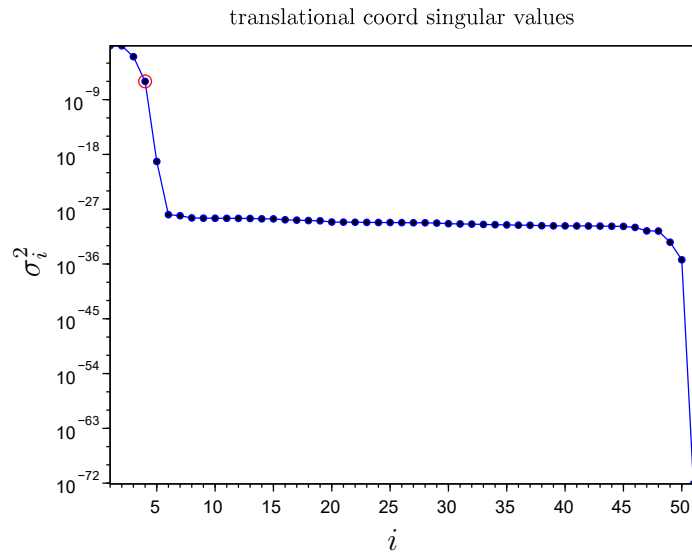


Figure 5.3: Translational velocity coordinate POVs - Rigid V8 crank drive

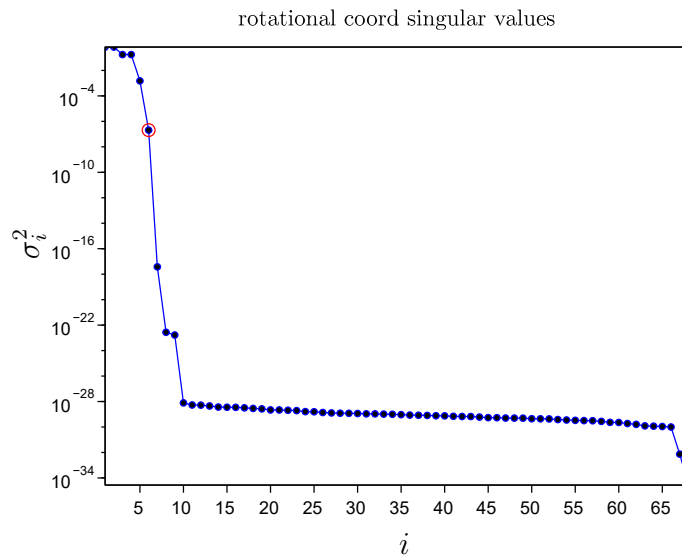


Figure 5.4: Rotational velocity coordinate POVs - Rigid V8 crank drive

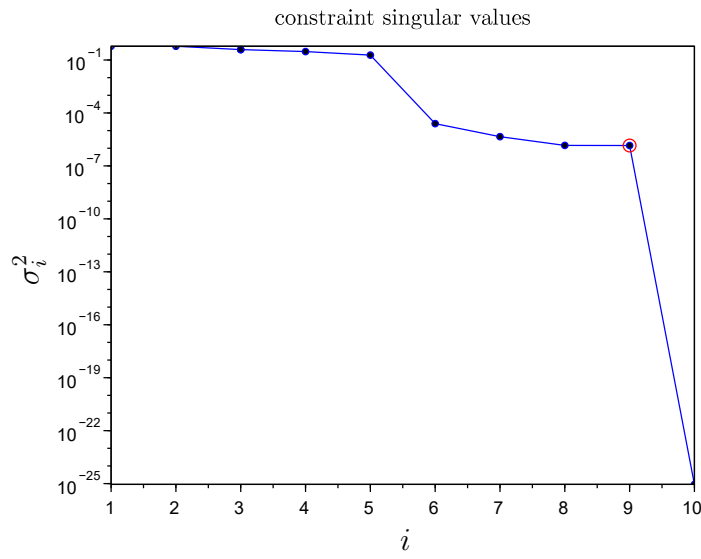


Figure 5.5: Constraint singular values - Rigid V8 crank drive

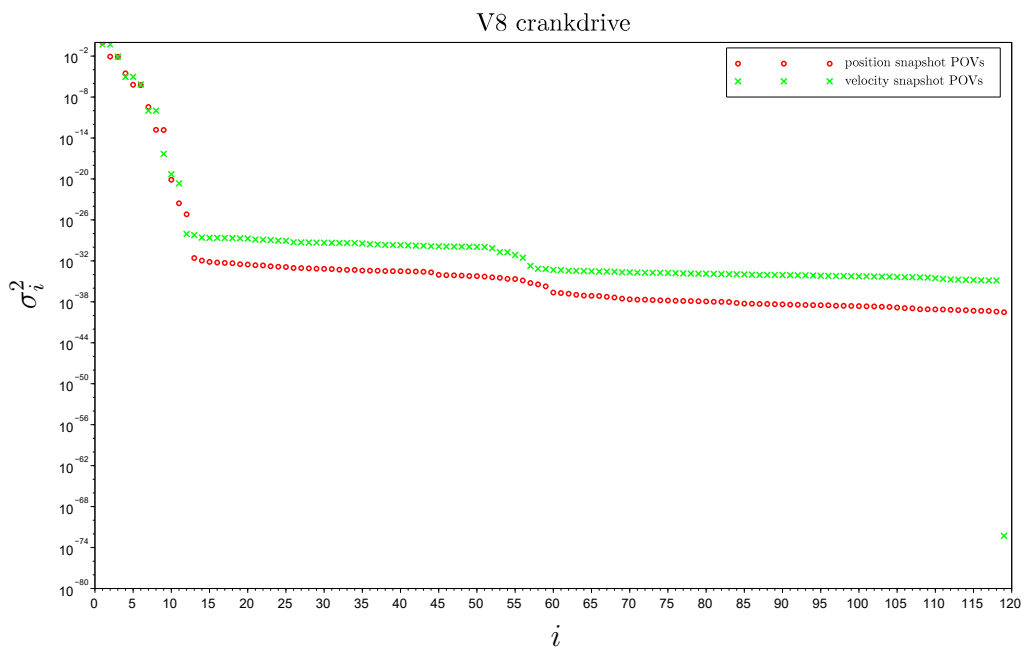


Figure 5.6: Combined position and velocity snapshot POD - Rigid V8 crank drive

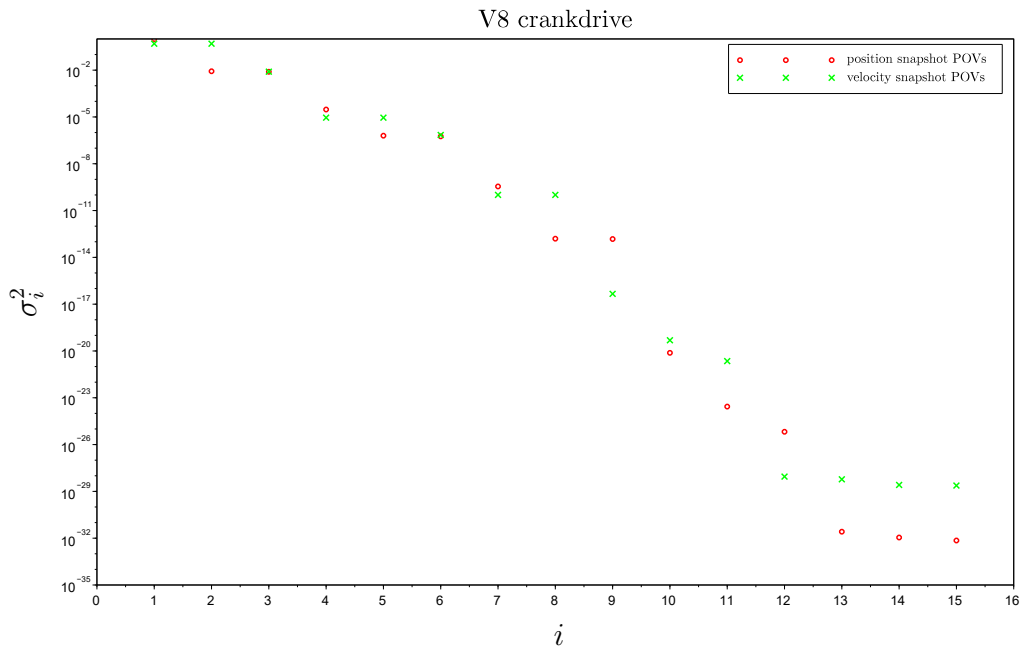


Figure 5.7: Zoom into the first 15 POVs - Combined position and velocity snapshot POD - Rigid V8 crank drive

coordinates, cf. Fig 5.4, point out a drop below $1\text{E-}16$ after POV number six. As a result, the reduced order model consists of six rotational coordinates only.

Due to this choice of ten reduced coordinates, the constraint singular values in Fig 5.5 are computed. It points out a drop below $1\text{E-}16$ after nine singular values. Thus, the reduced order model consists of nine reduced constraint equations. Note that the constraint singular values are normalized similar to the coordinate proper orthogonal values.

In contrast to these findings, the POD of combined position snapshots and the POD of combined velocity snapshots point out larger ROMs, see Fig. 5.6 and Fig. 5.7. Drops below approximately $1\text{E-}16$ are found after POV nine in the case of position snapshot data, and after POV eight in the case of velocity snapshot data. Unfortunately, the corresponding sets of proper orthogonal modes do not span sufficient subspaces to the full model. Hence the reduced simulations fail due to excessive physical coordinate error, as soon as the high-RPM area is reached. Valid subspaces, in terms of combined position data and combined velocity data, are in need of more than these eight or nine proper orthogonal modes. In the case of combined position snapshots a reasonable drop in magnitude is found after POV

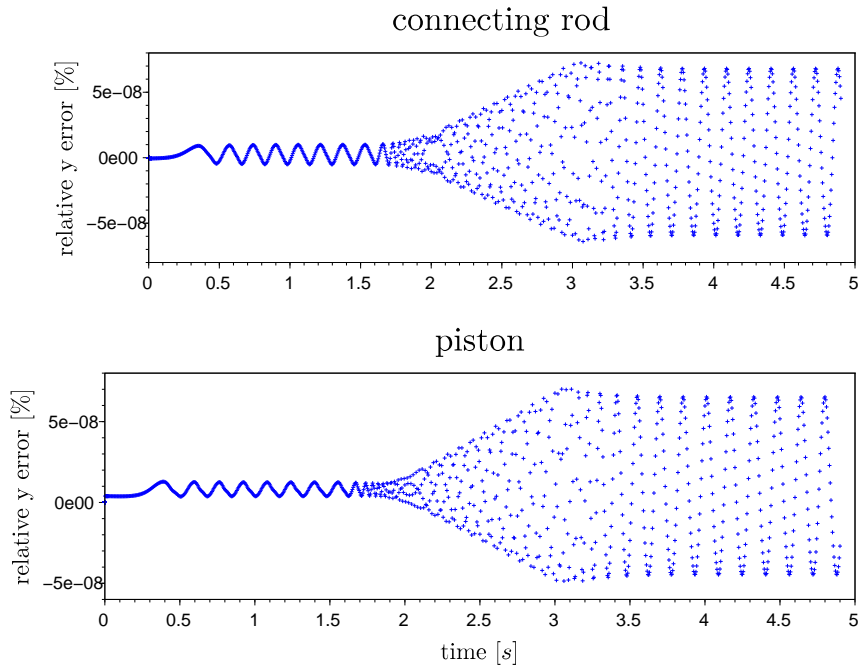


Figure 5.8: Time history of the relative position error - Rigid V8 crank drive

number twelve. For combined velocity data a reasonable drop is found after proper orthogonal value number eleven. Although the corresponding ROMs perform well in terms of the reduced order simulation, they are of larger dimension than the ROM computed by the new approach. They therefore take more computational time.

It should be noted that the reduced MBS is solvable only if the proposed constraint reduction is applied. This is regardless of the actual dimension of the classical POD subspace.

The results of the ROM derived by the new separated model order reduction approach are compared to the results of the full model simulation. Their validity is evaluated based on the relative position errors of several body coordinates. These are:

- the rotational e_0 parameters of the crankshaft and the connecting rod, and
- the y coordinate of the first cylinder's connecting rod and piston.

The relative position error plots in Figs. 5.8 and 5.9 point out that a maximum error of about $5E-8\%$ arises. Hence, the accuracy of the reduced order model is

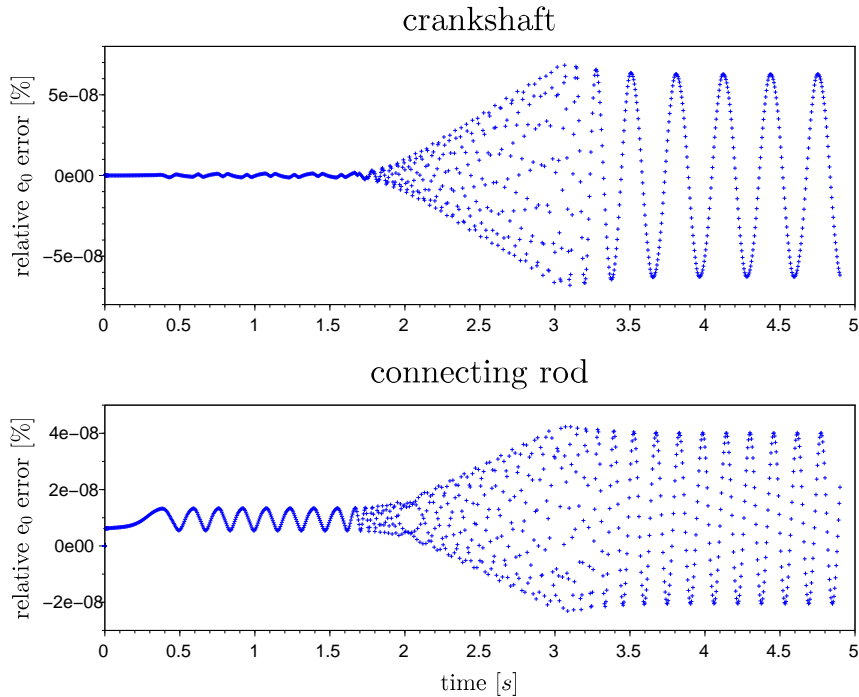


Figure 5.9: Time history of the relative e_0 error - Rigid V8 crank drive

high.

Summing up the findings of the separated POD approach, the number of translational coordinates is reduced by more than 92%. The number of rotational coordinates is reduced by more than 91%, and the number of constraint equations is also reduced by more than 92%.

The online simulation time is reduced from about 355s to approximately 179s. This is a reduction of roughly 50%.

5.2 A Rigid V8 Crank Drive in Mounting Condition

The former crank drive, depicted in Fig. 5.10, is extended by an engine housing. It is no longer fixed to the ground but supported by engine and gearbox mounts, as well as one torque roll restrictor. The engine supports are modeled by virtual spring and damper elements. These are indicated by three red colored coordinate systems in Fig. 5.10. Spring and damping parameters of the supports are chosen such that the static sinking is less than five millimeters. Furthermore, the rotation in the crank's longitudinal axis is less than five degrees at maximum rotation

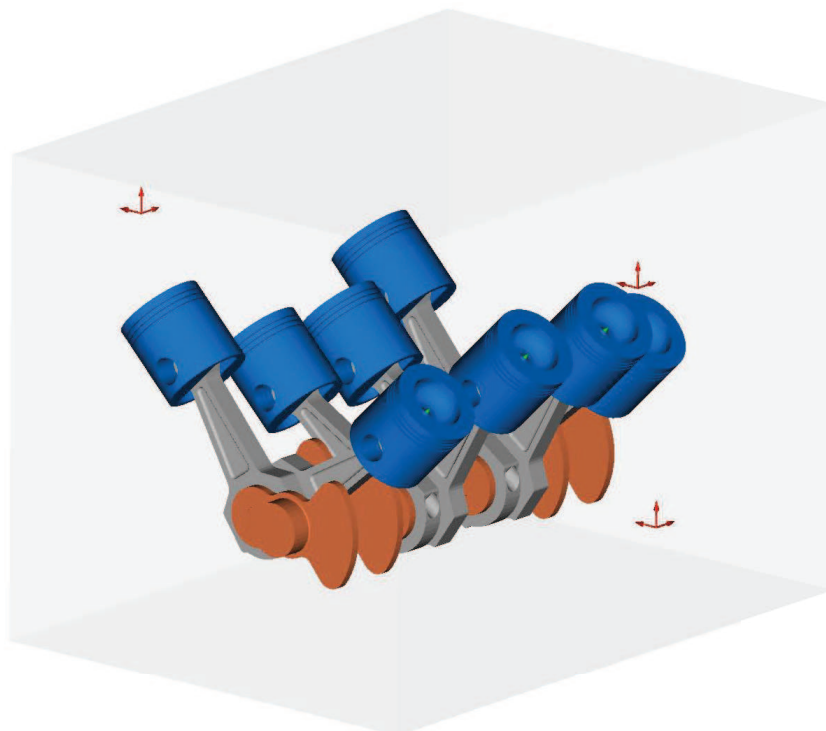


Figure 5.10: V8 crank drive in mounting condition

speed. The supports are built by a total of nine linear spring elements and nine linear damping elements. The support stiffness is $c_{\text{support spring}} = 75000$ [N/m] and the damping ratio is $d_{\text{support damper}} = 0.05$ [N · m · s]. The crank drive is dragged as presented in Sec. 5.1. Due to this setup the engine experiences superimposed vibrations.

5.2.1 Results

The results of the full system simulation are again investigated by the herein derived model order reduction method. By investigating the proper orthogonal value plot in Fig. 5.11 a drop in magnitude below $1\text{E-}16$ can be found after proper orthogonal value 22. This border is further highlighted by a flat spot. In the case of rotational POVs, see Fig. 5.12, the magnitude drops below $1\text{E-}16$ after proper orthogonal value 22. Hence, the coordinate-type sensitive POD approach suggests a reduced order model consisting of $n_{r,\text{trans}} = 22$ translational and $n_{r,\text{rot}} = 22$ rotational reduced coordinates.

Investigating the constraint singular value plot in Fig. 5.13, the magnitude drops rapidly after POV 37. Thus, the reduced order model consists of $m_r = 37$ con-

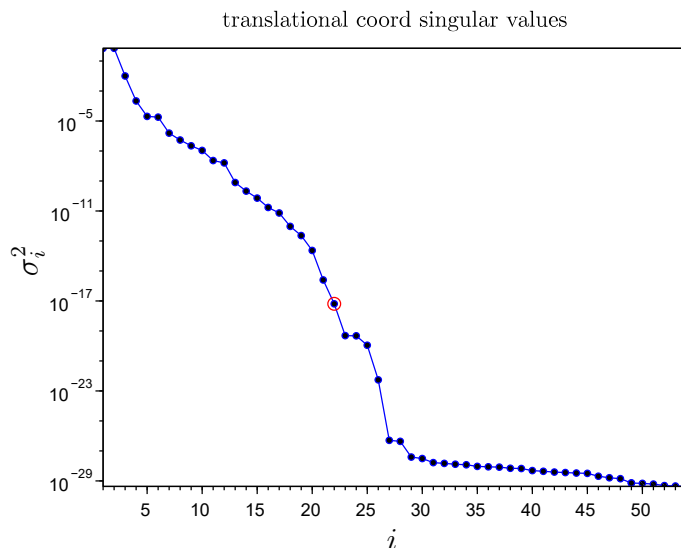


Figure 5.11: Translational velocity coordinate POVs - Rigid V8 crank drive in mounting condition

straint equations.

In contrast to these findings, the combined POD approach, see Fig 5.14, points out a drop below $1E-16$ after proper orthogonal value 31. This is a clearly smaller subspace than in the separated POD case. But, this set of proper orthogonal modes does not span a proper subspace to the full model, similar to the first numerical example in Sec. 5.1. The simulation fails due to excessive error in the physical coordinates, as soon as the high-RPM area is reached. Furthermore, a clear drop in magnitude is not found within a reasonable number of proper orthogonal values. Thus, a sufficient subspace to the original MBS is not directly derivable using the combined POD approach. The results of the reduced order model, consisting of ten reduced coordinates and nine reduced constraint equations, is compared to the results of the full model simulation. The relative position error measures are:

- the x, y, z coordinates of the crankshaft and the first cylinder's piston, and
- the rotational e_0 parameters of the crankshaft and the first cylinder's connecting rod and piston.

Investigating the relative position error plots in Figs. 5.15 to 5.17, the accuracy of the reduced order model is high. The maximum error is about $8E-6\%$ compared to the solution of the original system.

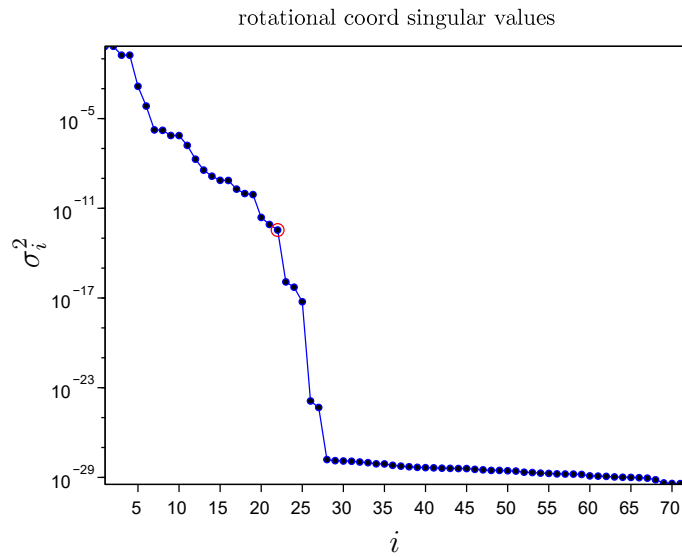


Figure 5.12: Rotational velocity coordinate POVs - Rigid V8 crank drive in mounting condition

In conclusion, the number of translational coordinates is reduced by almost 60%. The number of rotational coordinates is reduced by more than 69%. The number of constraint equations is also reduced by almost 69%.

Finally, the online simulation time is reduced from about 407s to approximately 311s. This is a reduction of about 24%.

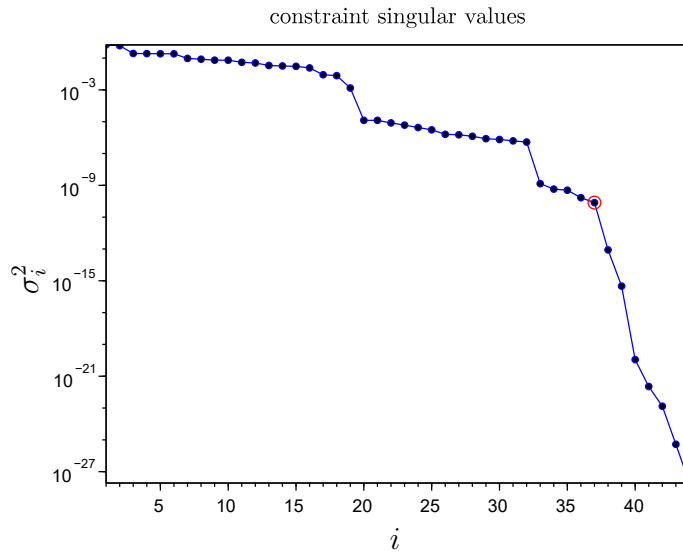


Figure 5.13: Constraint singular values - Rigid V8 crank drive in mounting condition

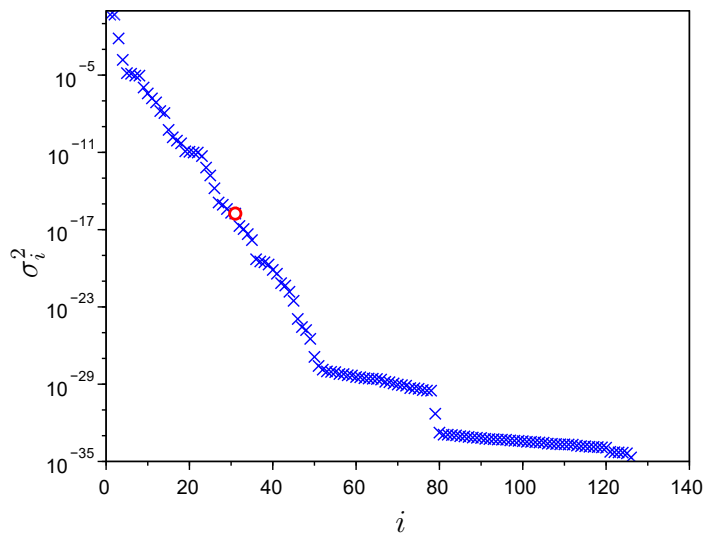


Figure 5.14: Position data POD - Plot of POVs computed from combined translational and rotational velocity information - Rigid V8 crank drive in mounting condition

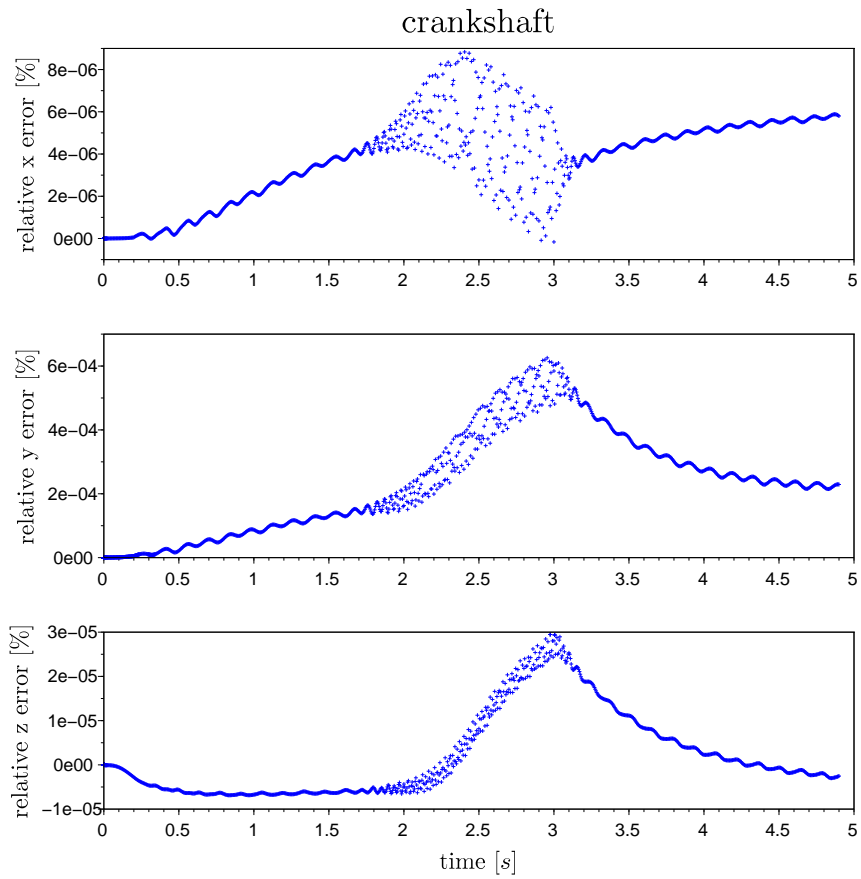


Figure 5.15: Time history of the relative crankshaft position error of the rigid V8 crank drive in mounting condition

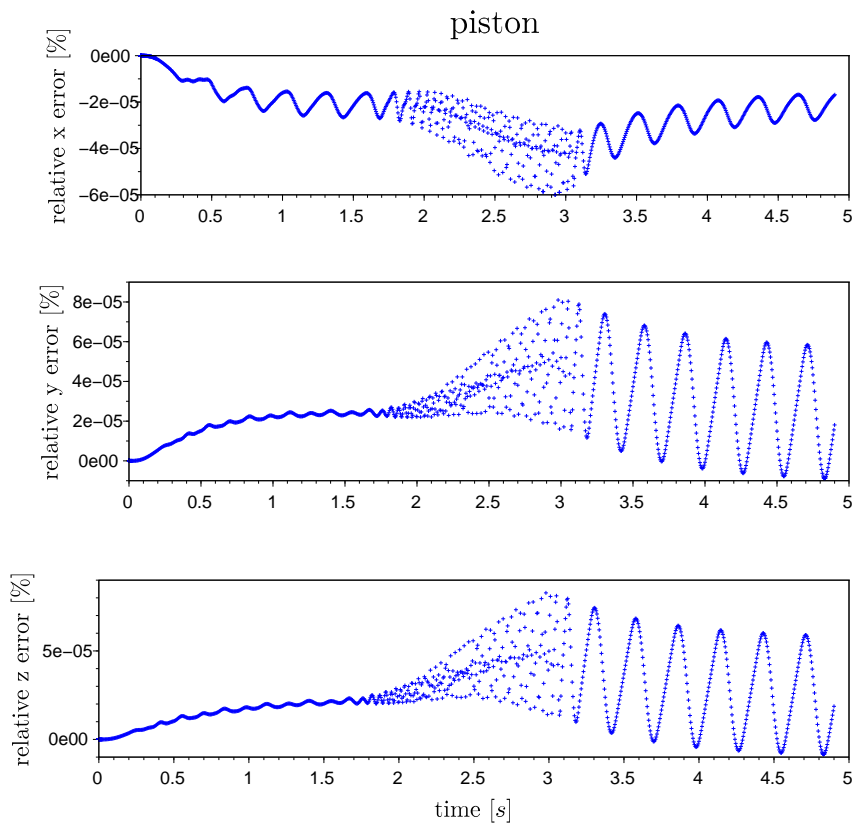


Figure 5.16: Time history of the relative piston position error of the rigid V8 crank drive in mounting condition

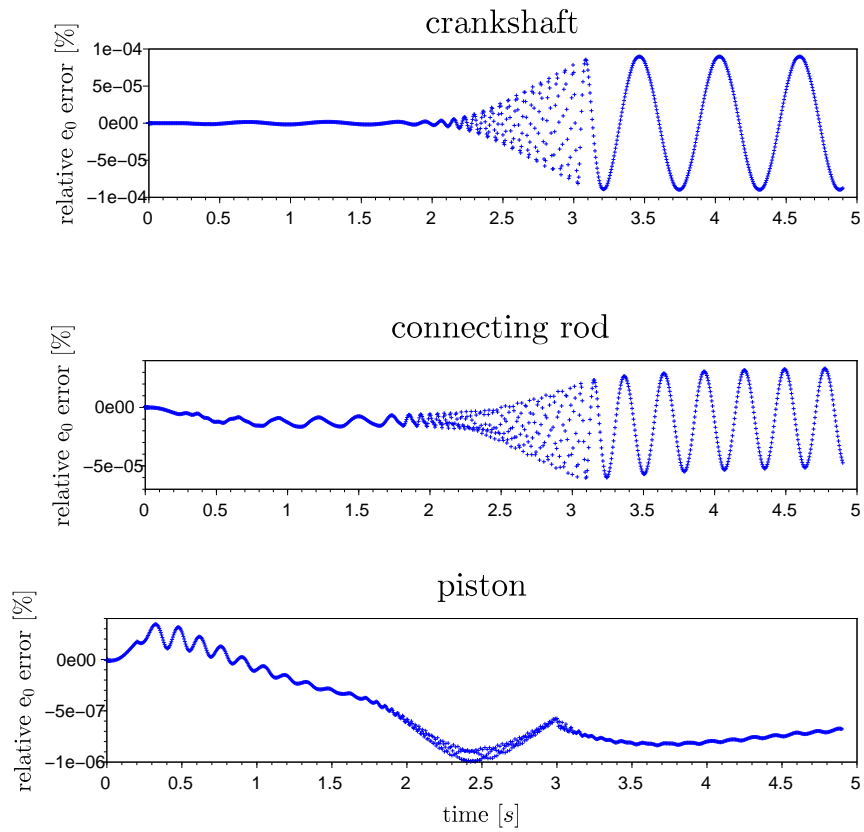


Figure 5.17: Time history of the relative e_0 error of the rigid V8 crank drive in mounting condition

5.3 A Partially Flexible Front Suspension

The front suspension in Fig. 5.18 originates from an offroad racing vehicle as used in the European Autocross Championship in 2016. The double wishbone suspension consists of the rigid parts

- steering knuckle, upper wishbone, steering rod and relay lever.

It further includes the flexible components

- lower wishbone and pushrod.

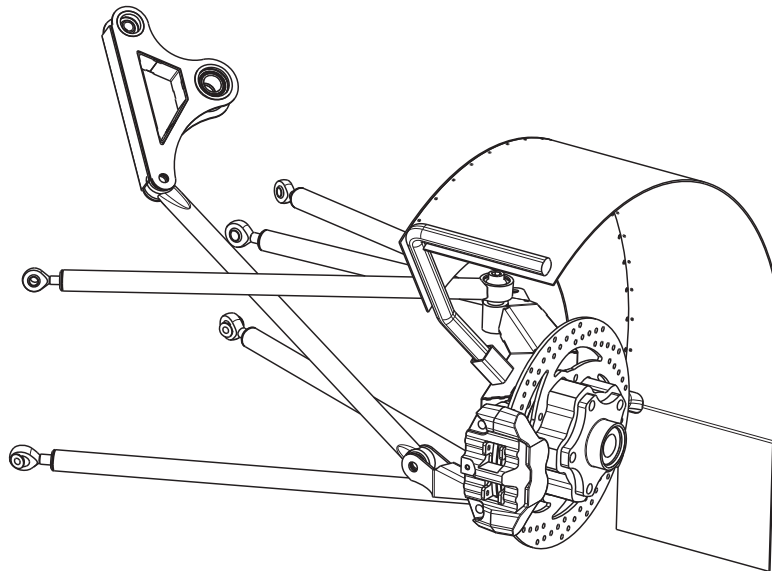


Figure 5.18: Double wishbone front suspension

Flexibility is introduced by a set of CMS modes which are computed in a preprocessing step utilizing a suitable FEM code.

This example should point out that the separated POD approach is able to reduce not only rigid but also flexible coordinates. To this end, the chosen mode bases, which describe the flexibility of the regarding bodies, consist of too many modes (flexible coordinates). The mode base describing the lower wishbone's flexibility covers the eigenfrequencies in Tab. 3. The mode base describing the pushrod's flexibility covers the eigenfrequencies in Tab. 4. As already mentioned in a previous Chapter, flexible bodies bring up the need of so-called zero inertia bodies (ZIB). These act as coupling elements between a flexible body's coupling point and the

rest of the MBS model. In the present case, the flexible lower wishbone consists of four coupling points. One allowing to establish a connection to the steering knuckle, one to connect to the flexible pushrod, and another two in the rear, allowing to connect to ground. Therefore, it introduces $n_{\text{rigid}} = 7$ rigid coordinates, and a set of $n_{\text{flex}} = 30$ flexible coordinates. Further, another 28 rigid coordinates are introduced which describe the ZIBs. Therefore, the flexible wishbone introduces a total of 64 coordinates to the MBS model.

In analogous manner, the flexible pushrod consists of two coupling points allowing to establish the connection to the flexible lower wishbone and to the relay lever. It introduces $n_{\text{rigid}} = 7$ rigid coordinates, and a set of $n_{\text{flex}} = 26$ flexible coordinates. Another 14 rigid coordinates are again introduced by the ZIBs. Therefore, the flexible pushrod introduces a total of 47 coordinates to the MBS model.

Moreover, the number of constraint equations increases. This is due to the ZIBs, which are coupled to the flexible body by a fix joint. Each of these couplings introduces six additional constraint equations.

Concluding, the MBS model consists of $b = 12$ bodies, $n = 140$ physical coordinates and $m = 84$ constraint equations. Detailed model data is summarized in Tab. 5.

The model is forced by vertical loading in the steering knuckle, according to the force time history in Fig. 5.19. A linear spring/damper element which acts on

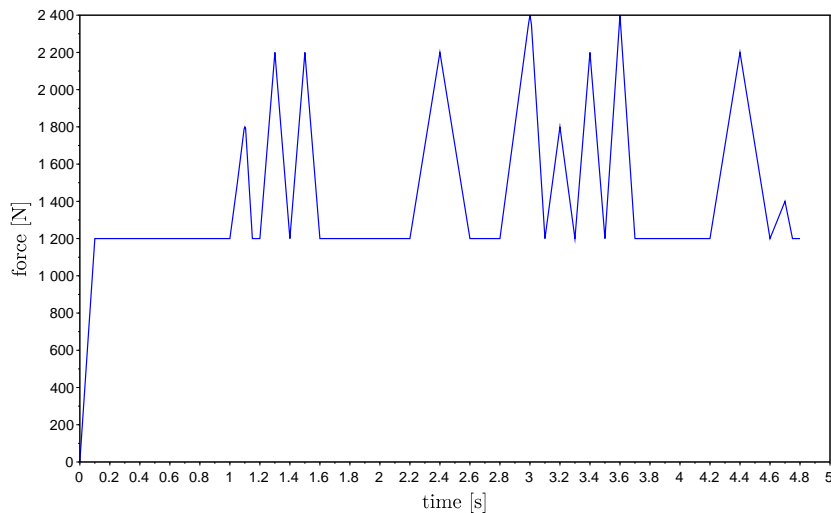


Figure 5.19: Vertical forcing acting on the steering knuckle - Partially flexible front suspension

the top eye of the relay lever opposes this force. The linear damping element is

designed such that the flexible bodies are allowed to reach high frequency areas and possibly cross eigenfrequencies. Force data are summarized in Tab. 6.

5.3.1 Results

The results of the full system simulation are again processed by the herein derived model order reduction method. By investigating the proper orthogonal value

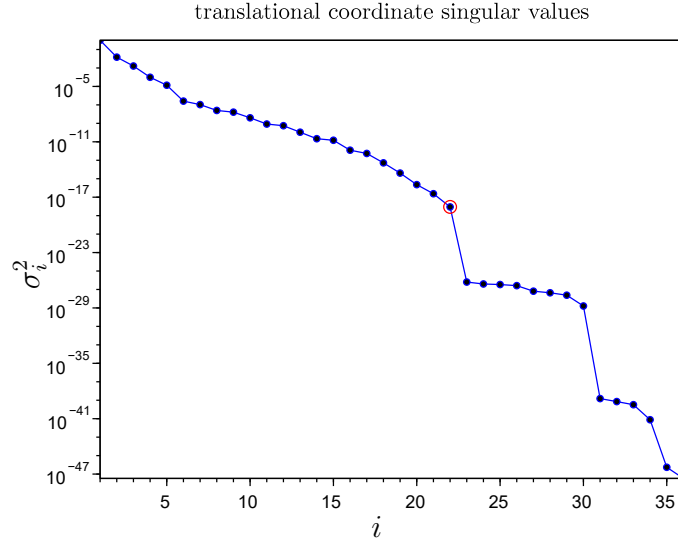


Figure 5.20: Translational velocity coordinate POVs - Partially flexible front suspension

plot in Fig. 5.20, a drop in magnitude below $1\text{E-}16$ can be found after POV 22. It is further highlighted by a flat spot. In the case of rotational POVs, see Fig. 5.21, the magnitude drops below $1\text{E-}16$ after proper orthogonal value 26. As for the rotational proper orthogonal value plot, the flexible POV plot does not indicate the reduced order model directly. Nevertheless, the flexible POV magnitude drops below $1\text{E-}16$ after proper orthogonal value 13. The coordinate-type sensitive POD approach therefore suggests a reduced order model consisting of $n_{r,\text{trans}} = 22$ translational, $n_{r,\text{rot}} = 26$ rotational and $n_{r,\text{flex}} = 13$ flexible reduced coordinates. Investigating the constraint singular value plot in Fig. 5.23, the magnitude drops rapidly after proper orthogonal value 48. The reduced order model therefore consists of $m_r = 48$ constraint equations.

In contrast, the combined POD approach does not point out any drop. Still, the absolute proper orthogonal value value drops below $1\text{E-}16$ after POV 20. This is a clearly smaller subspace than in the separated POD case. Again, this set

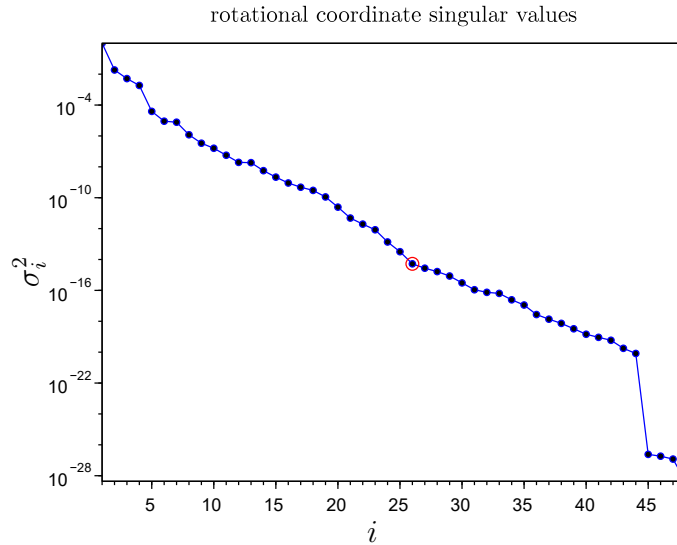


Figure 5.21: Rotational velocity coordinate POVs - Partially flexible front suspension

of proper orthogonal modes does not span a proper subspace to the full model. The simulation fails due to excessive error in the physical coordinates. Still, by sticking with the 20 proper orthogonal modes and artificially reducing the number of remaining constraint equations to twelve a vaguely approximating subspace can be spanned, see Figs. 5.25 to 5.27.

The results of the separated POD approach and the results of the (classical) combined snapshot POD approach are compared to the results of the full model simulation of several body coordinates. The relative position error measures are:

- the y coordinate of the steering knuckle, pushrod and lower wishbone,
- the rotational e_0 parameters of the relay lever, the pushrod and lower wishbone,
- the first two dominant flexible coordinates of the pushrod and the first dominant flexible coordinate of the lower wishbone.

Investigating Figs. 5.25 to 5.27, the separated POD approximate the original model with high accuracy. In contrast, the classical POD approach results in an insufficient reduced order model.

Summing up the findings of the separated POD approach, the number of translational coordinates is reduced by almost 39%. The number of rotational coordinates

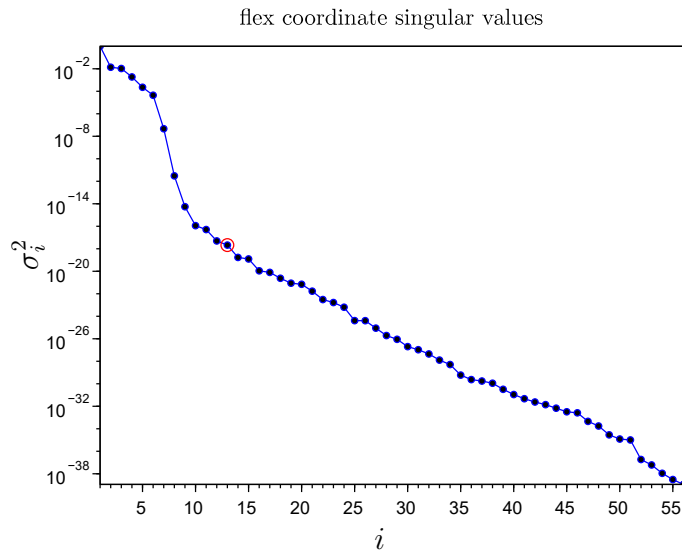


Figure 5.22: Flexible velocity coordinate POVs - Partially flexible front suspension

is reduced by nearly 16% and the number of flexible coordinates is reduced by almost 77%. Accordingly, the number of constraint equations reduces by almost 43%.

The online simulation time is reduced from about 615s to approximately 436s. This is a reduction of more than 29%.

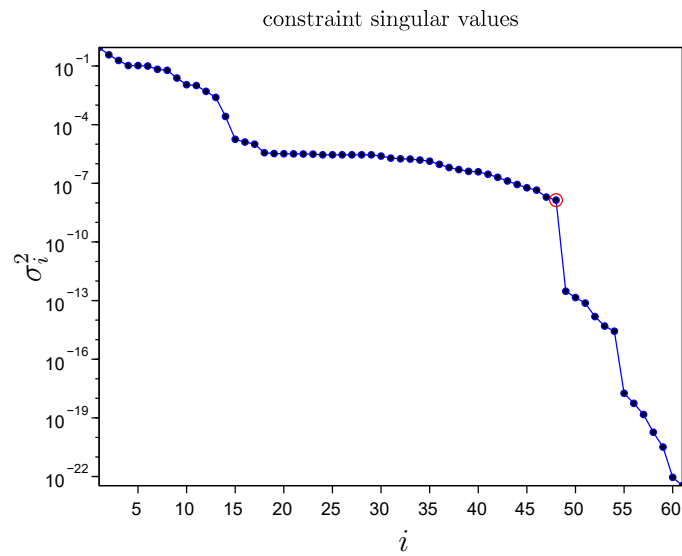


Figure 5.23: Constraint singular values - Partially flexible front suspension

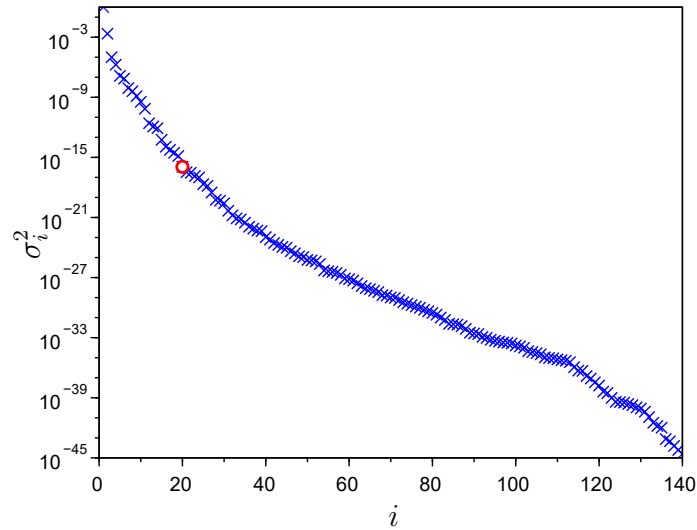


Figure 5.24: Classical POD approach - Plot of POVs computed from combined translational, rotational and flexible velocity information - Partially flexible front suspension

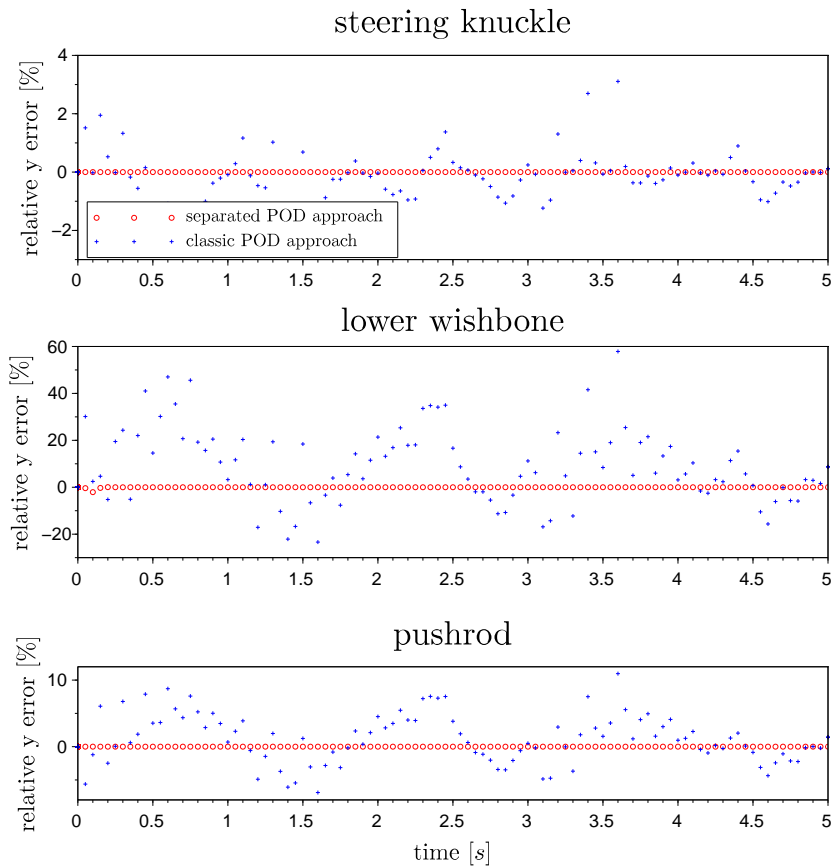


Figure 5.25: Time history of the relative y coordinate error of the partially flexible front suspension

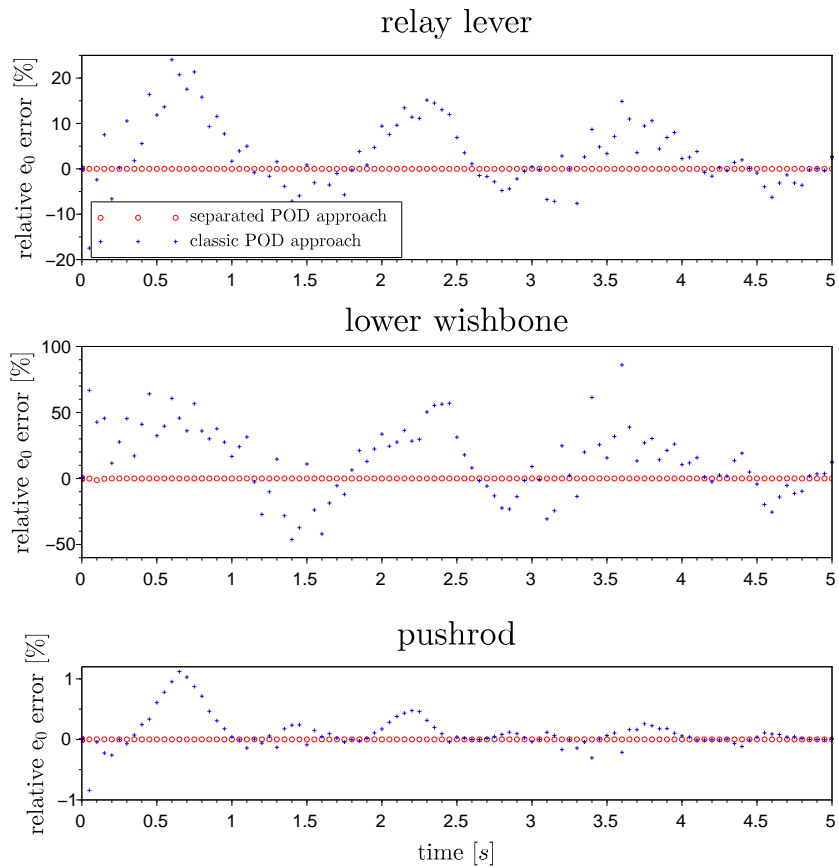


Figure 5.26: Time history of the relative e_0 error of the partially flexible front suspension

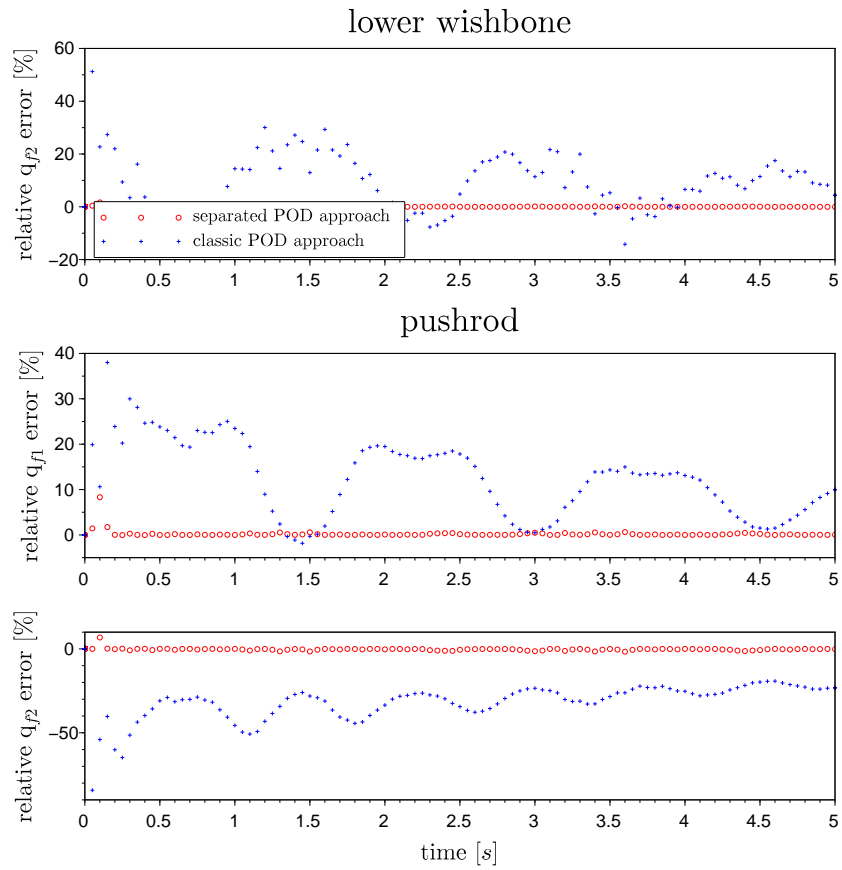


Figure 5.27: Time history of the relative flexible coordinate error of the partially flexible front suspension

5.4 A Rigid Junior Dirtbike

This example introduces the electrical junior dirtbike depicted in Fig. 5.28. The model consists of ten bodies, which are

- the frame,
- the front and the rear wheel,
- the battery,
- the swing arm including the electric motor,
- the upper and the lower part of the shock,
- the upper and the lower part of the fork including the handlebar, and
- a point mass, representing the physical properties of a dummy rider.

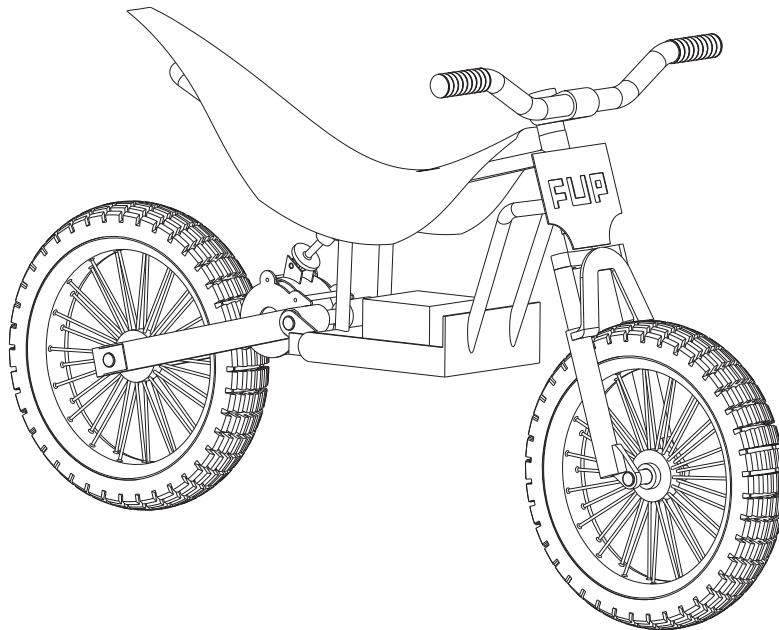


Figure 5.28: Electrical junior dirtbike

Detailed physical data is summarized in Tabs. 7 and 8. The model is subject to two linear spring/damper elements which represent the shock and fork behavior. The dirtbike is put on a virtual MBS test bench (two post test bench), in order to apply force measurements taken from test rides. One spring/damper element

is applied to each wheel, allowing the dirtbike to set into riding position at the beginning of the simulation. Afterwards, two time dependent forces are applied to the front and rear wheel, see Fig. 5.29. Detailed model data is summarized in

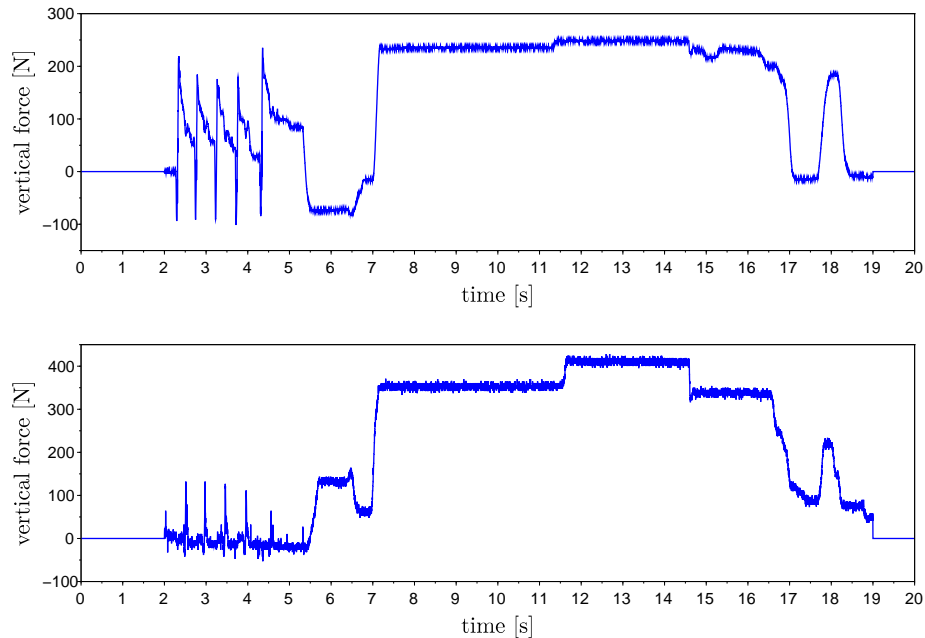


Figure 5.29: Vertical forcing acting on the wheels - Electrical junior dirtbike

Tab. 9.

5.4.1 Results

The results of the full system simulation are again investigated by the herein derived model order reduction method. By investigating the proper orthogonal value plot in Fig. 5.30, a huge drop in magnitude, even below approximately $1E-16$, can be found after POV nine. In the case of rotational proper orthogonal values, the proper orthogonal value magnitude drops significantly after proper orthogonal value six. Hence, the coordinate-type-sensitive POD approach suggests a reduced order model consisting of $n_{r,trans} = 9$ translational and $n_{r,rot} = 6$ rotational reduced coordinates.

Investigating the constraint singular value plot shown in Fig. 5.32, the magnitude drops rapidly after POV 11. Therefore, the reduced order model consists of $m_r = 11$ constraint equations.

In contrast, the combined snapshot data POD approach, cf. Fig. 5.33, points out a huge drop after proper orthogonal value ten. This is a smaller subspace than in

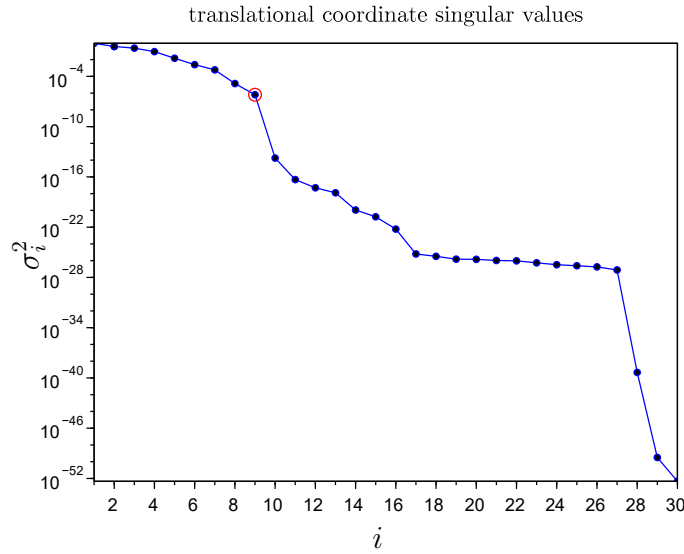


Figure 5.30: Translational coordinate POVs - Electrical junior dirtbike

the separated POD case.

The results of the separated POD approach, and the results of the classic POD approach are compared to the results of the full model simulation. The relative position error measures are:

- the x coordinate of the frame and shock,
- the z coordinate of the swing arm, and
- the rotational e_0 parameters of the rider dummy, the swing arm and the shock.

The subspace spanned by the combined snapshot data POD approach does not span a proper subspace to the full model. The simulation fails due to excessive error in the physical coordinates.

In contrast, the accuracy of the separated POD approach is again high with a maximum relative error of about 0.1%.

Summing up the findings of the separated POD approach, the number of translational coordinates is reduced by 70%. The number of rotational coordinates is reduced by 85%. Accordingly, the number of constraint equations decreases by more than 83%.

The online simulation time is reduced from about 1972s to approximately 971s. This is a reduction of more than 50%.

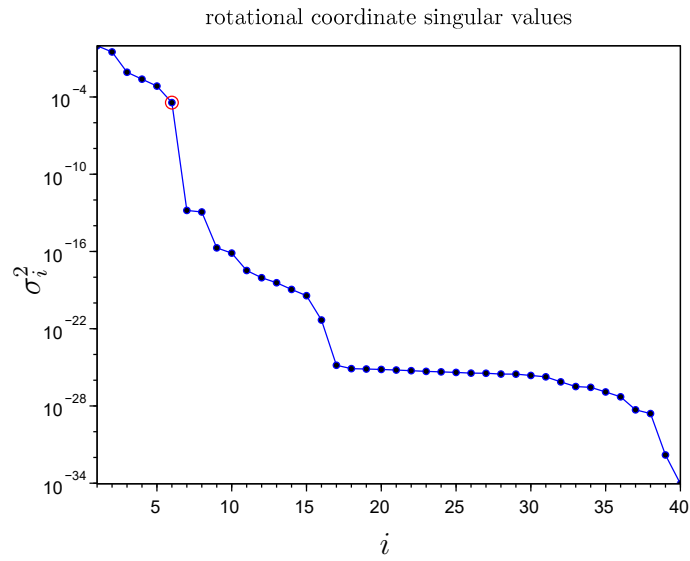


Figure 5.31: Rotational coordinate POVs - Electric junior dirtbike

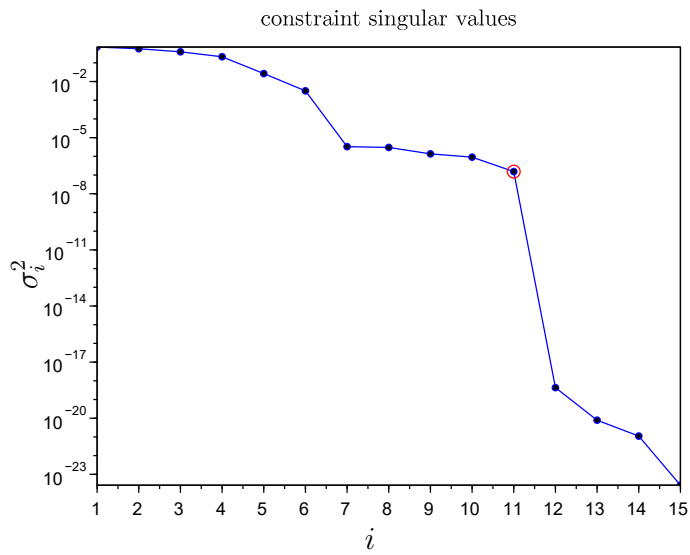


Figure 5.32: Constraint singular values - Electric junior dirtbike

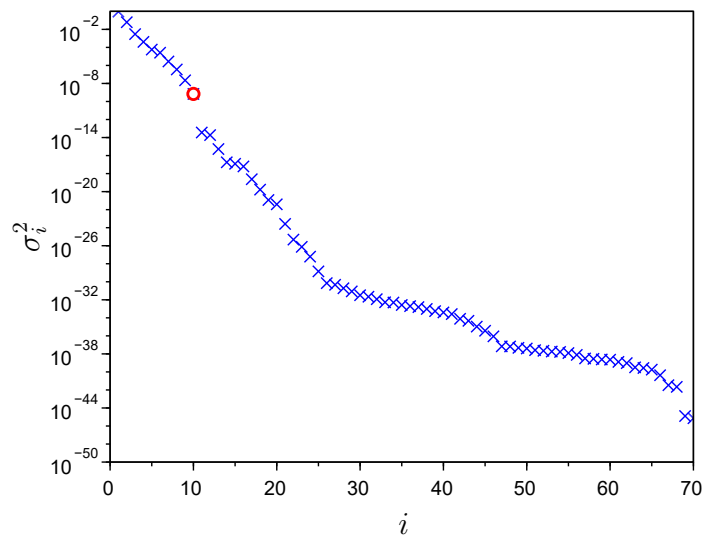


Figure 5.33: Combined snapshot data POD approach - Electrical junior dirtbike

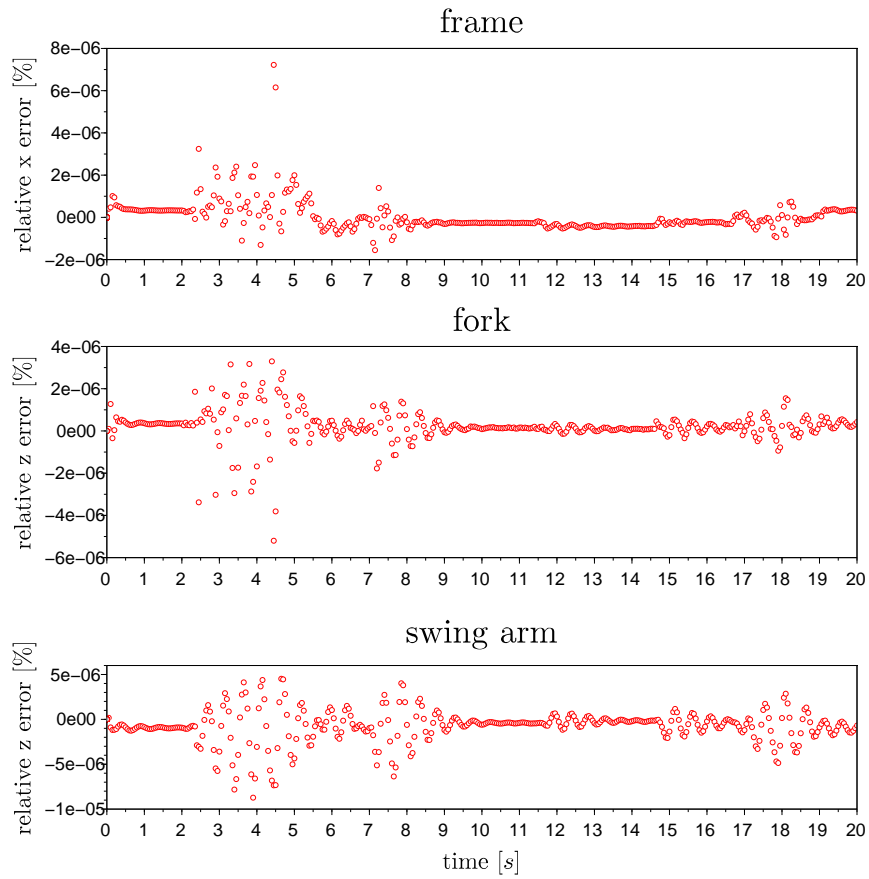
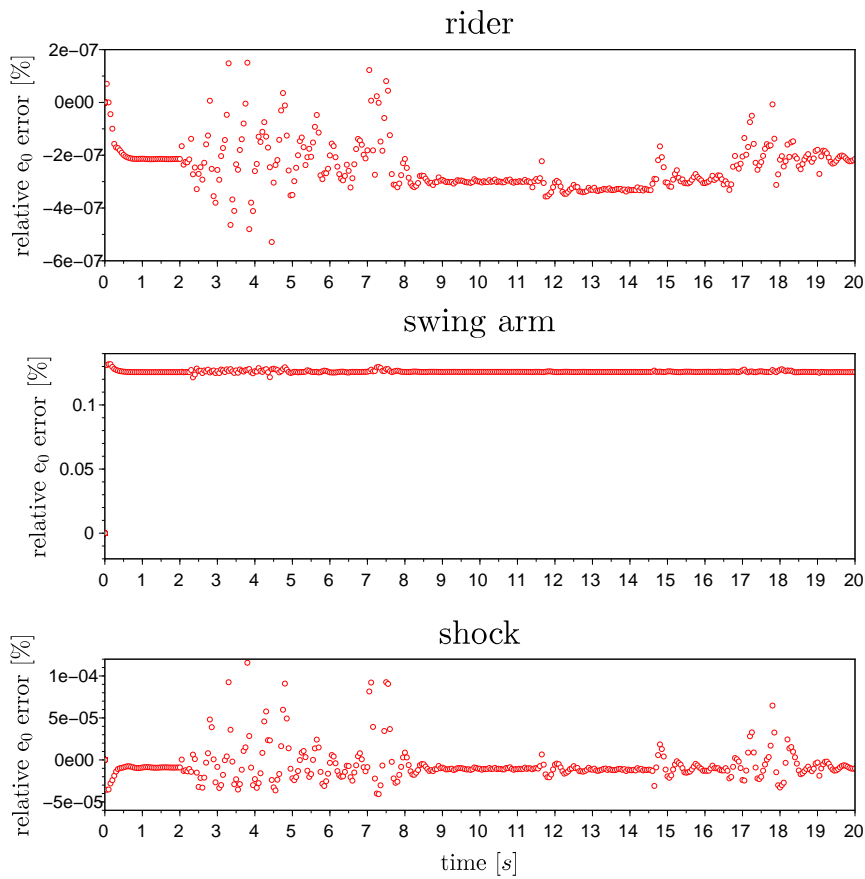


Figure 5.34: Time history of relative translational coordinate errors - Electrical junior dirtbike

Figure 5.35: Time history of the relative e_0 error - Electrical junior dirtbike

5.4.2 Discussion

The large scale examples presented in this Chapter point out the performance of the derived model order reduction approach.

As it becomes obvious a general indicator for the dimension of the ROM can not be ensured. For the standard POD approach, which processes all coordinate snapshots in once, it is often necessary to try different promising-looking sets of proper orthogonal modes.

For the coordinate-scale sensitive approach the choice of a sufficient number of reduced coordinates seems to be easier. Due to taking into account the different scales of translational, rotational and flexible coordinates, each motion-type is handled without under- or overestimation. The novel approach seems to allow an absolute proper orthogonal value value as indicator of the reduced order model. This seems to be due to the data which is always of the same scale. The indicator is in the range of approximately $1E-16$ for the numerical examples in this Chapter. Still it must be emphasized that this value is only applicable to the presented examples. It must not be thought of as a general indicator at all. The determination of the ROM is mainly due to user experience in "reading" the proper orthogonal values of a single set of snapshots.

In terms of the constraint coordinate reduction, the numerical examples show the ability to identify the set of regular constraint equations. The singular value plots point out a minimal set of constraint equations by drops in magnitude. Therefore, the singular values of the constraint coordinate reduction can be interpreted similar to proper orthogonal values. A choice on the number of unique constraint equations due to large drops or a drop below $1E-16$ is possible.

Talking about performance, a maximum reduction of more than 50% in the simulation time is achieved. Further, coordinate savings up to 90% and more are possible. The saving in physical and constraint coordinates is a hard fact. In contrast, time-savings of the former examples should not be taken as absolute values. This is due to the implementation of the MBS code in Scilab. Scilab is, in contrast to e.g. C++, an interpreted programming language. The reduced order model has to switch from the reduced to the approximated full space in every iteration, as all system matrices are built in terms of the full state vector. Due to the interpreter-like nature of the Scilab environment, back and forth projection of the reduced system takes excessive time. Therefore, absolute time savings could be further improved by switching from Scilab to a C++ implementation, which is planned in future work.

Application to Parameter Identification Tasks in Multibody Systems

The derived MOR method was developed under the long-term perspective of a parameter identification environment. As the MBS system has to be solved repetitively it is a suitable field of application to the derived MOR.

The computation of the gradient of the cost function is usually the most time consuming task, and the adjoint method is a highly efficient strategy to handle it in the field of multibody dynamics. It was used in the sensitivity analysis of systems of partial differential equations or systems of differential algebraic equations (DAE) by authors such as [47, 12, 29, 83, 16]. Nachbagauer et al. [76, 77] presented how to directly apply the adjoint method to redundantly formulated multibody system dynamics.

In terms of the parameter identification of unknown model parameters, the MBS model is enhanced by the unknown parameters \mathbf{u} :

$$\begin{aligned} \mathbf{M}(\mathbf{q}, \mathbf{u}) \ddot{\mathbf{q}} + \mathbf{C}_{\mathbf{q}}(\mathbf{q})^T \boldsymbol{\lambda} &= \mathbf{Q}(\mathbf{q}, \dot{\mathbf{q}}, \mathbf{u}) \\ \mathbf{C}(\mathbf{q}) &= \mathbf{0}. \end{aligned} \quad (6.1)$$

Note that in Eq. (6.1), unknown parameters are supposed to appear in the mass matrix and in the vector of applied forces.

The identification of unknown model parameters is represented by an optimization problem. Here, the goal is to minimize the root mean square error between (real) measured values and calculated simulation results. The cost function to be

minimized takes the general form

$$J = \int_0^T h(\mathbf{q}, \mathbf{v}, t) dt, \quad (6.2)$$

with $\mathbf{v} = \dot{\mathbf{q}}$. In our case, h is given by the root mean square error

$$h(\mathbf{q}, \mathbf{v}, t) = \sum_{i=1}^N \frac{1}{2} (\bar{\mathbf{s}}_i(t) - \mathbf{s}_i(\mathbf{q}, \mathbf{v}))^2. \quad (6.3)$$

Therein, $\bar{\mathbf{s}}_i$ are the measured signals and \mathbf{s}_i are the system outputs of the simulation.

The gradient of this cost function is efficiently calculated using the adjoint method.

6.1 Parameter Identification utilizing the Adjoint Method

According to Nachbagauer et al. [76], the cost function is enhanced by the multi-body model in Eq. (6.1):

$$J = \int_0^T \left\{ h(\mathbf{q}, \mathbf{v}, \mathbf{u}, t) + \mathbf{p}^\top (\dot{\mathbf{q}} - \mathbf{v}) + \mathbf{w}^\top [\mathbf{M}\dot{\mathbf{v}} - \mathbf{Q} + \mathbf{C}_q^\top \boldsymbol{\lambda}] + \boldsymbol{\mu}^\top \mathbf{C} \right\} dt. \quad (6.4)$$

$\mathbf{p} \in \mathbb{R}^n$, $\mathbf{w} \in \mathbb{R}^n$, $\boldsymbol{\mu} \in \mathbb{R}^m$ are the adjoint variables, which are arbitrary at this point. The variation of the function reads

$$\begin{aligned} \delta J = & \int_0^T \left\{ h_{\mathbf{q}} \delta \mathbf{q} + h_{\mathbf{v}} \delta \mathbf{v} + h_{\mathbf{u}} \delta \mathbf{u} + \mathbf{p}^\top (\delta \dot{\mathbf{q}} - \delta \mathbf{v}) \right. \\ & + \mathbf{w}^\top \left[(\mathbf{M}\dot{\mathbf{v}})_{\mathbf{q}} \delta \mathbf{q} + \mathbf{M} \delta \dot{\mathbf{v}} - \mathbf{Q}_{\mathbf{q}} \delta \mathbf{q} - \mathbf{Q}_{\mathbf{v}} \delta \mathbf{v} - \mathbf{Q}_{\mathbf{u}} \delta \mathbf{u} + (\mathbf{C}_q^\top \boldsymbol{\lambda})_{\mathbf{q}} \delta \mathbf{q} + \mathbf{C}_q^\top \delta \boldsymbol{\lambda} \right] \\ & \left. + \boldsymbol{\mu}^\top \mathbf{C}_q \delta \mathbf{q} \right\} dt. \end{aligned} \quad (6.5)$$

After applying partial integration to terms including $\delta \dot{\mathbf{q}}$ and $\delta \dot{\mathbf{v}}$ (cf. [76]), the adjoint variables are finally defined by the equations

$$\begin{aligned} \dot{\mathbf{p}} &= h_{\mathbf{q}}^\top + \left((\mathbf{M}\dot{\mathbf{v}})_{\mathbf{q}} - \mathbf{Q}_{\mathbf{q}} + (\mathbf{C}_q^\top \boldsymbol{\lambda})_{\mathbf{q}} \right)^\top \mathbf{w} + \mathbf{C}_q^\top \boldsymbol{\mu} \\ \frac{d}{dt} (\mathbf{M}\mathbf{w}) &= h_{\mathbf{v}}^\top - \mathbf{p} - \mathbf{Q}_{\mathbf{v}}^\top \mathbf{w} \\ \mathbf{0} &= \mathbf{C}_q \mathbf{w} \\ \mathbf{0} &= \mathbf{p}(T) \\ \mathbf{0} &= \mathbf{M}(T) \mathbf{w}(T) \end{aligned} \quad (6.6)$$

such that if Eqs. (6.6) are satisfied, the variation in Eq. (6.5) reduces to

$$\delta J = \int_0^T h_{\mathbf{u}} - \mathbf{w}^\top \mathbf{Q}_{\mathbf{u}} \delta \mathbf{u} dt = \left[\int_0^T (h_{\mathbf{u}} - \mathbf{w}^\top \mathbf{Q}_{\mathbf{u}}) dt \right] \delta \mathbf{u}. \quad (6.7)$$

Hence, the gradient of J with respect to \mathbf{u} is given by

$$\frac{\delta J}{\delta \mathbf{u}} = \int_0^T [h_{\mathbf{u}}^\top - \mathbf{Q}_{\mathbf{u}}^\top \mathbf{w}] dt. \quad (6.8)$$

For the adjoint gradient computation one first has to solve the original system in Eq. (6.1) forward in time. Secondly, by using the system information generated by the forward simulation (the snapshot data), the linear set of adjoint equations in Eqs. (6.6) is solved. Third, the gradient of the cost function in Eq. (6.8) is calculated. The gradient information is then processed by a suitable optimization strategy, e.g. the BFGS algorithm (see for instance [85]).

The literature deals with reduced order adjoint systems to ordinary and partial differential equations, c.f. [33, 28, 5, 44, 59]. But, the reduction of the adjoint system in the sense of [76] has, to the best knowledge of the author, not been investigated yet.

6.1.1 The Adjoint Method in the Context of Reduced Order Multibody Systems

This section presents the derivation of the adjoint system for a reduced multibody system by applying the introduced flat projection. The subspace on which the adjoint system is projected to, is the same as for the reduced forward simulation. The cost function in reduced coordinates takes the form

$$J = \int_0^T h(\tilde{\mathbf{q}}, \tilde{\mathbf{v}}, \mathbf{u}, t) dt = \int_0^T h(\mathbf{V}\mathbf{q}_r, \mathbf{V}\mathbf{v}_r, \mathbf{u}, t) dt. \quad (6.9)$$

Enhanced by the reduced multibody system in Eq. (4.35), the cost function reads

$$\begin{aligned} J = \int_0^T \left\{ h(\tilde{\mathbf{q}}, \tilde{\mathbf{v}}, \mathbf{u}, t) + \mathbf{p}_r^\top (\dot{\mathbf{q}}_r - \mathbf{v}_r) \right. \\ \left. + \mathbf{w}_r^\top \mathbf{V}^\top [\mathbf{M}(\tilde{\mathbf{q}}) \mathbf{V} \dot{\mathbf{v}}_r - \mathbf{Q}(\tilde{\mathbf{q}}, \tilde{\mathbf{v}}, \mathbf{u}) + \mathbf{C}_q^\top(\tilde{\mathbf{q}}) \mathbf{\Gamma}^\top \boldsymbol{\lambda}_l] \right. \\ \left. + \boldsymbol{\mu}_l^\top \mathbf{\Gamma} \mathbf{C}(\tilde{\mathbf{q}}) \right\} dt. \end{aligned} \quad (6.10)$$

The adjoint variables $\mathbf{p}_r \in \mathbb{R}^r$, $\mathbf{w}_r \in \mathbb{R}^r$, $\boldsymbol{\mu}_l \in \mathbb{R}^l$ are again arbitrary at this point. The variation of the reduced model's cost function is given by

$$\begin{aligned} \delta J = & \int_0^T \left\{ h_{\mathbf{q}_r} \delta \mathbf{q}_r + h_{\mathbf{v}_r} \delta \mathbf{v}_r + h_{\mathbf{u}} \delta \mathbf{u} + \mathbf{p}_r^\top (\delta \dot{\mathbf{q}}_r - \delta \mathbf{v}_r) \right. \\ & + \mathbf{w}_r^\top \mathbf{V}^\top \left[(\mathbf{M}\mathbf{V}\dot{\mathbf{v}}_r)_{\mathbf{q}_r} \delta \mathbf{q}_r + \mathbf{M}\mathbf{V} \delta \dot{\mathbf{v}}_r - \mathbf{Q}_{\mathbf{q}_r} \delta \mathbf{q}_r - \mathbf{Q}_{\mathbf{v}_r} \delta \mathbf{v}_r - \mathbf{Q}_{\mathbf{u}} \delta \mathbf{u} \right. \\ & + \left. \left. \left(\mathbf{C}_q^\top \Gamma^\top \boldsymbol{\lambda}_l \right)_{\mathbf{q}_r} \delta \mathbf{q}_r + \mathbf{C}_q^\top \Gamma^\top \delta \boldsymbol{\lambda}_l \right] \right. \\ & \left. + \boldsymbol{\mu}_l^\top (\Gamma \mathbf{C})_{\mathbf{q}_r} \delta \mathbf{q}_r \right\} dt. \end{aligned} \quad (6.11)$$

In order to eliminate the time derivatives, the integration by parts for the terms including $\delta \dot{\mathbf{q}}_r$ and $\delta \dot{\mathbf{v}}_r$ is computed:

$$\int_0^T \mathbf{p}_r^\top \delta \dot{\mathbf{q}}_r dt = - \int_0^T \dot{\mathbf{p}}_r^\top \delta \mathbf{q}_r dt + \mathbf{p}_r^\top \delta \mathbf{q}_r \Big|_{t=T} \quad (6.12)$$

$$\begin{aligned} \int_0^T \mathbf{w}_r^\top (\mathbf{V}^\top \mathbf{M}\mathbf{V} \delta \dot{\mathbf{v}}_r) dt &= - \int_0^T \frac{d}{dt} (\mathbf{w}_r^\top \mathbf{V}^\top \mathbf{M}\mathbf{V}) \delta \mathbf{v}_r dt \\ &+ \mathbf{w}_r^\top \mathbf{V}^\top \mathbf{M}\mathbf{V} \delta \mathbf{v}_r \Big|_{t=T}. \end{aligned} \quad (6.13)$$

Rearranging Eq. (6.11) and taking into account Eqs. (6.12-6.13), the variation of the cost function is given by

$$\begin{aligned} \delta J = & \int_0^T \left\{ \left[h_{\mathbf{q}_r} - \dot{\mathbf{p}}_r^\top + \mathbf{w}_r^\top \mathbf{V}^\top \left((\mathbf{M}\mathbf{V}\dot{\mathbf{v}}_r)_{\mathbf{q}_r} - \mathbf{Q}_{\mathbf{q}_r} + \left(\mathbf{C}_q^\top \Gamma^\top \boldsymbol{\lambda}_l \right)_{\mathbf{q}_r} \right) \right. \right. \\ & + \left. \left. \boldsymbol{\mu}_l^\top (\Gamma \mathbf{C})_{\mathbf{q}_r} \right] \delta \mathbf{q}_r \right. \\ & + \left[h_{\mathbf{v}_r} - \mathbf{p}_r^\top - \mathbf{w}_r^\top \mathbf{V}^\top \mathbf{Q}_{\mathbf{v}_r} - \frac{d}{dt} (\mathbf{w}_r^\top \mathbf{V}^\top \mathbf{M}\mathbf{V}) \right] \delta \mathbf{v}_r \\ & + \mathbf{w}_r^\top \mathbf{V}^\top \mathbf{C}_q^\top \Gamma^\top \delta \boldsymbol{\lambda}_l + \left[h_{\mathbf{u}} - \mathbf{w}_r^\top \mathbf{V}^\top \mathbf{Q}_{\mathbf{u}} \right] \delta \mathbf{u} \left. \right\} dt \\ & + \mathbf{p}_r^\top \delta \mathbf{q}_r \Big|_{t=T} + \mathbf{w}_r^\top \mathbf{V}^\top \mathbf{M}\mathbf{V} \delta \mathbf{v}_r \Big|_{t=T}. \end{aligned} \quad (6.14)$$

Due to the reduced order model under investigation, the Jacobians in Eq. (6.14) differ from the full model's equivalent. They may be rearranged in order to correspond to the full model Jacobians. By taking into account the flat projection, and

recalling that \mathbf{V} and $\mathbf{\Gamma}$ are constant, terms of the form $(\cdot)_{\mathbf{q}_r}$ can be rearranged as

$$(\cdot)_{\mathbf{q}_r} = \left. \frac{\partial(\cdot)}{\partial \mathbf{q}} \right|_{\substack{\mathbf{q}=\tilde{\mathbf{q}} \\ \mathbf{v}=\tilde{\mathbf{v}}}} \cdot \frac{\partial \mathbf{q}}{\partial \mathbf{q}_r} = (\cdot)_{\mathbf{q}} \cdot \mathbf{V}. \quad (6.15)$$

Using Eq. (6.15), Eq. (6.14) reads

$$\begin{aligned} \delta J = & \int_0^T \left\{ \left[h_{\mathbf{q}} \mathbf{V} - \dot{\mathbf{p}}_r^\top + \mathbf{w}_r^\top \mathbf{V}^\top \left((\mathbf{M}\dot{\mathbf{v}})_{\mathbf{q}} - \mathbf{Q}_{\mathbf{q}} + (\mathbf{C}_{\mathbf{q}}^\top \mathbf{\Gamma}^\top \boldsymbol{\lambda}_l)_{\mathbf{q}} \right) \right] \Phi \right. \\ & + \left. \boldsymbol{\mu}_l^\top \mathbf{\Gamma} \mathbf{C}_{\mathbf{q}} \mathbf{V} \right] \delta \mathbf{q}_r \\ & + \left[h_{\mathbf{v}} \mathbf{V} - \mathbf{p}_r^\top - \mathbf{w}_r^\top \mathbf{V}^\top \mathbf{Q}_{\mathbf{v}} \mathbf{V} - \frac{d}{dt} (\mathbf{w}_r^\top \mathbf{V}^\top \mathbf{M} \mathbf{V}) \right] \delta \mathbf{v}_r \\ & + \left[\mathbf{w}_r^\top \mathbf{V}^\top \mathbf{C}_{\mathbf{q}}^\top \mathbf{\Gamma}^\top \right] \delta \boldsymbol{\lambda}_l + \left[h_{\mathbf{u}} - \mathbf{w}_r^\top \mathbf{V}^\top \mathbf{Q}_{\mathbf{u}} \right] \delta \mathbf{u} \left. \right\} dt \\ & + \mathbf{p}_r^\top \delta \mathbf{q}_r \Big|_{t=T} + \mathbf{w}_r^\top \mathbf{V}^\top \mathbf{M} \mathbf{V} \delta \mathbf{v}_r \Big|_{t=T}. \end{aligned} \quad (6.16)$$

Terms depending on $\delta \mathbf{q}_r$ and $\delta \mathbf{v}_r$ are eliminated due to a special choice of the adjoint variables $\mathbf{p}_r, \mathbf{w}_r$ and $\boldsymbol{\mu}_l$. Therefore, the set of adjoint equations is defined by equating the expressions in square brackets to zero:

$$\begin{aligned} \frac{d\mathbf{p}_r}{dt} &= \mathbf{V}^\top h_{\mathbf{q}}^\top + \mathbf{V}^\top \left((\mathbf{M}\dot{\mathbf{v}})_{\mathbf{q}} - \mathbf{Q}_{\mathbf{q}} + (\mathbf{C}_{\mathbf{q}}^\top \mathbf{\Gamma}^\top \boldsymbol{\lambda}_l)_{\mathbf{q}} \right)^\top \mathbf{V} \mathbf{w}_r + \mathbf{V}^\top \mathbf{C}_{\mathbf{q}}^\top \mathbf{\Gamma}^\top \boldsymbol{\mu}_l \\ \frac{d}{dt} (\mathbf{V}^\top \mathbf{M} \mathbf{V} \mathbf{w}_r) &= \mathbf{V}^\top h_{\mathbf{v}}^\top - \mathbf{p}_r - \mathbf{V}^\top \mathbf{Q}_{\mathbf{v}}^\top \mathbf{V} \mathbf{w}_r \\ \mathbf{0} &= \mathbf{\Gamma}^\top \mathbf{C}_{\mathbf{q}} \mathbf{V} \mathbf{w}_r \end{aligned} \quad (6.17)$$

Moreover, the boundary conditions

$$\begin{aligned} \mathbf{0} &= \mathbf{p}_r(T) \\ \mathbf{0} &= \mathbf{V}^\top \mathbf{M}(T) \mathbf{V} \mathbf{w}_r(T) \end{aligned}$$

are used to eliminate the variations $\delta \mathbf{q}_r(T)$ and $\delta \mathbf{v}_r(T)$ in Eq. (6.16). Next, supposing Eqs. (6.17) are fulfilled, the variation of the cost function in Eq. (6.16) reduces to

$$\delta J = \int_0^T \left[h_{\mathbf{u}} - \mathbf{w}_r^\top \mathbf{V}^\top \mathbf{Q}_{\mathbf{u}} \right] \delta \mathbf{u} dt = \left(\int_0^T \left[h_{\mathbf{u}} - \mathbf{w}_r^\top \mathbf{V}^\top \mathbf{Q}_{\mathbf{u}} \right] dt \right) \delta \mathbf{u}. \quad (6.18)$$

This fully reduced parameter identification approach uses both, the reduction of the forward simulation, and the reduced gradient computation. Not only are the number of DAEs reduced, but also the number of adjoint equations in Eq. (6.17) is downsized.

6.1.2 Numerical Example

The reduced adjoint system is tested by the rather academical example of the cart-pendulum chain shown in Fig. 6.1. The test example consists of two carts with four pendula each. For simplicity, an Euler angle representation of the rotational DOFs is used, resulting in $n = 60$ DOFs. The system is subject to $m = 28$ algebraic constraint equations, which force the system to a planar behavior.

While the left cart is actuated by an external force ($F(t)$) the right cart is connected to ground by a linear spring (k_2). Furthermore, the carts are interconnected by a linear spring (k_1). Each pendulum is subject to a damping element with linear damping coefficients (d_{P_1}, \dots, d_{P_8}) acting on the joints.

The parameters to be identified are:

- the linear damping coefficients d_{P_1}, \dots, d_{P_4} ,
- the four masses m_{P_1}, \dots, m_{P_4} of the four pendula connected to the left cart, and
- the mass m_{C_1} of the left cart.

Initial and target values of the unknown parameters are summarized in Tab. 10. The parameter identification is based on fictitious measurement signals. These are generated by a forward simulation using the target parameters. The measured signals are:

- the oscillating angles $\varphi_{P_1}(t), \dots, \varphi_{P_4}(t)$,
- the oscillating angular velocities $\omega_{P_1}(t), \dots, \omega_{P_4}(t)$,
- the first cart's position $x_{C_1}(t)$,
- and the first cart's translational velocity $\dot{x}_{C_1}(t)$.

The model data is summarized in Tab. 10.

The system starts from its static equilibrium. The left cart is actuated by a ten second sinusoidal signal. It acts at a frequency of three hertz and an amplitude of 25 [N]. After ten seconds, the actuating force is deactivated and the system is allowed to oscillate for another five seconds. The example is run in Scilab [90] using the HHT-solver for the forward simulation. A BDF-solver, together with a BFGS optimization algorithm, is used to solve the adjoint system.

In Figs. 6.2 - 6.5 the cart positions and the oscillating angle of the first pendulum are shown exemplarily. The proposed MOR approach is applied to snapshots

collected from the forward simulation of the original system. The POV plots in Figs. 6.6 and 6.7 indicate a reduced order model consisting of 18 translational and eight rotational DOFs. The number of reduced DOFs correlates with the active DOFs in the model. These are one translational DOF for each cart, and two translational as well as one rotational DOF for each pendulum.

The constraint reduction approach computes the singular value decay shown in Fig. 6.8. It points out a set of 16 unique constraint equations. Using this setup, the online solver time of the forward simulation reduces from 29s to 22s, which is a reduction of more than 24%.

Next, the adjoint method is used to determine the gradient of the cost function in Eq. (6.2) and Eq. (6.10) respectively. The plots in Figs. 6.9 - 6.12 show:

- the decay of the cost function,
- the variation of the pendula damping parameters,
- the pendula mass parameters, and
- the first cart's mass parameter.

The plots show a congruent behavior, regardless of whether the identification is run in reduced form or not. Therefore, the reduction process does not change the information content of the measured signals or the cost functional. The parameter variation plots, see Figs. 6.10 - 6.12, indicate the correct parameter values after 25 iterations. Due to the cost function plot, shown in (Fig. 6.9), the final cost value reduces to about 10^{-4} . The parameter identification process takes 2655s for the original model. The simulation time reduces to 2247s in the case of reduced forward simulation only. In the case of reducing both, the forward and the adjoint system, the overall simulation time reduces to 2183s. This is a reduction of about 18%.

Figures 6.13 and 6.14 show the relative error plots of the first cart and the first pendulum, for the final parameter iteration. The error plots point out high consistency between the final trajectory of the original parameter identification procedure and the reduced parameter identification.

As the set of linear adjoint equations is of a good nature (in a computational sense), the numerical effort to solve this set of equations is small. The overall time savings presented by the numerical results is dominated by the reduction of the forward simulations. They make up about 97% of the time-saving while the reduced adjoint system results in about three percent only.

6.1.3 Discussion

The application of the proposed model order reduction approach to parameter identification tasks shows the close connection between the forward system reduction and the adjoint system reduction.

The subspace on which the set of adjoint equations is projected to is spanned by POD modes which also span the subspace for the forward simulation. The performance of the fully reduced parameter identification is compared to the performance of the non-reduced parameter identification method.

As the linear adjoint equations are of good nature (in a computational sense), the numerical effort to solve this set of equations is small. Hence, the overall time-saving is dominated by the reduced forward simulation. The computation of the reduced adjoint system enhances the simulation time saving only slightly.

As for any model order reduction its quality and validity is only as good as the system information contained in the basis vectors which span the reduction subspace. Hence, crucial changes in the system configuration must be detected and handled. One possibility to handle this is to compute the original MBS from time to time and check the validity of the reduced order model. Still, the question of how to automatically detect the switch from a meaningful reduced subspace to a useless one remains open.

Finally, as already mentioned in the preceding chapter, the time benefit gained by the model reduction procedure may be overridden by the Scilab scripting environment.

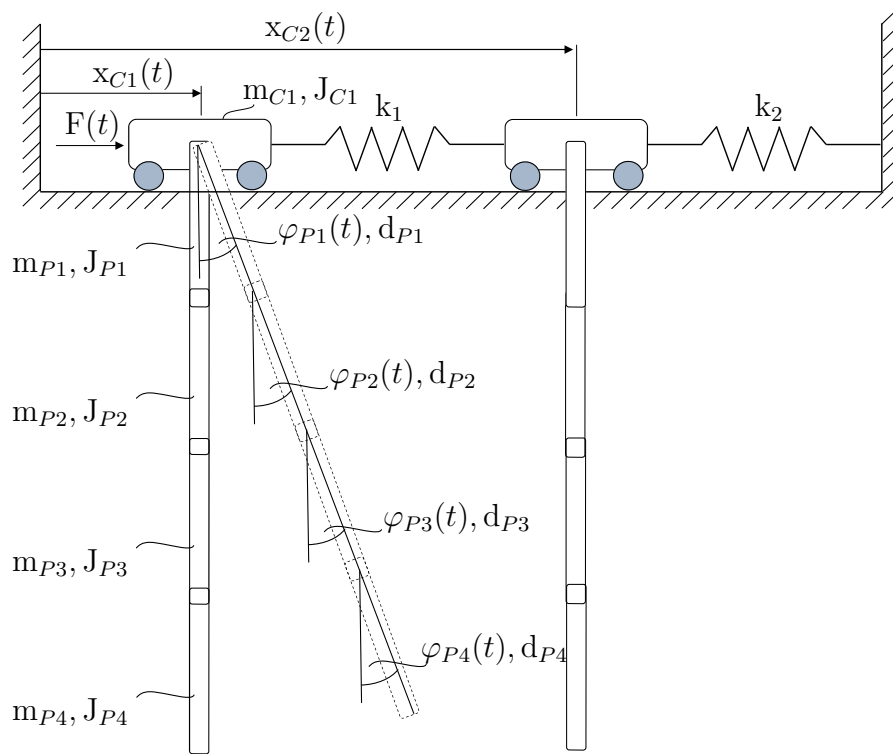


Figure 6.1: Cart-Pendulum chain

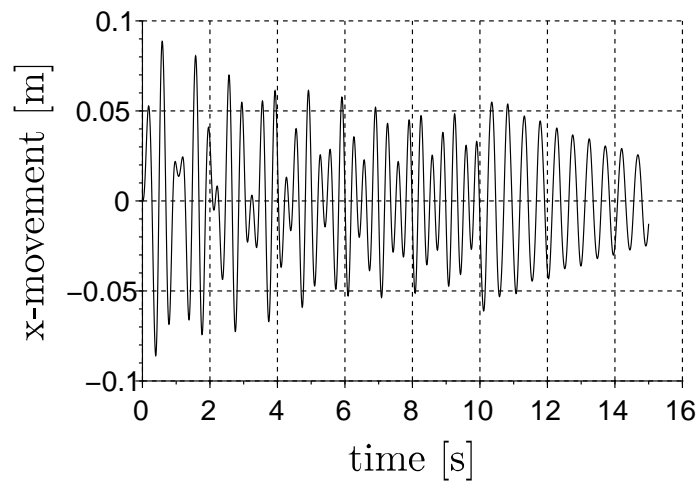


Figure 6.2: Time history of the left cart - Cart-pendulum chain

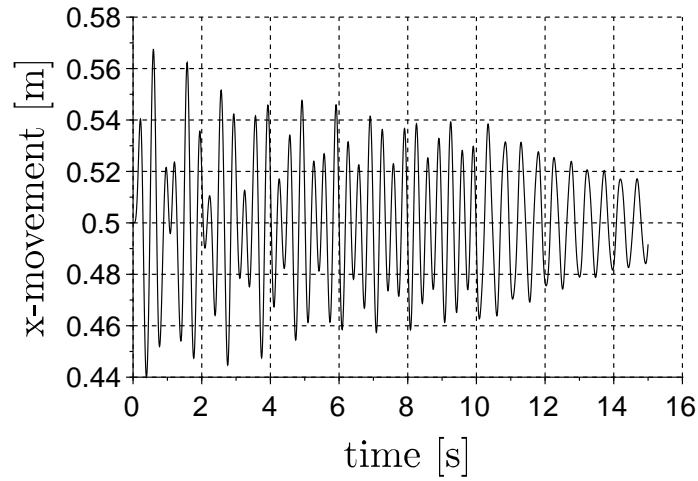


Figure 6.3: Time history of the right cart - Cart-pendulum chain

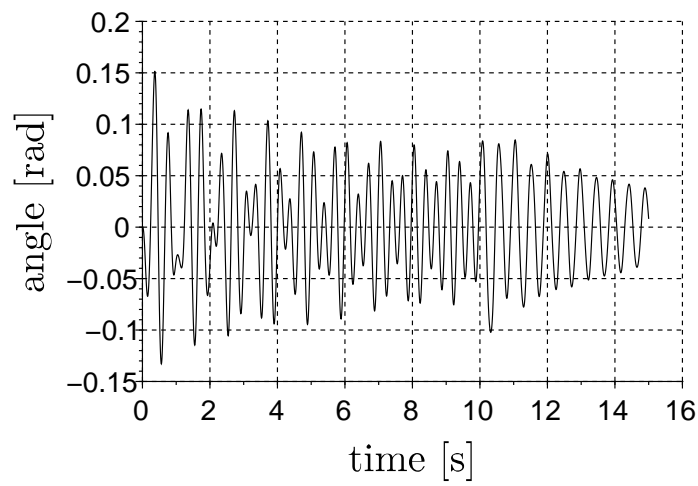


Figure 6.4: Time history of the first pendulum - Cart-pendulum chain

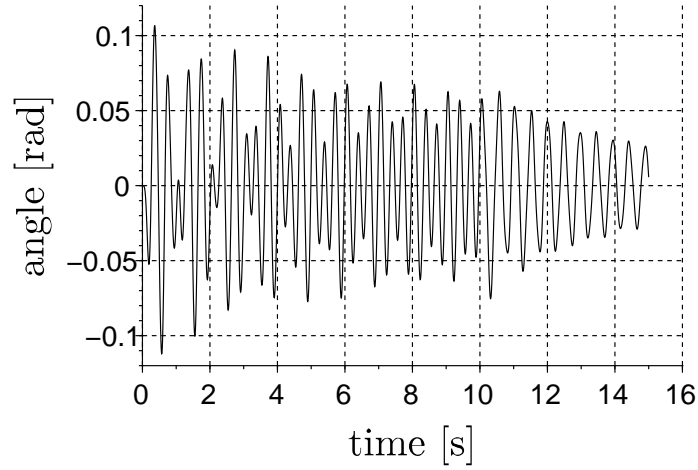


Figure 6.5: Time history of the fifth pendulum - Cart-pendulum chain

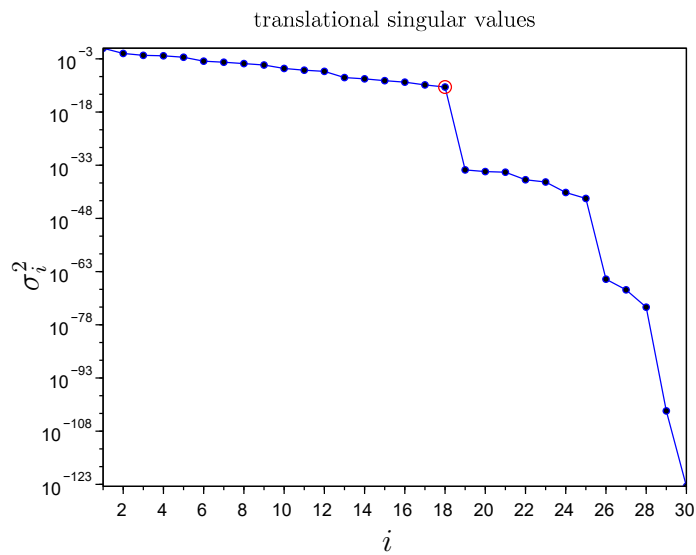


Figure 6.6: Translational velocity coordinate POVs - Cart-pendulum chain

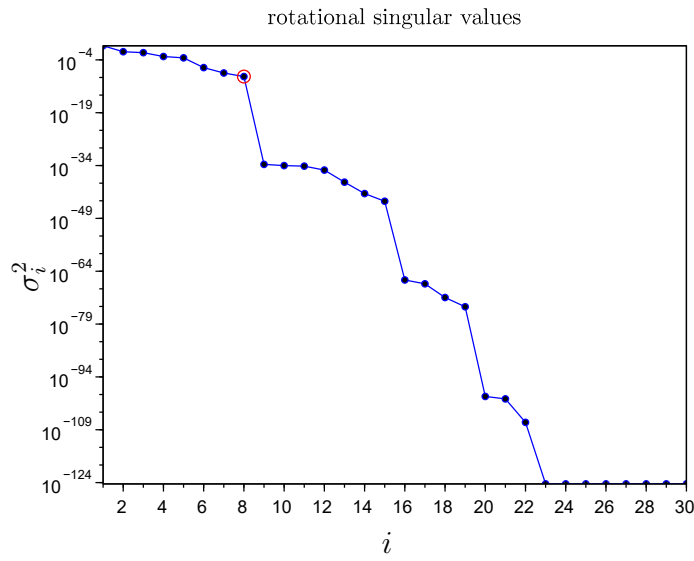


Figure 6.7: Rotational velocity coordinate POVs - Cart-pendulum chain

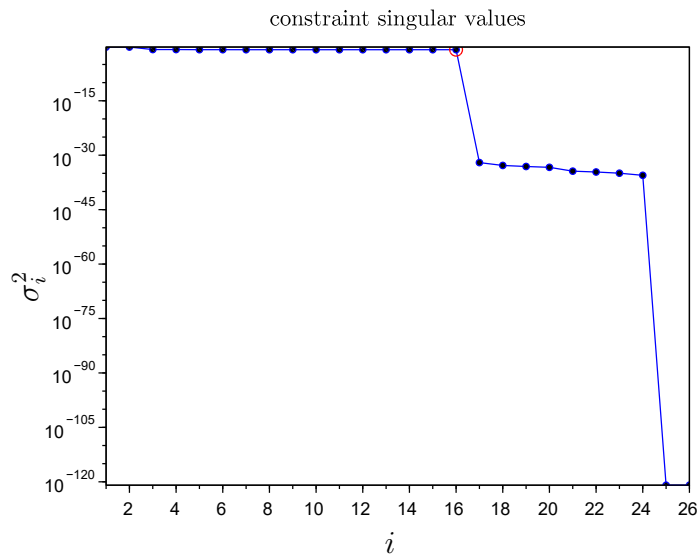


Figure 6.8: Constraint singular values - Cart-pendulum chain

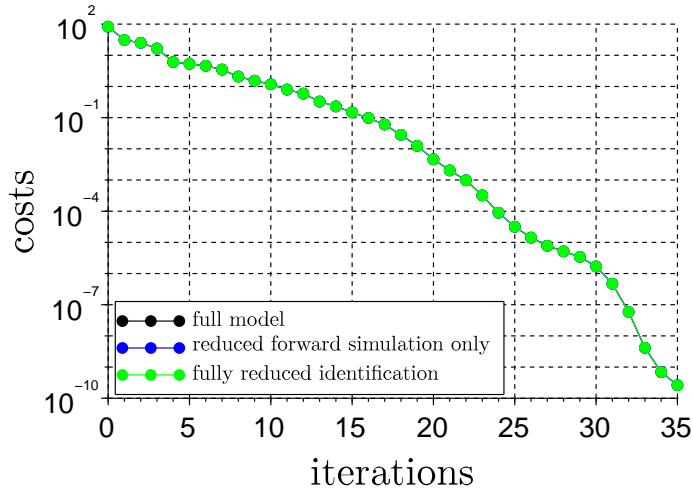


Figure 6.9: Cost Function decay - Cart-pendulum chain

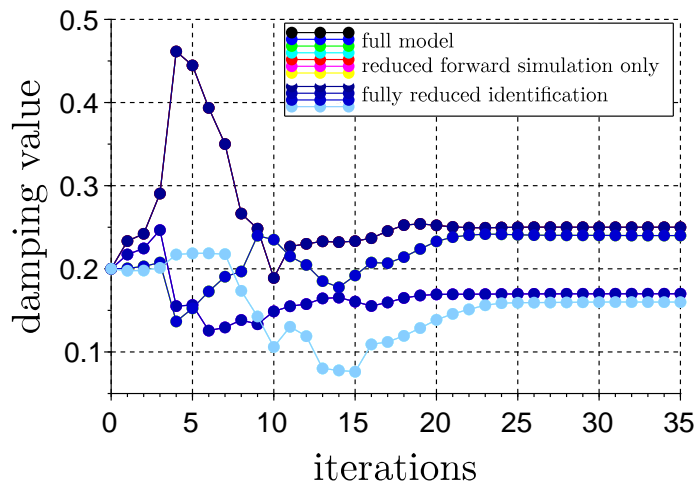


Figure 6.10: Pendula damping parameter variation - Cart-pendulum chain

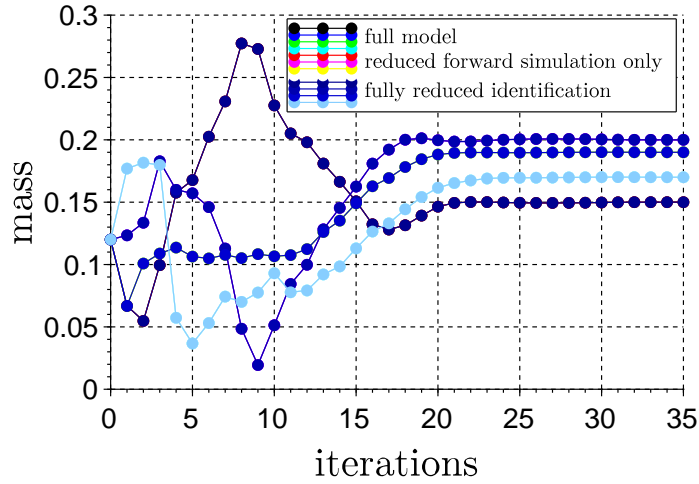


Figure 6.11: Pendula mass parameter variation - Cart-pendulum chain

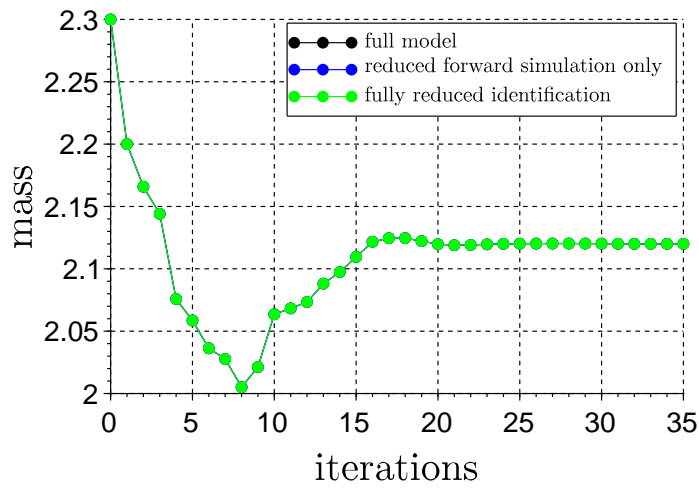


Figure 6.12: Cart mass parameter variation - Cart-pendulum chain

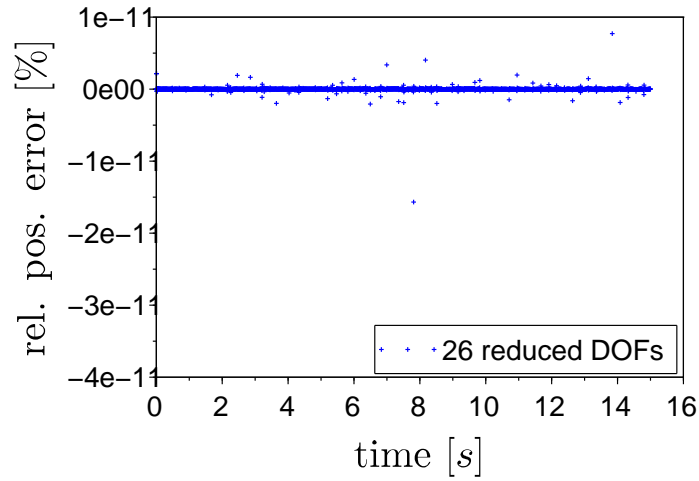


Figure 6.13: Relative position error of the left cart - Cart-pendulum chain

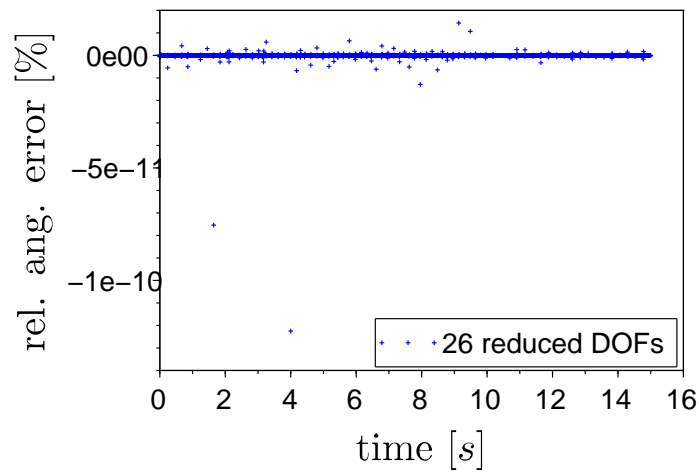


Figure 6.14: Relative angular error of the first pendulum - Cart-pendulum chain

Conclusion

The intention of this dissertation was to derive an efficient model order reduction approach to redundantly formulated general flexible multibody systems.

Due to the highly nonlinear state and time dependent character of the MBS, a data-driven model order reduction approach was chosen. Consequently, such a MOR method is meaningful in the context of repetitive simulation tasks, like parameter identification or design studies. Two circumstances, which evolve from the redundant formulation, are considered as crucial in terms of MOR: (1) the number of DOFs (and therefore differential equations) is typically larger than actually necessary, and (2) due to the redundant formulation, algebraic constraint equations, which describe the inter-DOF behavior of the MBS, have to be considered.

The herein derived model order reduction approach may be split into (a) the task of how to reduce the number of physical coordinates (DOFs) and (b) the task of how to reduce the number of algebraic equations (constraints).

Concerning the reduction of physical coordinates, the derived approach is based on a special set of POD modes, which is built from velocity coordinate data. The physical coordinate reduction matrix consists of POD submatrices, which are generated for translational, rotational and flexible DOF data separately. Therefore, the derived approach accounts for different snapshot scales evolving from e.g. small valued coordinates as in the case of Eulerparameters. Although the focus was not put on the question how to implement FEM bodies, the modal basis of flexible bodies is checked and, if necessary/possible, reduced. In order to overcome initial value issues the projection is expanded by a residual vector.

It has been shown, that the reduction of constraint equations is crucial to ensure the ROM to be determined and non-singular. By not reducing the constraint equations, as suggested in the literature [30], the resulting ROM could be overdetermined. This is the case if the number of reduced physical coordinates is smaller

than the number of algebraic constraint equations. As the physical coordinate POD subspace encloses constraint information, it spans at least a partially orthogonal subspace to the constraint equations. These constraint equations introduce redundant information to the ROM, and hence, have to be removed. To this end, a constraint reduction approach based on the principal component analysis has been developed. The reduced constraint Jacobian is investigated on its unique constraints, resulting in a unique-constraint-subspace. In order to ensure the ROM to be determined, the constraints and the constraint Jacobian are then projected onto this subspace.

It should be noted that the level of reduction is highly case sensitive. The level of reduction varies between 50% and 90% for the presented numerical examples. It was also shown that the approach is basically even able to reduce the set of redundant coordinates to the minimal set of coordinates.

It must be stated that the constraint forces of the ROM are no longer comparable to the original system, although the reduced order models show high consistency in the system states. Therefore, the method is not suitable to deliver the same joint reaction forces as the original MBS model. Hence, FEM simulations based on these joint reaction forces are to be handled with care. Moreover, the overall accuracy of the reduced order models is closely related to the processed snapshots. The used projection space may become insufficient in cases with critically changing excitation directions or model parameters. In such a case, it will become necessary to collect a new set of snapshots, renewing the reduction subspace and the set of unique constraints. This becomes especially important in terms of the presented, reduced parameter identification.

In conclusion, due to the derived MOR method the set of DAEs is reducible in its number of differential and algebraic equations. Furthermore, in terms of the reduced parameter identification the adjoint system is also reducible, utilizing the same reduction subspace. The simulation of a ROM takes less computational effort, and offers a considerable saving in coordinates and simulation time.

List of Figures

2.1	Vector diagram for derivation of rotation formula [81, p. 158]	6
2.2	Definition of a body fixed coordinate system	8
2.3	Floating reference frame description of a flexible body	10
3.1	Geometric interpretation of the linear Galerkin projection in \mathbb{R}^3 following [71]	20
3.2	Geometric interpretation of the linear and nonlinear (Petrov-)Galerkin projection	30
3.3	Bilinear two mass oscillator, following [108, p.1648]	42
3.4	Two mass oscillator	47
3.5	Centering the input data, following [18, p.812]	50
3.6	Two mass oscillator	50
3.7	POD and cyclic coordinates	54
3.8	Original cart-pendulum model	59
3.9	Time history of the pendulum's rotational e_3 coordinate	60
3.10	Proper orthogonal values - Reduced cart-pendulum model	61
3.11	Superposition of the cart movement in the original and the POD reduced model	62
4.1	Single mass under constant rotation and large translational movement .	66
4.2	Rigid pendulum	74
4.3	Single mass oscillator	80
5.1	V8 crank drive	84
5.2	V8 RPM plot	85
5.3	Translational velocity coordinate POVs - Rigid V8 crank drive	86
5.4	Rotational velocity coordinate POVs - Rigid V8 crank drive	86
5.5	Constraint singular values - Rigid V8 crank drive	87
5.6	Combined position and velocity snapshot POD - Rigid V8 crank drive .	87
5.7	Zoom into the first 15 POVs - Combined position and velocity snapshot POD - Rigid V8 crank drive	88
5.8	Time history of the relative position error - Rigid V8 crank drive . . .	89

5.9	Time history of the relative e_0 error - Rigid V8 crank drive	90
5.10	V8 crank drive in mounting condition	91
5.11	Translational velocity coordinate POVs - Rigid V8 crank drive in mounting condition	92
5.12	Rotational velocity coordinate POVs - Rigid V8 crank drive in mounting condition	93
5.13	Constraint singular values - Rigid V8 crank drive in mounting condition	94
5.14	Position data POD - Plot of POVs computed from combined translational and rotational velocity information - Rigid V8 crank drive in mounting condition	94
5.15	Time history of the relative crankshaft position error of the rigid V8 crank drive in mounting condition	95
5.16	Time history of the relative piston position error of the rigid V8 crank drive in mounting condition	96
5.17	Time history of the relative e_0 error of the rigid V8 crank drive in mounting condition	97
5.18	Double wishbone front suspension	98
5.19	Vertical forcing acting on the steering knuckle - Partially flexible front suspension	99
5.20	Translational velocity coordinate POVs - Partially flexible front suspension	100
5.21	Rotational velocity coordinate POVs - Partially flexible front suspension	101
5.22	Flexible velocity coordinate POVs - Partially flexible front suspension .	102
5.23	Constraint singular values - Partially flexible front suspension	103
5.24	Classical POD approach - Plot of POVs computed from combined translational, rotational and flexible velocity information - Partially flexible front suspension	103
5.25	Time history of the relative y coordinate error of the partially flexible front suspension	104
5.26	Time history of the relative e_0 error of the partially flexible front suspension	105
5.27	Time history of the relative flexible coordinate error of the partially flexible front suspension	106
5.28	Electrical junior dirtbike	107
5.29	Vertical forcing acting on the wheels - Electrical junior dirtbike	108
5.30	Translational coordinate POVs - Electrical junior dirtbike	109
5.31	Rotational coordinate POVs - Electrical junior dirtbike	110
5.32	Constraint singular values - Electrical junior dirtbike	110
5.33	Combined snapshot data POD approach - Electrical junior dirtbike	111

5.34	Time history of relative translational coordinate errors - Electrical junior dirtbike	112
5.35	Time history of the relative e_0 error - Electrical junior dirtbike	113
6.1	Cart-Pendulum chain	123
6.2	Time history of the left cart - Cart-pendulum chain	123
6.3	Time history of the right cart - Cart-pendulum chain	124
6.4	Time history of the first pendulum - Cart-pendulum chain	124
6.5	Time history of the fifth pendulum - Cart-pendulum chain	125
6.6	Translational velocity coordinate POVs - Cart-pendulum chain	125
6.7	Rotational velocity coordinate POVs - Cart-pendulum chain	126
6.8	Constraint singular values - Cart-pendulum chain	126
6.9	Cost Function decay - Cart-pendulum chain	127
6.10	Pendula damping parameter variation - Cart-pendulum chain	127
6.11	Pendula mass parameter variation - Cart-pendulum chain	128
6.12	Cart mass parameter variation - Cart-pendulum chain	128
6.13	Relative position error of the left cart - Cart-pendulum chain	129
6.14	Relative angular error of the first pendulum - Cart-pendulum chain	129

List of Tables

1	Physical properties - V8 crank drive	148
2	Forces/torques - V8 crankshaft	149
3	Eigenfrequencies of the flexible lower wishbone - Partially flexible front suspension	149
4	Eigenfrequencies of the flexible pushrod - Partially flexible front suspension	150
5	Physical properties - Partially flexible front suspension	151
6	Forces/torques - Partially flexible front suspension	152
7	Physical properties part 1 - Electrical junior dirtbike	153
8	Physical properties part 2 - Electrical junior dirtbike	154
9	Forces/torques - Electrical junior dirtbike	154
10	Cart-Pendulum chain - model data	155

List of Symbols

General

\mathbf{I} ... Identity matrix.

$(\dot{})$... Time derivative.

$()^\top$... Transpose of a vector/matrix.

Multibody System

$\mathbf{q}(t) \in \mathbb{R}^n$... Vector of physical coordinates.

$\mathbf{v}(t) \in \mathbb{R}^n$... Vector of physical velocity coordinates of the first order MBS.

$\boldsymbol{\lambda}(t) \in \mathbb{R}^m$... Vector of Lagrangian multipliers.

$\mathbf{u} \in \mathbb{R}^u$... Vector of unknown model parameters.

$\mathbf{M}(\mathbf{q}) \in \mathbb{R}^{n \times n}$... Global mass matrix.

$\mathbf{C}(\mathbf{q}) \in \mathbb{R}^m$... Vector of algebraic constraint equations.

$\mathbf{C}_q(\mathbf{q}) \in \mathbb{R}^{m \times n}$... Constraint Jacobian matrix.

$\mathbf{Q}(\mathbf{q}, \dot{\mathbf{q}}, t) \in \mathbb{R}^n$... Vector of generalized and gyroscopic forces.

Reduced Multibody System

$\mathbf{q}_r \in \mathbb{R}^r$... Vector of reduced physical coordinates.

$\mathbf{v}_r \in \mathbb{R}^r$... Vector of reduced physical velocity coordinates of the first order MBS.

$\boldsymbol{\lambda}_l \in \mathbb{R}^l$... Vector of reduced Lagrangian multipliers.

$\tilde{\mathbf{q}} = \mathbf{V}\mathbf{q}_r \in \mathbb{R}^n$... Vector of approximated, original physical coordinates.

$\mathbf{C}_l \in \mathbb{R}^l$... Vector of reduced algebraic constraint equations.

$\mathbf{C}_{\mathbf{q},r} = \mathbf{C}_{\mathbf{q}}\mathbf{V} \in \mathbb{R}^{m \times r}$... Constraint Jacobian of the physical coordinate reduced system.

$\mathbf{C}_{\mathbf{q},l} = \mathbf{\Gamma}\mathbf{C}_{\mathbf{q}}\mathbf{V} \in \mathbb{R}^{l \times r}$... Constraint Jacobian of the physical coordinate and constraint coordinate reduced system.

Model Reduction

$\mathbf{X} \in \mathbb{R}^{n \times h}$... Matrix of position level snapshots.

$\dot{\mathbf{X}} \in \mathbb{R}^{n \times h}$... Matrix of velocity level snapshots.

$\Phi \in \mathbb{R}^{n \times n}$... Matrix of left singular vectors.

$\Sigma \in \mathbb{R}^{n \times m}$... Diagonal matrix of singular values.

$\Psi \in \mathbb{R}^{m \times m}$... Matrix of right singular vectors.

$\mathbf{V} \in \mathbb{R}^{n \times r}$... Global physical coordinate reduction matrix.

$\mathbf{\Gamma} \in \mathbb{R}^{m \times l}$... Constraint coordinate reduction matrix.

$\mathbf{R}_0 \in \mathbb{R}^n$... Initial conditions residual vector.

Parameter Identification

h ... Error function.

$h_{\mathbf{q}} \in \mathbb{R}^n$... Derivative of h with respect to \mathbf{q} .

$h_{\mathbf{v}} \in \mathbb{R}^n$... Derivative of h with respect to \mathbf{v} .

$h_{\mathbf{u}} \in \mathbb{R}^u$... Derivative of h with respect to \mathbf{u} .

$\mathbf{Q}_{\mathbf{q}} \in \mathbb{R}^{n \times n}$... Jacobian matrix of \mathbf{Q} with respect to \mathbf{q} .

$\mathbf{Q}_{\mathbf{v}} \in \mathbb{R}^{n \times n}$... Jacobian matrix of \mathbf{Q} with respect to \mathbf{v} .

$\mathbf{Q}_{\mathbf{u}} \in \mathbb{R}^{n \times u}$... Jacobian matrix of \mathbf{Q} with respect to \mathbf{u} .

$\mathbf{p} \in \mathbb{R}^n$... Vector of adjoint variables.

$\mathbf{w} \in \mathbb{R}^n$... Vector of adjoint variables.

$\boldsymbol{\mu} \in \mathbb{R}^m$... Vector of adjoint variables.

Reduced Parameter Identification

$h_{\mathbf{q}_r} \in \mathbb{R}^r$... Derivative of the error function with respect to the reduced state variables.

$h_{\mathbf{v}_r} \in \mathbb{R}^r$... Derivative of the error function with respect to the reduced velocity variables.

$h_{\mathbf{u}_u} \in \mathbb{R}^r$... Derivative of the error function with respect to the reduced velocity variables.

$\mathbf{p}_r \in \mathbb{R}^r$... Vector of reduced adjoint variables.

$\mathbf{w}_r \in \mathbb{R}^r$... Vector of reduced adjoint variables.

$\boldsymbol{\mu}_l \in \mathbb{R}^l$... Vector of reduced adjoint variables.

Bibliography

- [1] H. Abdi. Singular value decomposition (svd) and generalized singular value decomposition (gsvd). In N. J. Salkind, editor, *Encyclopedia of Measurement and Statistics*, Conference Proceedings of the Society for Experimental Mechanics Series, pages 907–912. Thousand Oaks (CA): Sage., 2007.
- [2] A. Alla and S. Volkwein. Asymptotic stability of pod based model predictive control for a semilinear parabolic pde. *Advances in Computational Mathematics*, 41(5):1073–1102, 2015.
- [3] O. Alter, P. Brown, and D. Botstein. Generalized singular value decomposition for comparative analysis of genome-scale expression data sets of two different organisms. *Proceedings of the National Academy of Sciences of the United States of America*, 100:3351–3356, 2003.
- [4] E. Anderson, Z. Bai, C. Bischof, L. S. Blackford, J. Demmel, J. J. Dongarra, J. Du Croz, S. Hammarling, A. Greenbaum, A. McKenney, and D. Sorensen. *LAPACK Users' Guide (Third Ed.)*. Society for Industrial and Applied Mathematics, Philadelphia, PA, USA, 1999.
- [5] H. Antil, M. Heinkenschloss, and R. Hoppe. Domain decomposition and balanced truncation model reduction for shape optimization of the stokes system. *Optimization Methods and Software*, 26(4-5):643–669, 2011.
- [6] A. C. Antoulas. *Approximation of Large-Scale Dynamical Systems*. SIAM, 2005.
- [7] Z. Bai. The csd, gsvd, their applications and computations. In *IMA preprint 958*, pages 3–5, 1992.
- [8] S. Bellizzi and R. Sampaio. Model reduction based on Karhunen-Loeve decomposition and smooth decomposition for random mechanical systems. In P. Sas and B. Bergen, editors, *International Conference on Noise and Vibration Engineering (ISMA2010)*, pages 5157–5172, Leuven, Belgium, Sept. 2010.

- [9] S. Bellizzi and R. Sampaio. The smooth decomposition as a nonlinear modal analysis tool. *Mechanical Systems and Signal Processing*, 64–65:245 – 256, 2015.
- [10] P. Benner, V. Mehrmann, and D. Sorensen. *Dimension Reduction of Large-Scale Systems*. Springer, 2003.
- [11] B. Besselink, U. Tabak, A. Lutowska, N. van de Wouw, H. Nijmeijer, D. Rixen, M. Hochstenbach, and W. Schilders. A comparison of model reduction techniques from structural dynamics, numerical mathematics and system control. *Journal of Sound and Vibration*, 332:4403–4422, 2013.
- [12] D. Bestle and P. Eberhard. Analyzing and optimizing multibody systems. *Mech. Struc. Mach.*, 20:67–92, 1992.
- [13] D. A. Bistrián and I. M. Navon. An improved algorithm for the shallow water equations model reduction: Dynamic mode decomposition vs pod. *International Journal for Numerical Methods in Fluids*, 78(9):552–580, 2015. fd.4029.
- [14] O. Brüls, P. Duysinx, and J.-C. Golinval. The global modal parameterization for non-linear model-order reduction in flexible multibody dynamics. *International Journal for Numerical Methods in Engineering*, 69(5):948–977, 2007.
- [15] O. Brüls, P. Duysinx, and J.-C. Golinval. A model reduction method for the control of rigid mechanisms. *Multibody System Dynamics*, 15(3):213–227, 2006.
- [16] Y. Cao, S. Li, L. Petzold, and R. Serban. Adjoint Sensitivity Analysis for Differential-Algebraic Equations: The Adjoint DAE System and Its Numerical Solution. *SIAM Journal on Scientific Computing*, 24(3):1076–1089, 2003.
- [17] J. Carr. *Applications of Centre Manifold Theory*. Springer Verlag, 1981.
- [18] A. Chatterjee. An introduction to the Proper Orthogonal Decomposition. *Current Science*, 75:808–817, 2000.
- [19] D. Chelidze. Identifying robust subspaces for dynamically consistent reduced-order models. In G. Kerschen, editor, *Nonlinear Dynamics, Volume 2*, Conference Proceedings of the Society for Experimental Mechanics Series, pages 123–130. Springer International Publishing, 2014.

- [20] D. Chelidze and M. Liu. Smooth orthogonal decomposition based reconstruction of a slow-time trajectory. In *Proceedings of the ENOC-2005 Fifth EUROMECH Nonlinear Dynamics Conference, Eindhoven, The Netherlands, August 7-12, 2005*, 2005.
- [21] D. Chelidze and W. Zhou. Smooth orthogonal decomposition-based vibration mode identification. *Journal of Sound*, 292:461–473, 2006.
- [22] R. Craig. A review of time-domain and frequency-domain component mode synthesis method. *Journal of Modal Analysis*, 2:59–72, 1985.
- [23] R. Craig. Coupling of substructures for dynamic analyses: An overview. In *Structural Dynamics, and Materials Conference and Exhibit*, 2000.
- [24] R. Craig and M. Bampton. Coupling of substructures for dynamic analyses. *AIAA Journal*, 6:1313–1319, 1968.
- [25] D. de Clerk, D. Rixen, and S. Vormeerren. General framework for dynamic substructuring: History, review and classification of techniques. *AIAA Journal*, 46:1169–1181, 2008.
- [26] J. G. de Jalon and M. Gutierrez-Lopez. Multibody dynamics with redundant constraints and singular mass matrix: existence, uniqueness and determination of solutions for accelerations and constraint forces. *Multibody System Dynamics*, 30:311–341, 2013.
- [27] J. Diebel. Representing attitude: Euler angles, unit quaternions, and rotation vectors. *Matrix*, 58(15-16):1–35, 2006.
- [28] M. Dihlmann and B. Haasdonk. Certified PDE-constrained parameter optimization using reduced basis surrogate models for evolution problems. *Computational Optimization and Applications*, 60(3):753–787, 2015.
- [29] P. Eberhard. Adjoint variable method for sensitivity analysis of multibody systems interpreted as a continuous, hybrid form of automatic differentiation. *Proceedings of the 2nd Int. Workshop on Computational Differentiation, Santa Fe. Philadelphia, SIAM*, pages 319–328, 1996.
- [30] F. Ebert. A note on POD model reduction methods for DAEs. *Mathematical and Computer Modeling of Dynamical Systems*, 16:115–131, 2010.
- [31] T. Ersal, H. Fathy, and J. Stein. Orienting body coordinate frames using Karhunen-Loeve expansion for more effective structural simplification. *Simulation Modelling Practice and Theory*, 17:197–210, 2009.

- [32] T. Ersal, H. K. Fathy, D. G. Rideout, L. S. Louca, and J. L. Stein. A review of proper modeling techniques. *Journal of Dynamic Systems, Measurement, and Control*, 130(6):061008, 2008.
- [33] M. Fahl and E. Sachs. Reduced order modelling approaches to pde-constrained optimization based on proper orthogonal decomposition. In L. Biegler, M. Heinkenschloss, O. Ghattas, and B. van Bloemen Waanders, editors, *Large-Scale PDE-Constrained Optimization*, volume 30 of *Lecture Notes in Computational Science and Engineering*, pages 268–280. Springer Berlin Heidelberg, 2003.
- [34] U. Farooq and B. Feeny. Smooth orthogonal decomposition for modal analysis of randomly excited systems. *Journal of Sound and Vibration*, 316(1–5):137 – 146, 2008.
- [35] B. Feeny. On the proper orthogonal modes and normal modes of continuous vibration systems. *Journal of Vibration and Acoustics, Transactions of the ASME*, 124(1):157–160, 1 2002.
- [36] B. Feeny and R. Kappagantu. On the physical interpretation of proper orthogonal modes in vibrations. *Journal of Sound and Vibration*, 211:607–616, 1998.
- [37] G. Fix and R. Heiberger. An algorithm for the ill-conditioned generalized eigenvalue problem. *SIAM Journal on Numerical Analysis*, 9:78–88, 1972.
- [38] C. Foias, M. Jolly, I. Kevrekidis, G. Sell, and E. Titi. On the computation of inertial manifolds. *Physics Letters*, 131:433–436, 1988.
- [39] C. Foias, O. Manley, and R. Temam. Modelling of the interaction of small and large eddies in two-dimensional turbulent flows. *Mathematical Modelling and Numerical Analysis*, 22:93–114, 1988.
- [40] C. Foias, G. Sell, and R. Temam. Inertial manifolds for nonlinear evolutionary equations. *Journal of Differential Equations*, 73:309–353, 1988.
- [41] FreeDyn. Freedyn version 2015.10 (x64). <http://www.freedyn.at>, 2015.
- [42] G. Fuchs, A. Steindl, and S. Jakubek. Order reduction for a realtime engine model using flat and nonlinear galerkin methods. *Advances in Communications, Computers, Systems, Circuits and Devices*, pages 255–260, 2010.
- [43] B. Garchia-Archilla, J. Novo, and E. Titi. Postprocessing the galerkin method: A novel approach to approximate inertial manifolds. *SIAM Journal of Numerical Analysis*, 35:941–972, 1998.

- [44] J. Gohlke. Reduced order modeling for optimization of large scale dynamical systems. Master's thesis, Department of Computational and Applied Mathematics, Rice University, Houston, TX, 2013.
- [45] F. Gonzalez and J. Kövecses. Use of penalty formulations in dynamic simulation and analysis of redundantly constrained multibody systems. *Multibody System Dynamics*, 29:57–76, 2013.
- [46] E. Haug. *Computer Aided Kinematics and Dynamics of Mechanical Systems*. Allyn and Bacon series in engineering. Allyn and Bacon, 1989.
- [47] E. Haug, R. Wehage, and N. Mani. Design sensitivity analysis of large-scaled constrained dynamic mechanical systems. *Trans ASME*, 106:156–162, 1984.
- [48] G. Heirman, O. Brüls, P. Sas, and W. Desmet. Coordinate transformation techniques for efficient model reduction in flexible multibody dynamics. In *Proceedings of ISMA*, 2008.
- [49] G. Heirman, F. Naets, and W. Desmet. A system-level model reduction technique for the efficient simulation of flexible multibody systems. *International Journal for Numerical Methods in Engineering*, 85(3):330–354, 2011.
- [50] H. Hilber, T. Hughes, and R. Taylor. Improved numerical dissipation for time integration algorithms in structural dynamics. *Earthquake engineering and structural dynamics*, 5:283–292, 1977.
- [51] S. Ilbeigi and D. Chelidze. Model order reduction of nonlinear euler-bernoulli beam. In G. Kerschen, editor, *Nonlinear Dynamics, Volume 1*, Conference Proceedings of the Society for Experimental Mechanics Series, pages 377–386. Springer International Publishing, 2015.
- [52] S. Ilbeigi and D. Chelidze. *Reduced Order Models for Systems with Disparate Spatial and Temporal Scales*, pages 447–455. Springer International Publishing, Cham, 2017.
- [53] G. Kerschen and J. Golinval. Physical interpretation of the proper orthogonal modes using the singular value decomposition. *Journal of Sound and Vibration*, 249(5):849 – 865, 2002.
- [54] G. Kerschen, J. Golinval, A. Vakakis, and L. Bergman. The method of proper orthogonal decomposition for dynamical characterization and order reduction of mechanical systems: An overview. *Nonlinear Dynamics*, 41:147–169, 2005.

- [55] G. Kerschen, M. Peeters, J. Golinval, and A. Vakakis. Nonlinear normal modes, part i: A useful framework for the structural dynamicist. *Mechanical Systems and Signal Processing*, 23:170–194, 2009.
- [56] D. Kosambi. Statistics in function space. *Journal of the Indian Mathematical Society*, 7:76–78, 1943.
- [57] P. Koutsovasilis and M. Beitelschmidt. Comparison of model reduction techniques for large mechanical systems. *Multibody System Dynamics*, 20:111–128, 2008.
- [58] D. Kovacs. *Inertial Manifolds and Nonlinear Galerkin Methods*. PhD thesis, Virginia Polytechnic Institute and State University, 2005.
- [59] K. Kunisch and S. Volkwein. Proper orthogonal decomposition for optimality systems. *ESAIM: Mathematical Modelling and Numerical Analysis*, 42(1):1–23, 2008.
- [60] A. Laulusa and O. Bauchau. Review of classical approaches for constraint enforcement in multibody systems. *Journal of Computational and Nonlinear Dynamics*, 3:1–8, 2007.
- [61] C. Leblond, C. Allery, and C. Inard. An optimal projection method for the reduced-order modeling of incompressible flows. *Computer Methods in Applied Mechanics and Engineering*, 200(33-36):2507–2527, 2011.
- [62] M. Lehner. *Modellreduktion in elastischen Mehrkoerpersystemen*. PhD thesis, Fakultät fuer Maschinenbau, Universitaet Stuttgart, 2007.
- [63] M. Lehner and P. Eberhard. Modellreduktion in elastischen Mehrkörpersystemen. *at-Automatisierungstechnik*, 54:170–177, 2006.
- [64] M. Lehner and P. Eberhard. On the use of moment-matching to build reduced order models in flexible multibody dynamics. *Multiple Sclerosisbody System Dynamics*, 16:191–211, 2006.
- [65] F. Liu, Q. Sun, J. Zhang, and D. Xia. Generalized canonical correlation analysis using gsvd. In *International Symposium on Computer Science and Computational Technology*, 2008.
- [66] B. Lohmann and B. Salimbahrami. Ordnungsreduktion mittels Krylov-Unterraummethoden. *at-Automatisierungstechnik*, 52:30–38, 2004.
- [67] R. E. Madsen, L. K. Hansen, and O. Winther. Singular value decomposition and principal component analysis. Technical report, Technical University of Denmark, DTU Compute, Intelligent Signal Processing Group, 2004.

- [68] C. Martin and M. Porter. The Extraordinary SVD. *The American Mathematical Monthly*, 119:838–851, 2012.
- [69] R. Masoudi, T. Uchida, and J. McPhee. Reduction of multibody dynamic models in automotive systems using the proper orthogonal decomposition. *Journal of Computational and Nonlinear Dynamics*, 10:031007, 2015.
- [70] D. Meyer and S. Srinivasan. Balancing and model reduction for second-order form linear systems. *IEEE Transactions on Automatic Control*, 41:1632–1644, 1996.
- [71] M. Meyer. Computational model order reduction of linear and nonlinear dynamical systems - an introduction -, 2006.
- [72] A. A. Miranda, Y.-A. Le Borgne, and G. Bontempi. New routes from minimal approximation error to principal components. *Neural Processing Letters*, 27(3):197–207, 2008.
- [73] A. H. Monahan, J. C. Fyfe, M. H. P. Ambaum, D. B. Stephenson, and G. R. North. Empirical orthogonal functions: The medium is the message. *Journal of Climate*, 22(24):6501–6514, 2009.
- [74] L. Mráz and M. Valášek. Solution of three key problems for massive parallelization of multibody dynamics. *Multibody System Dynamics*, 29(1):21–39, 2013.
- [75] MSC software. MSC Adams. <http://www.mscsoftware.com>, 2015.
- [76] K. Nachbagauer, S. Oberpeilsteiner, K. Sherif, and W. Steiner. The use of the adjoint method for solving typical optimization problems in multibody dynamics. *Journal of Computational and Nonlinear Dynamics*, 10:061011, 2014.
- [77] K. Nachbagauer, S. Oberpeilsteiner, and W. Steiner. Enhancement of the adjoint method by error control of accelerations for parameter identification in multibody dynamics. *Universal Journal of Control and Automation*, 3:47–52, 2015.
- [78] R. Narasimha. Kosambi and proper orthogonal decomposition. *Resonance*, 16(6):574–581, 2011.
- [79] D. Negrut, G. Ottarsson, R. Pampalli, and A. Sadjak. On an implementation of the hilber-hughes-taylor method in the context of index 3 differential-algebraic equations of multibody dynamics. *Journal of Computational and Nonlinear Dynamics*, 2, 2006.

- [80] N. Newmark. A method of computation for structural dynamics. *Journal of the Engineering Mechanics Division - ASCE*, pages 67–94, 1959.
- [81] P. Nikravesh, R. Wehage, and O. Kwon. Euler parameters in computational kinematics and dynamics, part 1. *Journal of Mechanical Design*, 107:358–365, 1985.
- [82] E. Pennestri and P. Valentini. Coordinate reduction strategies in multibody dynamics: A review. In *XXVII National Conference on Multibody System Dynamics, Pitesti, Romania*, pages 1–12, 2007.
- [83] L. Petzold, S. Li, Y. Cao, and R. Serban. Sensitivity analysis for differential-algebraic equations and partial differential equations. *Computers and Chemical Engineering*, 30:1553–1559, 2006.
- [84] Z. Qu. *Model Order Reduction Techniques with Applications in Finite Element Analysis*. Springer, 2004.
- [85] S. Rao. *Engineering Optimization: Theory and Practice: Fourth Edition*. John Wiley and Sons, 6 2009.
- [86] M. Reit, J.-K. Bremer, W. Mathis, and R. Stoop. Ansätze zur ordnungsreduktion von nichtlinearen oszillatormodellen zur anwendung im schaltungsentwurf. *Advances in Radio Science*, 8:151–160, 2010.
- [87] J. Robinson. Finite-dimensional behavior in dissipative partial differential equations. *Chaos*, 5:330–345, 1995.
- [88] B. Salimbahrami and B. Lohmann. Krylov subspace methods for the reduction of first and second order large-scale systems. In *Proceedings of 8th DFMRs Conference*, 2004.
- [89] W. H. A. Schilders, H. A. van der Vorst, and J. Rommes. *Model Order Reduction - Theory, Research Aspects and Applications*. Springer Verlag, 2008.
- [90] Scilab enterprises. Scilab version 5.5.1 (x64). <http://www.scilab.org>, 2014.
- [91] D. B. Segala, D. H. Gates, J. B. Dingwell, and D. Chelidze. Nonlinear smooth orthogonal decomposition of kinematic features of sawing reconstructs muscle fatigue evolution as indicated by electromyography. *Journal of biomechanical engineering*, 133(3):031009, 2011.
- [92] A. A. Shabana. *Dynamics of Multibody Systems - Third edition*. Cambridge University Press, 2005.

- [93] K. Sherif, H. Irschik, and W. Witteveen. Transformation of arbitrary elastic mode shapes into pseudo-free-surface and rigid body modes for multibody dynamic systems. *ASME J COMPUT NONLIN DYN*, 7, 2012.
- [94] K. Sherif and K. Nachbagauer. A detailed derivation of the velocity-dependent inertia forces in the floating frame of reference formulation. Technical report, 2014.
- [95] J. Shlens. A tutorial on principal component analysis. *CoRR*, abs/1404.1100, 2014.
- [96] L. Sirovich. Turbulence and the dynamics of coherent structures. *Quarterly of applied mathematics*, 45:561–571, 1987.
- [97] A. Sridhar, P. Tiso, and T. Hardeman. Configuration-dependent reduced order model for cable slab nonlinear dynamics. In G. Kerschen, editor, *Nonlinear Dynamics, Volume 1*, Conference Proceedings of the Society for Experimental Mechanics Series. Springer International Publishing, 2015.
- [98] D. Stadlmayr and W. Witteveen. Model reduction for nonlinear multibody systems based on proper orthogonal- & smooth orthogonal decomposition. In G. Kerschen, editor, *Nonlinear Dynamics, Volume 1*, Conference Proceedings of the Society for Experimental Mechanics Series, pages 449–458. Springer International Publishing, 2015.
- [99] D. Stadlmayr, W. Witteveen, and W. Steiner. A generalized constraint reduction method for reduced order mbs models. *Multibody System Dynamics*, pages 1–16, 2016.
- [100] D. Stadlmayr, W. Witteveen, and W. Steiner. Reduction of Physical and Constraint DOF of Redundant Formulated Multibody Systems. *Journal of Computational and Nonlinear Dynamics*, 11, 2016.
- [101] G. Stewart. On the sensitivity of the eigenvalue problem $Ax = \lambda Bx$. *SIAM Journal on Numerical Analysis*, 9:669–686, 1972.
- [102] G. Stewart. The decompositional approach to matrix computation. *Computing in Science & Engineering*, 2:50–59, 2000.
- [103] R. Ștefănescu, A. Sandu, and I. M. Navon. Comparison of pod reduced order strategies for the nonlinear 2d shallow water equations. *International Journal for Numerical Methods in Fluids*, 76(8):497–521, 2014.
- [104] R. Temam. Inertial manifolds. *Mathematical Intelligencer*, 12:68–74, 1990.

- [105] P. Tiso and D. Rixen. Reduction methods for mems nonlinear dynamic analysis. In *Proceedings of the IMAC-XXVII*, 2010.
- [106] E. Titi. On approximate inertial manifolds to the navier-stokes equations. *Journal of mathematical analysis and applications*, 149:540–557, 1990.
- [107] C. F. van Loan. Generalizing the singular value decomposition. *SIAM Journal on Numerical Analysis*, 13:76–83, 1976.
- [108] A. van Wynsberghe and Q. Cui. Interpreting correlated motions using normal mode analysis. *Structure*, 14:1647–1653, 2006.
- [109] S. Volkwein. *Model Reduction Using Proper Orthogonal Decomposition*. Lecture Notes - University of Constance, 2008.
- [110] M. E. Wall, A. Rechtsteiner, and L. M. Rocha. Singular value decomposition and principal component analysis. *ArXiv Physics e-prints*, Aug. 2002.
- [111] L. Wang. *Karhunen-Loève expansions and their applications*. PhD thesis, London School of Economics and Political Science (United Kingdom), 2008.
- [112] R. Wehage and E. Haug. Generalized coordinate partitioning for dimension reduction in analysis of constrained dynamic systems. *ASME Journal of Mechanical Design*, 104:247–255, 1982.
- [113] K. Willcox and J. Peraire. Balanced model reduction via the proper orthogonal decomposition. *AIAA Journal*, 40:2323–2330, 2002.
- [114] W. Witteveen. On the modal and non-modal model reduction of metallic structures with variable boundary conditions. *World Journal of Mechanics*, 2:311–324, 2012.
- [115] M. Wojtyra. Joint reactions in rigid body mechanisms with dependent constraints. *Mechanism and Machine Theory*, 44:2265–2278, 2009.
- [116] M. Wojtyra and H. Fraczek. Comparison of selected methods of handling redundant constraints in multibody system simulations. *Journal of Computational and Nonlinear Dynamics*, 8:CND–11–1179, 2012.
- [117] B. Yan, S. Tan, and B. McCaughy. Second-order balanced truncation for passive-order reduction of rlc circuits. *IEEE Transactions on Circuits and Systems - II: Express Briefs*, 55:942–946, 2008.

Appendix

crankshaft				
	value/direction	unit		
m_{crank}	9.5	[kg]		
PAI_x	(1, 0, 0)	[-]		
PAI_y	(0, 1, 0)	[-]		
PAI_z	(0, 0, 1)	[-]		
I_x	0.015	[kg · m ²]		
I_y	0.128	[kg · m ²]		
I_z	0.138	[kg · m ²]		

PAI Principal Axis of Inertia
in the global coordinate system

connecting rod (1st cyl.)			piston (1st cyl.)		
	value/direction	unit		value/direction	unit
$m_{\text{con rod}}$	0.9	[kg]	m_{piston}	0.7	[kg]
PAI_x	(0, 0.571, 0.821)	[-]	PAI_x	(1, 0, 0)	[-]
PAI_y	(0, -0.821, 0.571)	[-]	PAI_y	(0, 0.71, -0.71)	[-]
PAI_z	(1, 0, 0)	[-]	PAI_z	(0, 0.71, 0.71)	[-]
I_x	0.00031	[kg · m ²]	I_x	0.00066	[kg · m ²]
I_y	0.0031	[kg · m ²]	I_y	0.00068	[kg · m ²]
I_z	0.0033	[kg · m ²]	I_z	0.00068	[kg · m ²]

Table 1: Physical properties - V8 crank drive

	value	unit
T_{idle}	20	$[N \cdot m]$
T_{peak}	200	$[N \cdot m]$
$d_{\text{crank,rot}}$	500	$[N \cdot m \cdot s]$

Table 2: Forces/torques - V8 crankshaft

	value	unit		value	unit
f_1	60.9	[Hz]	f_{16}	2141.3	[Hz]
f_2	247.9	[Hz]	f_{17}	2498.4	[Hz]
f_3	317.5	[Hz]	f_{18}	2651.6	[Hz]
f_4	375.1	[Hz]	f_{19}	2879.5	[Hz]
f_5	393.2	[Hz]	f_{20}	3063.2	[Hz]
f_6	696.6	[Hz]	f_{21}	3233.2	[Hz]
f_7	894.7	[Hz]	f_{22}	3335.9	[Hz]
f_8	1022.9	[Hz]	f_{23}	3780.0	[Hz]
f_9	1092.8	[Hz]	f_{24}	4294.9	[Hz]
f_{10}	1206.8	[Hz]	f_{25}	4518.2	[Hz]
f_{11}	1379.9	[Hz]	f_{26}	4985.1	[Hz]
f_{12}	1651.7	[Hz]	f_{27}	5117.6	[Hz]
f_{13}	1838.1	[Hz]	f_{28}	5267.9	[Hz]
f_{14}	1952.8.1	[Hz]	f_{29}	5627.28	[Hz]
f_{15}	2006.8	[Hz]	f_{30}	5718.3	[Hz]

Table 3: Eigenfrequencies of the flexible lower wishbone - Partially flexible front suspension

	value	unit			
f ₁	564.3	[Hz]	f ₁₄	7260.6	[Hz]
f ₂	565.0	[Hz]	f ₁₅	7277.75	[Hz]
f ₃	1510.8	[Hz]	f ₁₆	8437.1	[Hz]
f ₄	1517.9	[Hz]	f ₁₇	9441.3	[Hz]
f ₅	2791.0	[Hz]	f ₁₈	9530.3	[Hz]
f ₆	2819.3	[Hz]	f ₁₉	9738.1	[Hz]
f ₇	3094.7	[Hz]	f ₂₀	10126.1	[Hz]
f ₈	4217.7	[Hz]	f ₂₁	10132.8	[Hz]
f ₉	4277.6	[Hz]	f ₂₂	10168.9	[Hz]
f ₁₀	4969.5	[Hz]	f ₂₃	10539.5	[Hz]
f ₁₁	5684.1	[Hz]	f ₂₄	11515.1	[Hz]
f ₁₂	5752.9	[Hz]	f ₂₅	11698.1	[Hz]
f ₁₃	5958.0	[Hz]	f ₂₆	12359.6	[Hz]

Table 4: Eigenfrequencies of the flexible pushrod - Partially flexible front suspension

steering knuckle			steering rod		
	value/direction	unit		value/direction	unit
m	4.4	[kg]	m	0.4	[kg]
PAI _x	(0.86, 0.37, 0.33)	[-]	PAI _x	(0.02, 0.99, -0.03)	[-]
PAI _y	(0.44, -0.27, -0.84)	[-]	PAI _y	(0.83, 0.0, 0.55)	[-]
PAI _z	(-0.22, 0.88, -0.40)	[-]	PAI _z	(0.55, -0.04, -0.83)	[-]
I _x	0.014	[kg · m ²]	I _x	0.00048	[kg · m ²]
I _y	0.030	[kg · m ²]	I _y	0.0055	[kg · m ²]
I _z	0.035	[kg · m ²]	I _z	0.0055	[kg · m ²]

lower wishbone			upper wishbone		
	value/direction	unit		value/direction	unit
m	1.68	[kg]	m	1.07	[kg]
PAI _x	(1, 0, 0)	[-]	PAI _x	(-0.50, 0.85, -0.03)	[-]
PAI _y	(0, 1, 0)	[-]	PAI _y	(-0.85, -0.50, 0.10)	[-]
PAI _z	(0, 0, 1)	[-]	PAI _z	(0.06, 0.08, 0.99)	[-]
I _x	0.050	[kg · m ²]	I _x	0.016	[kg · m ²]
I _y	0.030	[kg · m ²]	I _y	0.026	[kg · m ²]
I _z	0.00060	[kg · m ²]	I _z	0.042	[kg · m ²]

pushrod			relay lever		
	value/direction	unit		value/direction	unit
m	0.58	[kg]	m	1.1	[kg]
PAI _x	(1, 0, 0)	[-]	PAI _x	(0.49, 0.57, 0.64)	[-]
PAI _y	(0, 1, 0)	[-]	PAI _y	(-0.81, 0.57, 0.11)	[-]
PAI _z	(0, 0, 1)	[-]	PAI _z	(-0.30, -0.58, 0.75)	[-]
I _x	0.012	[kg · m ²]	I _x	0.0021	[kg · m ²]
I _y	0.0036	[kg · m ²]	I _y	0.0036	[kg · m ²]
I _z	0.0094	[kg · m ²]	I _z	0.0056	[kg · m ²]

Table 5: Physical properties - Partially flexible front suspension

	value	unit
c_{spring}	80000	$[N/m]$
d_{spring}	0.1	$[N \cdot m \cdot s]$

Table 6: Forces/torques - Partially flexible front suspension

frame			battery		
	value/direction	unit		value/direction	unit
m	11.3	[kg]	m	2.2	[kg]
PAI _x	(0.98, 0.0, -0.21)	[-]	PAI _x	(0, 1, 0)	[-]
PAI _y	(-0.21, 0.0, -0.98)	[-]	PAI _y	(1, 0, 0)	[-]
PAI _z	(0.0, 1.0, 0.0)	[-]	PAI _z	(0, 0, 1)	[-]
I _x	0.197	[kg · m ²]	I _x	0.0039	[kg · m ²]
I _y	0.339	[kg · m ²]	I _y	0.0039	[kg · m ²]
I _z	0.475	[kg · m ²]	I _z	0.005	[kg · m ²]

front wheel			rear wheel		
	value/direction	unit		value/direction	unit
m	4.4	[kg]	m	4.4	[kg]
PAI _x	(0.31, 0.0, -0.95)	[-]	PAI _x	(1, 0, 0)	[-]
PAI _y	(-0.95, 0.0, -0.31)	[-]	PAI _y	(0, 0, 1)	[-]
PAI _z	(0.0, 1, 0.0)	[-]	PAI _z	(0, -1.0)	[-]
I _x	0.072	[kg · m ²]	I _x	0.072	[kg · m ²]
I _y	0.072	[kg · m ²]	I _y	0.072	[kg · m ²]
I _z	0.140	[kg · m ²]	I _z	0.140	[kg · m ²]

swing arm			rider dummy		
	value/direction	unit		value/direction	unit
m	4.0	[kg]	m	30	[kg]
PAI _x	(0.96, -0.0, 0.26)	[-]	PAI _x	(1, 0, 0)	[-]
PAI _y	(-0, -1, 0)	[-]	PAI _y	(0, 1, 0)	[-]
PAI _z	(0.27, 0.0, 0.96)	[-]	PAI _z	(0, 0, 1)	[-]
I _x	0.011	[kg · m ²]	I _x	0.5	[kg · m ²]
I _y	0.036	[kg · m ²]	I _y	0.6	[kg · m ²]
I _z	0.044	[kg · m ²]	I _z	0.2	[kg · m ²]

Table 7: Physical properties part 1 - Electrical junior dirtbike

shock prt.1			shock prt.2		
	value/direction	unit		value/direction	unit
m	0.49	[kg]	m	0.15	[kg]
PAI _x	(0.74, 0.0, 0.67)	[-]	PAI _x	(0.74, 0.0, 0.67)	[-]
PAI _y	(0, -1, 0)	[-]	PAI _y	(0.67, 0.0, -0.74)	[-]
PAI _z	(0.67, 0.0, 0.74)	[-]	PAI _z	(0.1.0)	[-]
I _x	0.0001	[kg · m ²]	I _x	0.00002	[kg · m ²]
I _y	0.00018	[kg · m ²]	I _y	0.00009	[kg · m ²]
I _z	0.00018	[kg · m ²]	I _z	0.00009	[kg · m ²]

fork prt.1			fork prt.2		
	value/direction	unit		value/direction	unit
m	2.7	[kg]	m	2.4	[kg]
PAI _x	(-0.17, 0.0, 0.98)	[-]	PAI _x	(-0.30, 0.0, 0.96)	[-]
PAI _y	(0, -1, 0)	[-]	PAI _y	(0, -1, 0)	[-]
PAI _z	(0.98, 0.0, 0.17)	[-]	PAI _z	(0.95, 0.0, 0.3)	[-]
I _x	0.043	[kg · m ²]	I _x	0.0081	[kg · m ²]
I _y	0.057	[kg · m ²]	I _y	0.021	[kg · m ²]
I _z	0.098	[kg · m ²]	I _z	0.028	[kg · m ²]

Table 8: Physical properties part 2 - Electrical junior dirtbike

	value	unit
c_{shock}	50000	[N/m]
d_{shock}	1000	[N · m · s]
c_{fork}	8000	[N/m]
d_{fork}	1000	[N · m · s]
$c_{\text{testbench}}$	50000	[N/m]
$d_{\text{testbench}}$	500	[N · m · s]

Table 9: Forces/torques - Electrical junior dirtbike

	value	unit		value	unit
$m_{C1,initial}$	2.3	[kg]	k_2	1000	[N/m]
$m_{C1,target}$	2.12	[kg]	$J_{C1} = J_{C2}$	0.02	[kg m ²]
m_{C2}	4.6	[kg]	$J_{P1} = \dots = J_{P8}$	0.00079	[kg m ²]
$m_{P1,initial} = \dots = m_{P4,initial}$	0.12	[kg]	$l_{P1} = \dots = l_{P8}$	0.22	[m]
$m_{P1,target}$	0.15	[kg]	$d_{P1,initial} = \dots = d_{P4,initial}$	0.2	[Nms]
$m_{P2,target}$	0.2	[kg]	$d_{P1,target}$	0.25	[Nms]
$m_{P3,target}$	0.19	[kg]	$d_{P2,target}$	0.17	[Nms]
$m_{P4,target}$	0.17	[kg]	$d_{P3,target}$	0.24	[Nms]
$m_{P5} = \dots = m_{P8}$	0.12	[kg]	$d_{P4,target}$	0.16	[Nms]
k_1	1000	[N/m]	$d_{P5} = \dots = d_{P8}$	0.2	[Nms]

Table 10: Cart-Pendulum chain - model data

Daniel Stadlmayr

Kainzing 26
4753 Taiskirchen im Innkreis, Austria
☎ +43 (0699) 19870827
✉ stadlmayr.daniel@gmail.com

Biographical

Date of birth 27.08.1987
Place of birth Bad Ischl, Austria
Nationality Austrian
ORCID-ID 0000-0001-8969-4827

Professional experience

Current position

- 03.2018 – **Interim head of software development**, *SLM Solutions Software GmbH*, Perg, Austria.
Responsible for overall software development on an interim basis
- 03.2017 – **Head of technical R&D**, *SLM Solutions Software GmbH*, Perg, Austria.
Responsible for simulation related R&D topics in the field of metal powder bed additive manufacturing

Previous Employment

- 08.2013 – **Research fellow**, *Upper Austrian University of Applied Sciences - Research and Development GmbH*, Wels, Austria.
Engaged in research towards model order reduction in the multibody dynamics research group
- 10.2012 – **CAE engineer**, *WP Performance Systems GmbH - Division Suspension*, Munderfing, Austria.
Development of a CAE-simulation working group and implementation of CFD and FEM simulation in the product development process
- 02.2012 – **Intern/Graduand**, *WP Performance Systems GmbH - Division Suspension*, Munderfing, Austria.
Internship resulting in my master's thesis

Education

- 2014 – **Dr. techn.**, *Institute of Mechanics and Mechatronics – Technical University Vienna*, Vienna, Austria.
PhD-thesis on *Model Order Reduction of Redundant Multibody System Dynamics*

2007 – 2012 **Dipl.Ing**, *Mechanical Engineering - Upper Austrian University of Applied Sciences, Campus Wels, Wels, Austria.*
Master's thesis on *Motorcycle Air Suspension Systems*

Teaching activities

2014 – 2017 **Exercise**, *Mechanics (Strength of materials)*, Upper Austrian University of Applied Sciences - Campus Wels.

2014 – 2017 **Exercise**, *Finite Element Method*, Upper Austrian University of Applied Sciences - Campus Wels.

2015 **Exercise**, *Mechanics (Dynamics)*, Upper Austrian University of Applied Sciences - Campus Wels.

2015 **Tutorial**, *Introduction to LaTeX*, Upper Austrian University of Applied Sciences - Campus Wels.

Attended workshops

2015 – Advanced School on “The Art of Modeling Mechanical Systems”, CISM - AIMETA , Udine (Italy)

2013 – Model Reduction of Complex Dynamical Systems, Max Planck Institute for Dynamics of Complex Technical Systems, Magdeburg (Germany)

List of publications

Peer-reviewed papers

- [1] Stadlmayr, D., Witteveen, W., and Steiner, W. Reduction of Physical and Constraint DOF of Redundant Formulated Multibody Systems. *Journal of Computational and Nonlinear Dynamics*, 11(3):031010, 2016.
- [2] Stadlmayr, D., Witteveen, W., and Steiner, W. A generalized constraint reduction method for reduced order mbs models. *Multibody System Dynamics*, pages 1–16, 2016.

Book chapters

- [1] Stadlmayr, D. and Witteveen, W. Model Reduction for Nonlinear Multibody Systems based on Proper Orthogonal- & Smooth Orthogonal Decomposition. In Kerschen, G., Editor, *Nonlinear Dynamics, Volume 1*, Conference Proceedings of the Society for Experimental Mechanics Series, pages 449–458. Springer International Publishing, 2015.

Conference contributions

- [1] Stadlmayr, D., Witteveen, W., and Steiner, W. Physical and constraint DOF reduction of redundant multibody systems using the proper orthogonal decomposition. In *MoRePaS 2015 - Model Reduction of Parameterized Systems III, SISSA, Trieste, Italy*, 2015.